Circadian and circatidal oscillations of clock gene expression in brains of *Eurydice pulchra* and *Parhyale hawaiensis*.

Oliphant, A. [1]*, Sia, C.Y. [1]*, Kyriacou, C.P. [2], Wilcockson, D.C. [3], Hastings, M.H. [1]

* Equal contribution.

[1]MRC Laboratory of Molecular Biology, Cambridge, CB2 0QH, UK

[2]Department of Genetics, Genomics and Cancer Sciences, University of Leicester, Leicester LE1 7RH, UK

[3]Department of Life Sciences, Aberystwyth University, Aberystwyth SY23 3DA, UK

ORCiD

AO	0000-0002-4867-5352
CYS	0009-0004-1138-000X
CPK	0000-0003-4889-7606
DCW	0000-0002-5923-4472
MHH	0000-0001-8576-6651

Abstract

Coastal organisms express daily and tidal rhythms of physiology and behaviour to adapt to their intertidal environments. Although the molecular-genetic basis of the circadian clocks driving daily rhythms is well understood, the nature and mechanism of circatidal clocks remain a mystery. Using fluorescent *in situ* hybridisation, we mapped discrete clusters of putative "clock" cells co-expressing canonical circadian clock genes across the brains of the intertidal crustaceans *Eurydice pulchra* and *Parhyale hawaiensis*. Tidally rhythmic, field-collected *E. pulchra* exhibited ~12-hour and ~24-hours rhythms of gene expression in discrete cell groups. Laboratory-reared *P. hawaiensis* entrained to 24-hour light:dark cycles (LD) and exhibiting daily behaviour exhibited robust 24-hour rhythms of gene expression in several cell groups. In *P. hawaiensis* showing circatidal behaviour following tidal entrainment by agitation cycles under LD, circadian gene expression was evident in some of the daily rhythmic cell groups, but cells in the dorsal-lateral cluster exhibited robust ~12-hour, i.e., circatidal, transcriptional rhythms. This oscillation was phased to the prior tidal agitation, not to LD. These brain networks of cell groups with circadian or circatidal periodicities tracking LD or tidal agitation, respectively, reveal a neural substrate for the interactive generation of rhythms appropriate to complex intertidal habitats.

57

58 **Introduction:**

59

60 Organisms adapt to their cyclical environments through rhythms of metabolism, physiology
61 and behaviour that are driven by internal biological clocks [1]. Terrestrial environmental cycles
62 are predominantly daily, leading to the evolution of clocks with an autonomous period of
63 approximately one day (hence circadian) and which are entrained to the cycle of light and
64 darkness. In contrast, marine and coastal environments present much greater temporal
65 complexity and marine organisms have additionally evolved a range of circatidal (~12.4
66 hours), circasemilunar (~14.8 days) and circalunar (~29.5 days) timing mechanisms [2 3] that
67 co-ordinate adaptive rhythms of behaviour, metabolism and reproduction. Despite more than
68 six decades of research, the mechanistic underpinnings of circatidal clocks remain a mystery.
69 Observations of behavioural phenotypes have given rise to three principal hypotheses [2]. First,
70 circatidal and circadian rhythms are driven by a single oscillatory system that is plastic,
71 adapting to the period of the dominant environmental cue [4]. Second, paired lunidian (~24.8-
72 hour, i.e., slightly modified circadian) oscillators run in antiphase to create 12.4-hour rhythms
73 [5]. Third, 12.4-hour circatidal and 24-hour oscillators co-exist to drive circatidal and daily
74 phenotypes [6]. Testing these models requires identification of the clock cells and genes
75 responsible for circatidal rhythms.

76

77 The recurrent motif of eukaryotic circadian clocks is a transcriptional/ translational feedback
78 loop (TTFL) in which positive factors transactivate the expression of genes that encode
79 negative regulators [7]. Accumulating negative regulators progressively suppress their
80 transactivation and following their degradation the cycle restarts every ~24 hours [8]. In
81 mammals and flies, heterodimers of CLOCK (CLK) and BMAL1 (or CYC in flies) transactivate
82 the negative regulators PERIOD (PER) and CRYPTOCHROME (CRY) (and/ or TIMELESS
83 (TIM) depending on species) through E-box promotor sites [9]. The intertidal isopod *Eurydice*
84 *pulchra* and the amphipod *Parhyale hawaiensis* can express autonomous circadian and/ or
85 circatidal rhythms of locomotor behaviour in the absence of environmental cues [10 11 12 13].
86 However, the only molecular markers of tidal timekeeping relate to mitochondrial gene
87 expression and cellular redox state in *E. pulchra* [14]. Nevertheless, genes encoding CLOCK,
88 BMAL1, PER and CRY2 are present in both species [12 15] and *tim* expression in the head of *E.*
89 *pulchra* is circadian [12 16] (*P. hawaiensis* lacks *tim* [15]). *E. pulchra* CLOCK:BMAL1 heterodimers
90 can transactivate E-boxes and are suppressed by PER and CRY2 [12], whilst PhBMAL1 co-
91 expressed with mouse CLK can also transactivate E-boxes [13]. Are these conserved circadian
92 factors involved in circatidal time-keeping? Genomic deletion (*P. hawaiensis*) or RNAi-knock-
93 down (*E. pulchra*) of *Bmal1* compromises tidal activity rhythms[13 16], raising the intriguing

possibility of interactions at the molecular-genetic level between circadian and circatidal clocks.

The current aim, therefore, was to describe the expression of *Bmal1*, *Clk*, *per* and *cry2* (together with *tim* in *E. pulchra* and *vrille* in *P. hawaiensis*) across the brain and test its relationship to circadian and circatidal behaviour. We present the first evidence of multiple cell groups in the crustacean brain capable of tracking circadian time, encoded as the rhythmic expression of canonical clock genes. Furthermore, we reveal the presence of cells capable of tracking circatidal time, independently of circadian time, encoded as the expression of *per* and *cry2* with ~12-hour rhythms. These brain networks of cell groups with circadian or circatidal periodicities reveals a neural substrate for the interactive generation of rhythms appropriate to complex intertidal habitats and further implicates canonical circadian genes in circatidal timekeeping.

Results

Free-running activity rhythms in E. pulchra *and* P. hawaiensis

When placed into free-running conditions (DD) in the laboratory, field-collected *E pulchra* displayed strong circatidal activity rhythms with a period of 12.36 ±0.02 h, (mean ±SEM) (Figure 1a, b, Supplementary Figure 1a). From analysis of 11 independent field collections, an average of 54.5 ±6.5% of animals were tidally rhythmic (range: 20–76%, Supplementary Figure 1b) with peak activity corresponding to the expected time of high water on the home beach.

After being entrained in the laboratory to a 12h:12h light/dark (LD) cycle, 58.6 ±4.4% of *P. hawaiensis* across 7 experiments exhibited daily activity cycles (range: 45 -80%, total N =189), with elevated activity at night (Figure 1C, Supplementary Figure 2 a- f). When released into constant darkness, animals showed persistent circadian rhythms in their locomotor activity (Figure 1c, Supplementary Figure 2c, g, h), with an average period of 24.17 ±0.17 h SEM (Figure 1d). Activity levels were significantly higher during the subjective night than in the subjective day (Figure 1C, Supplementary Figure 2 g, h, i). It should be noted, however, that the percentage of rhythmic animals was lower in DD than under LD (22.9 ±7.5%, range: 0 - 50%, Supplementary Figure 2e).

In addition to circadian behaviour, the activity of *P. hawaiensis* can be entrained in a laboratory setting by tidal cycles of inundation [13]. We demonstrated that *P. hawaiensis* held under LD can also be entrained to tidal cycles of mechanical agitation to simulate wave action, as is the case for *E. pulchra* [11]. After over 30 days of tidal entrainment, individual *P. hawaiensis* showed circatidal locomotor behaviour under free-running conditions of DD and no further agitation (Figure 1e, Supplementary Figure 3a-c) with a mean period of 12.40 ±0.02 h SEM (Figure 1f). Across 13 experiments 52.8 ±2.8% of animals showed circatidal behaviour (range 40 –70%, total N =456, Supplementary Figure 3d), with significantly greater activity at subjective high tide than at low tide (Supplementary Figure 3c, e). To confirm that the circatidal behaviour was phased by the agitation and not by the LD cycle, animals were subjected to a phase-shift entrainment regime over 6 days in which tidal agitation occurred every 12.9 hours rather than every 12.4 hours. It therefore moved progressively later relative to the LD cycle than in the initial 12.4 hours paradigm, with an accumulated delay of ~6 hours (0.5 hours per cycle over 12 cycles/ 6 days). On release to DD, phase-shifted animals exhibited circatidal behavioural rhythms with a mean period of 12.4 hours (Figure 1g, Supplementary Figure 3f) and with peak activity again at projected high tide. Importantly, across 4 independent experiments with

147 control and phase-shifted animals, the phase of the circatidal behaviour relative to the prior
148 LD cycle was delayed by 4.94 hours, relative to that set by the original schedule (Figure 1h,
149 Supplementary Figure 3g). The overall quality of the rhythms and the effectiveness of the
150 phase-shifted entrainment were comparable to those seen after the original phase
151 (Supplementary Figure 3h-j). Our data thereby confirm the endogenous tidal rhythmicity of
152 both species, with appropriate periods and phased to their respective entrainment regimes.
153 We also demonstrate the ability of *P. hawaiensis* to exhibit either circadian or circatidal
154 behaviour, subject to prior laboratory entrainment by LD cycles and tidal agitation,
155 respectively.
156
157
158 ***Cellular expression of circadian clock genes in the brains of* E. pulchra *and* P.**
159 **hawaiensis*.***
160 To examine gene expression across the brain, we generated reference brains for each species
161 by averaging confocal image stacks of brains immunolabelled with anti-SYNORF1
162 (Supplementary Figure 4). The brains of *E. pulchra* and *P. hawaiensis* are flexed dorsally
163 around the oesophagus and lie approximately perpendicular to the ventral nerve cord.
164 Descriptions of gross brain anatomy and later naming of clock cell groups are relative to the
165 body axis and our neuroanatomical descriptions of *E. pulchra* are based on the valviferan
166 isopod *Saduria entomon* [17]. For *P. hawaiensis* we refer to [18] and [19] (Supplementary Figure 5,
167 Supplementary Material, Results).
168
169 Given that *Bmal1* has been implicated in circadian and circatidal timekeeping in both *E.*
170 *pulchra* and *P. hawaiensis*, we first localised *Bmal1* transcript as our entry point for a
171 neuroanatomical investigation of putative "clock" cells. Whole-mount HCR-FISH revealed that
172 *Bmal1* is widely expressed across the brain of *E. pulchra* (Figure 2a). This pan-cellular
173 expression and the intensity of *Bmal1* labelling did not change over time in LD (Supplementary
174 Figure 6a), supporting our earlier study using whole head qPCR [12] and suggesting that we
175 did not overlook possibly phase-dependent cell-specific enriched expression. The signals we
176 observed were specific, insofar as control HCR-FISH probes against the *deGFP* gene, which
177 is not expressed in *E. pulchra*, showed no labelling (Supplementary Figure 8). We next
178 examined the expression of *Clk* mRNA that encodes CLOCK, the heterodimeric partner of
179 BMAL1. This revealed similarly widespread expression in the brain of *E. pulchra*, with most
180 cells expressing specific but low levels of *Clk* mRNA (Figure 2b). In contrast to *Bmal1*,
181 however, there was a condensation of higher intensity signals in ~60 cells, located principally
182 in the cell rinds overlaying the median protocerebrum. These *Bmal1* and *Clk* expression

183 patterns in the brain of *E, pulchra* were confirmed using RNAscope on brain sections
184 (Supplementary Figure 7).
185
186 The pan-cellular expression of *Bmal1* was also evident in the brain of *P. hawaiensis* (Figure
187 2c) and, again, this did not change across the LD cycle (Supplementary Figure 6b). In
188 contrast, the expression of *Clk* in *P. hawaiensis* was less widespread than in *E. pulchra* and
189 there was a clear enrichment of expression in cells in the median protocerebrum. These were
190 comparable in number and location to those seen in *E. pulchra* (Figure 2d). Thus,
191 notwithstanding the requirement for *Bmal1* to sustain circatidal behaviour in both species [13 16],
192 the pattern of its expression did not reveal a population of dedicated clock cells. In contrast,
193 the expression of *Clk* was significantly elevated in discrete cell populations in the median
194 protocerebrum of both *E. pulchra* and *P. hawaiensis*.
195
196 Given that TTFL-based clocks require negative regulators, we next mapped the expression
197 across the brain of *E. pulchra* of *cryptochrome 2* (*cry2*), *period* (*per*) and *timeless* (*tim*). This
198 revealed strong, specific signal but in contrast to the widespread expression of the positive
199 regulators, transcripts encoding the negative regulators were invariably restricted to discrete
200 cell clusters in the median protocerebrum (Figure 2e, f, g). In the *P. hawaiensis* brain the
201 expression of *per* and *cry2* exhibited a similar pattern to *E. pulchra*, with high levels of both
202 transcripts localised to ~60 cells in the median protocerebrum (Figure 2h, i). *Tim* is absent
203 from the *P. hawaiensis* genome [15] and so we probed *P. hawaiensis* for *vrille* (*vri*), which in
204 *Drosophila* is colocalised to circadian cells and whose expression is driven by dCLK and CYC
205 [20 21] and this revealed a widespread expression pattern (Figure 2j).
206
207
208 ***Co-expression of circadian clock genes in distinct cell groups of* E. pulchra *and* P.**
209 **hawaiensis *brains*.**
210 On the basis that CLOCK:BMAL1 heterodimers are required for transactivation of *per* and *tim*
211 within the TTFL of *Drosophila*, the co-expression of *Bmal1* and *Clk* was compared by
212 multiplexed HCR-FISH of *E. pulchra* brains dissected in the light phase. The *Clk*-enriched
213 cells not only expressed *Bmal1* at a level seen in other cells across the brain, but also highly
214 expressed *per* (Figure 3a). *Per*-expressing cells also express *cry2* (Figure 3b) and *tim* (Figure
215 3c). This relatively small population of cells in the median protocerebrum of *E. pulchra*
216 therefore co-expressed the full complement of genes required for a functional TTFL,
217 supporting the view that they may be functional clock cells. Notably, *per* and *cry2* encode the
218 principal negative regulators of E-box-mediated transcription in *E. pulchra* [12]. We then applied
219 a similar analysis to *P. hawaiensis* and found, again, that *Clk*-enriched cells express *Bmal1*

220 and high levels of *cry2* (Figure 3d). Furthermore, the *cry2*- (and hence, *Clk*-) enriched cells
221 also expressed both *per* and *vri* (Figure 3e), highlighting them as likely clock-competent cells.
222
223
224 ***Regional expression of circadian clock genes in the brains of* E. pulchra *and* P.**
225 **hawaiensis.**
226 By combining HCR-FISH with anti-SYNORF1 immunofluorescence and registering images to
227 the reference brains, we delineated and localised putative clock cell clusters (Supplementary
228 Figure 9). All groups were bilaterally symmetrical in both species, the cell numbers stated
229 below being per hemisphere. In *E. pulchra, per*- and *cry2*-expressing cells were primarily
230 found in the posterior cell body rind overlying the medial protocerebrum (MP), hemi-ellipsoid
231 body and medulla terminalis (HE/MT, Figure 4a, b). There were nine somata in the rind
232 posterior to the protocerebral bridge (rPBp) [22], which we termed the "medioposterior" cells.
233 Dorsal and anterior to these cells was a cluster of 5 somata in the cell body rind dorsal to the
234 PB (rPBd) that we assigned as "medial" cells. Lateral to these medial and medioposterior
235 cells was a cell pair in the rind posterior of the medulla terminalis (rMTp) which we named
236 "lateroposterior" cells. In the cell body rind posterior to the hemi-ellipsoid body/ medulla
237 terminalis (rHEp/MTp) were 4 "dorsal" cells, one of which was larger than the others and we
238 refer to as "large dorsal" cell. In the dorsal region of the cell body rind posterior of the MP
239 (rMPp) ~4-6 "ventroposterior" cells. In the anterior aspect of the brain, we found fewer cells;
240 in the cell body rind lateroanterior of the hemi-ellipsoid body/medulla terminalis (rHE/MTla)
241 was a single pair of cells, the "dorsoanterior" cells. A single "lateroanterior" cell was in the rind
242 ventral and anterior of the lobula (rLOva). Finally, a pair of cells on the midline (one per
243 hemisphere), anterior of the medial protocerebrum were named "medioanterior" cells (rMPa).
244 Cell groups and their given nomenclature are summarised in Supplementary Table 1.
245
246 In *P. hawaiensis*, *per*- and *cry2*-enriched cells were found throughout the anterior and posterior
247 aspects of cell body rind overlying MP and HE/MT. In the cell body rind posterior and lateral
248 to the PB (rPBp) were ten *per*- and *cry2*-enriched somata that we assigned as "medioposterior"
249 cells (Figure 4c, d). Dorsoanterior to these cells were three cells, two of which were closer to
250 each other than the last one; these we termed "medial-2" and "medial-1", respectively, and
251 collectively, the medial cells. In the cell body rind dorsal of the HE/MT (rHE/MTd), we identified
252 two somata as the "dorsal-lateral" cells, and antero-medial to these cells were six cells that
253 we called the "dorsal" cells. On the anterior aspect of the brain, we identified one cell in the
254 cell body rind anterior of the HE/MT (rHE/MTa) as "anterior-lateral" cells. Lastly, we found 8 –
255 9 cells on the anterior aspect of the medial protocerebrum (rPMa). We refer to these cells
256 collectively as the "anterior-medial" cells and they can be divided into 4 groups. "Anterior-

257 medial b" cells described two cells with distinctive location lateral to the myoarterial formation.
258 Dorsal to the anterior-medial b cells were two cells, in which one was positioned medially to
259 the other. These, we termed "anterior-medial a1" and "anterior-medial a2" cells, respectively.
260 The "anterior-medial c" cells were a group of 4 – 5 cells located dorsal to the anterior-medial
261 a1-2 cells.
262
263
264 ***Pigment dispersing hormone cells are distinct from clock cells.***
265 In *Drosophila melanogaster* the neuropeptide pigment-dispersing factor (PDF) is a marker for
266 the ventral lateral (LN_v) circadian clock neurons, and it signals temporal cues within the clock
267 neurocircuitry [23]. The expression of the gene encoding the crustacean homologue, pigment-
268 dispersing hormone (PDH), was mapped and compared to that of the *per*- and *cry2*-enriched
269 cells. In *E. pulchra*, *pdh* transcript was expressed strongly in five cell bodies in the anterior
270 HE/ MT and weakly in two cells anterior and medial of the HE/MT (Figure 5a, b) [24]. In both
271 regions, cells expressing *per* and *cry2* were absent. Dual-labelling confirmed that, in contrast
272 to fruit flies, none of the *cry2*-enriched cells expressed *pdh* (Figure 5c). Similar analysis in *P.*
273 *hawaiensis* produced the same results: dual-labelling showed that *pdh* was not expressed in
274 the cells expressing *cry2*, and by extension the other circadian regulators (Figure 5d-f). These
275 results do not exclude *pdh* cells from clock functions, but they do show that the putative neural
276 circuitry underlying circadian time-keeping and its neuropeptidergic components differ
277 between *D. melanogaster* and these two crustaceans.
278
279
280 ***Rhythmic expression of circadian clock genes in circatidally rhythmic* E. pulchra *under***
281 ***a light:dark cycle.***
282 A canonical feature of the TTFL is the rhythmic expression of one or more negative regulators.
283 In *E. pulchra*, the accumulation of *Eptim*, as determined by qPCR of pooled heads, exhibits a
284 circadian cycle with a peak in late circadian day (~CT16-18), but rhythmic expression of *Epper*
285 or *Epcry2* was not detected [12]. It is possible, however, that rhythmic gene expression in
286 individual cell populations is masked by bulk sampling. To determine whether individual clock
287 cells, or clusters of cells, exhibit rhythms of expression, we performed whole-mount,
288 multiplexed HCR-FISH on dissected brains of circatidally rhythmic, beach-caught *E. pulchra*
289 sampled every 2 hours under LD (16:8) for 24 hours and quantified the number of HCR-FISH
290 spots as a proxy for transcript abundance. We considered transcript levels to be rhythmic only
291 when Kruskal-Wallis/ ANOVA identified a significant time effect and both JTK_CYC [25] and
292 RAIN [26] exceeded significance thresholds at a period of 12 hours ($p<0.05$) or 24 hours for
293 circatidal and daily rhythms, respectively. First, we aggregated counts across all putative clock

294 cells as a proxy for total brain expression, i.e., the total, specific signal fluorescence per brain
295 (Figure 6a). Both *per* and *cry2* showed a strong daily (24-hour) rhythm in expression, peaking
296 in the later dark phase. Aggregate levels of *tim* also showed an effect of time but it was more
297 complex, being statistically significant at both 24-hour and 12-hour periods.
298
299 An attractive hypothesis as to how circatidal and circadian behavioural phenotypes are driven
300 in coastal animals is that different cell populations contain ~12-hour and ~24-hour molecular
301 timers and entrain to appropriate stimuli for each time domain. To test this, we analysed
302 expression at the level of individual cell groups (Figure 6b, c, Supplementary Figure 10). In
303 the largest cell group, the medioposterior cells, both *per* and *cry2* showed a strong daily cycle,
304 again peaking in late dark phase, whereas *tim* transcript abundance did not vary significantly
305 between time points (Supplementary Table 2). In the medial cell group, *per* showed a daily
306 cycle peaking in late dark phase, but *cry2* did not vary significantly (Supplementary Table 2).
307 Expression of *tim*, however, showed a 12-hour pattern with elevated counts after subjective
308 high water (Figure 6d, e). A 12-hour cycle was also found for *tim* in the lateroposterior cells,
309 but *per* was non-rhythmic and *cry2* did not vary significantly between time points in these cells
310 (Supplementary Figure 10b, c, Supplementary Table 2). In the lateroanterior cells *per* and
311 *cry2* did not vary significantly. In these same cells, *tim* expression cycled with a 24-hour
312 rhythm (Supplementary Figure 10d, e) and a 24-hour rhythm was found for *cry2* in the large
313 dorsal cells. In the large dorsal cells (*per* and *tim*) and dorsoanterior cells, *per, cry2* and *tim*
314 expression either did not vary significantly between time points or cyclic expression was not
315 detected (Supplementary Figure 10, Supplementary Table 2). Thus, in circatidally behaving
316 *E. pulchra* sampled under LD, aggregate expression of *per* and *cry2* tracked daily time, whilst
317 aggregate levels of *tim* reflected both daily and circatidal time. When examined across distinct
318 cell groups, daily cycles of *per* and *cry2* were evident in some groups whilst a circatidal pattern
319 of *tim* expression was detected in a limited number of cells.
320
321
322 ***Rhythmic expression of circadian clock genes in* P. hawaiensis *under a light:dark cycle.***
323 In contrast to wild-caught *E. pulchra*, *P. hawaiensis* is amenable to daily and tidal entrainment
324 in a controlled setting, thereby allowing for more rigorous dissection of 24-hour and 12.4-hour
325 timing (Figure 1) [13 10]. Taking advantage of this, we first examined the expression of circadian
326 genes in animals entrained to LD cycles without tidal agitation. Correspondingly, these
327 animals exhibited daily behavioural rhythms prior to sampling (Supplementary Figure 11a).
328 When examined in aggregate across all cells as a proxy for total brain expression, *per* levels
329 changed significantly across 24 h time (Figure 7a), with higher levels during the late night
330 (ZT17-23) and an afternoon nadir (ZT9-ZT13). In contrast, although it was statistically

331 significant, the daily cycles of *cry2* and *Clk* expression were less marked (Figure 7a). When
332 examined within discrete cell groups, however, the rhythmic expression of these genes was
333 more pronounced. For example, the anterior-medial a1 cells exhibited highly significant daily
334 cycles of *per*, *cry2* and *Clk* expression (Figure 7b, c). *Per* was again high in the dark phase
335 whereas expression of *cry2* and *Clk* cycled in antiphase to *per* with a daytime elevation and
336 nocturnal decline. Circadian gene expression in the anterior-medial a1 cells is therefore able
337 to track the light-dark cycle. Rhythmic expression of *per* was shared across several cell
338 groups, including the medioposterior cells (Supplementary Figure 11b, c), the dorsal cells
339 (Supplementary Figure 11d, e) and the anterior-medial b cells (Supplementary Figure 11f, g),
340 in all cases peaking in the night. The rhythms of *cry2* and *Clk* were more variable across
341 these cell groups. In contrast, anterior-medial c cells did not exhibit clear rhythms, and only
342 *cry2* expression rhythm was statistically significant, albeit with a low amplitude
343 (Supplementary Figure 11h, i). Similarly, the medial-1, medial-2, dorsal-lateral, anterior-lateral
344 and anterior-medial a2 cells did not shown significant rhythms of expression of *per*, *cry2* or
345 *Clk* (Supplementary Figure 12). Overall, the phase of peak *per* expression in those cell groups
346 that were rhythmic was consistently nocturnal (ZT20.85 $\pm$1.02 SEM), whereas the phase of
347 *cry2* and *Clk* rhythms varied between cell groups (Figure 7d).
348
349
350 ***Rhythmic expression of circadian clock genes in circatidally active* P. hawaiensis*.***
351 Having established that circadian gene expression could track the LD cycle in a gene-specific
352 and cell-type-specific manner, we then tested whether any cell groups in *P. hawaiensis* could
353 track tidal time. Animals were entrained for over 30 days by cycles of swirling agitation at 12.4
354 h intervals under 12:12 LD regimes and were then allowed to free-run after transfer to DD in
355 the absence of swirling, with the first two expected high tides beginning at ~CT9.2 and
356 ~CT21.6. The animals exhibited a clear pattern of circatidal activity before harvest
357 (Supplementary Figure 13a). Aggregate expression of *per* was circadian, with peak
358 expression in circadian night, consistent with the daily rhythm seen in animals entrained to the
359 LD cycle (Figure 8a). The aggregate expression of *cry2* and *vri* was not notably circadian.
360 When examined by cell groups, expression of *per* was strongly circadian in anterior-medial a1
361 cells (Figure 8b, c) and in medioposterior cells (Figure 8d, e). These cells also showed
362 circadian cycles of *cry2* expression, in antiphase to the *per* cycle, recapitulating the patterns
363 observed on LD cycles. Expression of *vri* was marginally rhythmic in these cells. Importantly,
364 therefore, *per* and *cry2* expression in these cells continued to track circadian time rather than
365 tidal time in circatidally rhythmic animals. This was not the case for the dorsal-lateral cells.
366 Under LD cycles with no agitation the expression of *per*, *cry2* and *Clk* in animals showing daily
367 behaviour was not rhythmic (Supplementary Figure 12e, f). In contrast, in animals showing

368 circatidal behaviour there was a significant 12-hour cycle of *per*, *cry2* and *vri* transcripts in the
369 dorsal-lateral cells (Figure 9a, b). Furthermore, *per* and *cry2* oscillated almost in phase, both
370 peaking after subjective high tide. The experiment was repeated with tidal swirling applied
371 slightly later (+1.2 hours) relative to the LD cycle and the animals again exhibited robust
372 circatidal activity rhythms (Supplementary Figure 14a). Aggregate expression of *per* was
373 again circadian (Supplementary Figure 14a), as was expression of *per* and *cry2* in the anterior-
374 medial a1 and medioposterior cells (Supplementary Figure 14c, d and e, f). Nevertheless, the
375 dorsal-lateral cells again showed a strong circatidal pattern of expression of *per* and *cry*, which
376 oscillated in phase, peaking after subjective high tide (Figure 9c, d).
377
378 A key criterion for a *bona fide* clock is that it phase-entrains to appropriate environmental
379 stimuli. To test whether we could phase-entrain these putative tidal cells, and to differentiate
380 them from circadian cells exhibiting bimodal 24-hour rhythms, we sampled animals when the
381 tidal stimulus regime was 5.4-hour phase-shifted relative to the 12:12LD cycle (i.e., subjective
382 high tide at ~CT3.8 and ~CT16.2). The animals exhibited appropriately phased robust
383 circatidal rhythms of activity, again peaking at subjective high tide (Supplementary Figure
384 15a). The aggregate expression of *per* as well as cell-specific levels in anterior-medial a1 and
385 medioposterior cells remained circadian, with a peak in subjective night (Supplementary
386 Figure 15b-f). In contrast, the dorsal-lateral cells again showed 12 h cycles of *per*, *cry2* and
387 *vri* expression which peaked after subjective high tide (Figure 9e, f). Therefore, the profiles
388 were phase-shifted relative to the prior LD cycle by ~6 hours, corresponding to the altered
389 phase of tidal entrainment.
390
391 The distinctions between circatidal and circadian rhythms of gene expression are evident in
392 the combined analysis across the three tidal entrainment studies, registered in either tidal or
393 circadian time. When examined across all three experiments and six tidal cycles, the
394 expression of *per*, *cry2* and *vri* in dorsal-lateral cells was highly circatidal (Figure 10c), with
395 mean acrophases of CTT4.4, CTT5.8 and CTT1.9 (circatidal time, CTT =0 at subjective high
396 tide onset) respectively (Figure 10e). In the same circatidally behaving animals, the
397 expression of *per*, *cry2* and *vri* was highly circadian in the anterior-medial a1 and
398 medioposterior cells (Figure 10a, b), with the latter two genes oscillating in anti-phase to *per*
399 (Figure 10d). This mapping of the tidal oscillations to the phase of tidal entrainment in all three
400 experiments confirmed that the dorsal-lateral cells were able to express a free-running
401 molecular signature of tidal time that was independent of circadian time and revealed that the
402 brain of *P. hawaiensis* contains both circadian and circatidally rhythmic cell populations.
403

404 **Discussion**

405

406 Examination of the expression of canonical circadian clock genes across the brains of both *E.*
407 *pulchra* and *P. hawaiensis* identified ~60 cells co-expressing *Clk*, *Bmal1*, *cry2* and *per*,
408 arranged into distinct groups across the protocerebrum. Although the loss of *Bmal1*
409 compromises circatidal behaviour in *E. pulchra* [16] and in *P. hawaiensis* [13], its brain-wide
410 expression showed no local enrichment and so did not highlight any potential circatidal clock
411 cells. This broad distribution is, however, concurrent with BMAL1 having diverse, pleiotropic
412 actions beyond timekeeping [27]. On the other hand, the observed enrichment of *Clk*, *per*, and
413 *cry2* expression (alongside *tim* in *E. pulchra*) in specific cell groups indicated their potential
414 function as circadian oscillators. In contrast to *Drosophila* and other insects [28 29], however,
415 none of these putative clock cells in *E. pulchra* or *P. hawaiensis* co-expressed *pdh*/ *pdf*,
416 emphasising a major neurochemical difference between the insect and crustacean clock
417 circuits [30].

418

419 In circatidally active *E. pulchra* sampled under LD cycles, the aggregated signals for *per* and
420 *cry2* were daily, reflective of their putative circadian roles, and both peaked in the late night as
421 expected for negative co-regulators of the TTFL. In contrast, aggregate brain expression of
422 *tim* showed significant patterning not only at 24 hours, consistent with circadian cycling of *tim*
423 in whole heads assayed by qPCR [12], but also at 12 hours. Analysis at the level of individual
424 cell groups, however, provided a more granular insight, revealing ~24-hour rhythms of *per* and
425 *cry2* in medioposterior and *per* in medial cells, with peak expression in late night. This
426 absence of circatidal rhythmicity of *per* expression resonates with the finding that knockdown
427 of *per* to ~20% of wild-type levels, had no effect on circatidal activity in *E. pulchra*, although it
428 did disrupt circadian phenotypes [12]. Alternatively, *tim* showed ~12-hour accumulation in both
429 the medial and the lateroposterior cells, peaking ~2 hours after expected high water, indicative
430 of tidal time-keeping in these cells. The cell-specific differences in *tim* expression therefore
431 explain the compound periodicity evident in the aggregate expression and associate the
432 medial and the lateroposterior cells with the circatidal behaviour.

433

434 In *P. hawaiensis*, aggregate expression of *per* tracked daily time under LD and circadian time
435 under DD, with elevated levels during the dark phase and subjective night, respectively. Daily
436 and circadian patterning was even more pronounced when examined in individual cell groups,
437 with rhythmic expression of *per* notable in anterior-medial a1, medioposterior, dorsal and
438 anterior-medial b cells. Notably, whereas *per* and *cry2* were in phase in daily cells of *E.*
439 *pulchra*, expression of *per* and *cry2* in daily and circadian cells in *P. hawaiensis* was antiphasic,
440 suggesting inter-species differences in the molecular architecture of putative clock cells.

441

442 Remarkably, following entrainment of *P. hawaiensis* to artificial tidal cycles under LD and then
443 subsequent transfer to free-running conditions, dorsal-lateral cells were robustly rhythmic for
444 *per*, *cry2* and *vri* expression, with a circatidal period that reflects with the circatidal behaviour
445 of the animals. Across independent trials, these cells tracked experimental tidal time,
446 regardless of prior LD phase. In contrast, clock gene expression in these cells was arrhythmic
447 when analysed across individuals sampled under LD without tidal cues. These observations
448 place the dorsal-lateral cells as strong candidates for circatidal oscillators, especially when
449 other cell groups in the same brains (e.g., anterior-medial a1 cells), remained circadian,
450 phased to prior LD and ignoring tidal cues. Notably, *per* and *cry2* in these tidal cells oscillated
451 in phase, in contrast to the antiphasic rhythms of *per* and *cry2* in daily/ circadian cells. The
452 functional significance of these varying relationships, which are surprising in terms of the
453 canonical TTFL, is not clear but they suggest that a common molecular architecture may have
454 diverged, evolving to operate under different time-bases, in different cells.
455

456 Even though both *E. pulchra* and tidally entrained *P. hawaiensis* were strongly circatidal in
457 terms of behaviour, numerous cells in their brain oscillated at ~24 hours (for example, 22 in *P.*
458 *hawaiensis*), and only a few tidal oscillators were observed (4 in *P. hawaiensis*). This raises
459 the question of why strong tidal phenotypes are organised by relatively few tidal cells. Of
460 course, day/ night cycles are highly predictable in the wild and it is therefore expected that
461 circadian systems will be a prominent and robust feature. Nevertheless, coastal animals have
462 evolved temporally complex behaviours to match their habitats [11 12 13 10] and so it may be that
463 gene expression can be circatidal in additional cell groups. This may have evaded statistical
464 detection in the current study because of the high variance intrinsic to population-based
465 measures. Alternatively, it may be that different tidal cells respond to distinct entraining cues,
466 including mechanical agitation (current) or immersion/ emersion [13], and so only a subset is
467 revealed in an experimental setting. Such a cell- and stimulus-specific entrainment repertoire
468 raises the question of how tidal stimuli are transduced to the central brain, and whether the
469 subsets of cells we describe here as non-rhythmic might be recruited by tidal stimuli of other
470 modalities. Such a distributed network would potentially broaden the capacity for tidal
471 entrainment and reinforce it in diverse natural settings.
472

473 In considering the three hypotheses of circatidal time-keeping [4 5 6], our data concur most with
474 the model of dedicated tidal and daily timers proposed by Naylor [6], with canonical circadian
475 genes in distinct cell groups tuning to either circatidal or circadian periodicities. Our
476 demonstration that dual circatidal and circadian systems operate in parallel also corroborates
477 other work on circatidal clocks. For example, surgical removal of optic lobes of the mangrove

478 cricket, *Apteronemobius asahinai*, abrogates circadian but not circatidal locomotor
479 phenotypes, indicative of two anatomically separable timers [31] [32]. In contrast, evidence in
480 favour of a circadian/ tidal timer based on a single "plastic" clock influenced by the prevailing
481 dominant temporal cue, as proposed by Enright [4], received support from studies on the coastal
482 oyster *Crassostrea gigas*, which shows ~12-hour and/ or ~24-hour expression of circadian
483 gene homologues [33]. Importantly, these models are not mutually exclusive. Given the
484 evolutionary distance between molluscs and arthropods, it is entirely possible that tidal timing
485 machinery has evolved independently. In fact, a parsimonious explanation of the evolution of
486 clock cells with different periodicities would be that pre-existing circadian clock components
487 were co-opted to track relevant tidal cues. The cells we identified invariably co-expressed the
488 rudiments of a circadian TTFL but with either daily or tidal frequencies in the same brain and
489 it is possible that they evolved in parallel, diverging under the influence of photic and
490 mechanosenory (tidal) inputs, respectively.
491
492 Kwiatkowski et al. [10] asked how *P. hawaiensis* 'chooses' between 12.4-hour and 24-hour
493 environmental rhythms during entrainment. Our observation that distinct circadian and
494 circatidal cells groups entrain independently to light and mechanical stimuli, respectively,
495 provides a solution to this problem. Similarly, the authors also questioned whether neurons
496 coordinating rhythmic behaviour in *P. hawaiensis* have two different timers with differential
497 sensitivity to light and tides, or two cell types exist. Whilst we cannot currently exclude the
498 former, our data align better with the latter. This does not preclude interactions of the two
499 systems, however, and the genetic and behavioural malleability of *P. hawaiensis* should
500 enable their decipherment. Thus, our findings now enable the examination of input and output
501 pathways of tidal and daily cues at cellular resolution, progressing towards defining the nature
502 and connectivity of circadian and circatidal neural clockworks.
503
504
505

Acknowledgements

We thank Sebastian Cachero and Gregory Jefferis for their guidance on reference brain generation and their algorithms, as well as Aziz Aboobaker for gifting us a starting culture of Chicago-F *P. hawaiensis*. We also thank Mechanical and Electronics Workshops and Light Microscopy Facility at the MRC Laboratory of Molecular Biology for technical support. This work was supported by core funding from Medical Research Council (MRC), as part of United Kingdom Research and Innovation (also known as UK Research and Innovation) (MRC File Reference No. MC_U105170643) to M.H.H. C.Y.S. was supported by a Boehringer Ingelheim Fonds PhD fellowship (2023-2025). For the purpose of open access, the author has applied a CC BY public copyright licence to any Author Accepted Manuscript version arising.

Author contributions.

All Authors contributed to the direction of the project and the writing of the manuscript.
AO and CYS designed and conducted behavioural and neuroanatomical experiments and analysed data.
DCW conducted neuroanatomical experiments and analysed data.
MHH arranged funding.

530 **Methods**

531

532 ***Eurydice pulchra* collection and phenotypic analysis**

533 Animals were collected from Llanddona beach, Anglesey, UK, during spring high tides during
534 the months May to October [12]. Swimming behaviour of both females and males was recorded
535 in DAM10 and LAM10 activity monitors (Trikinetics Inc., USA) ambient lighting (LD) at 16°C
536 with animals housed individually in 3 ml (Ø: 11 mm) plastic vials containing 33 psu artificial
537 seawater (ASW, Reef Salt, Tropical Marine Centre, Germany) and ~5 mm depth of fine sand.
538 Infrared beam interruptions were recorded using the DAMSystem3 software (TriKinetics Inc.,
539 USA) in one-minute bins. The first peak in tidal swimming activity was omitted from analysis
540 and behavioural rhythmicity was assessed over the subsequent six tidal cycles using chi-
541 squared periodogram analysis in Rethomics R package [34].

542

543 ***Parhyale hawaiensis* husbandry and behavioural analysis**

544 Chicago F strain *P. hawaiensis* were maintained in 6.5 L polypropylene containers (h: 125 mm,
545 w: 260 mm, d: 260 mm) containing 30 –35 psu ASW and a layer of crushed coral substrate
546 (grain size 2 –20 mm). Animals were reared at 25°C under 12h light:dark (LD) cycles. The
547 containers were covered with clear Perspex lids to prevent evaporation and aerated using
548 aquarium air pumps and air stones. Animals were fed carrots, goldfish flakes (Tetra GmbH,
549 Germany), algae wafers (Kyorin Food Ind. Ltd., Japan), freeze-dried brine shrimps, and/or
550 freeze-dried Tubifex (Interpret, UK) once weekly. Full water changes were performed
551 fortnightly. For locomotor activity monitoring, female and male animals were placed
552 individually into 23 mL polystyrene vials (h: 75 mm, Ø: 23.5 mm) containing a layer (~2 mm)
553 of crushed coral substrate (grain size 2 –5 mm) and approximately 6 cm of 30 psu ASW at
554 25°C. Tubes were loosely covered with parafilm and loaded into two-tier activity monitors
555 modified from the LAM25 Locomotor Activity Monitors (TriKinetics Inc., USA; Supplementary
556 Figure 2a) configured to record swimming and/or roaming activity. Infrared beam interruptions
557 were recorded using the DAMSystem3 software (TriKinetics Inc., USA).

558

559 Beam interruptions were collected into 30-minute bins and normalised within each animal by
560 dividing the count in each bin by the average count across all bins for that animal.
561 Autocorrelation periodogram was used to determine whether animals were rhythmic, with a
562 significance threshold of $\alpha = 0.05$ [35]. The period and the power of rhythmicity were determined
563 using Lomb-Scargle periodogram analysis [36] of binned and normalised data at the significance
564 level $\alpha = 0.05$. For circatidal experiments, the first subjective high tide after loading was omitted
565 from analysis and behavioural rhythmicity was assessed over the subsequent six tidal cycles.

566 For circadian entrainment experiments, animals loaded into the monitor were subjected to at
567 least four 12:12 LD (ZT0/lights-on at 0600 local time) cycles before being allowed to free run
568 in DD. For tidal entrainment, animals were kept under LD as above but mechanically agitated
569 on an orbital shaker set at 50 –60 rpm for 2 hours at 12.4-hour intervals. For behavioural
570 monitoring, animals were taken from entrainment regimes during the agitation phase and
571 placed in the activity monitor as described above to free-run without agitation in DD.
572
573 **Brain collection and processing for immunohistochemistry and HCR-FISH**
574 Animals were anaesthetised in ice-cold seawater, and their brains dissected using sharpened
575 watch-maker's forceps in ice-chilled physiological saline [37] (*E. pulchra)* or 0.22 µm filter-
576 sterilised ASW (30 -35 psu, FASW; *P. hawaiensis*). Tissues were immediately fixed in 4%
577 paraformaldehyde (made in PBS for *E. pulchra* and FASW for *P. hawaiensis*) for 1 hour at
578 room temperature, dehydrated serially in 33%, 66%, 100% methanol in PBST (PBS
579 supplemented with 0.1% Tween20), and stored in 100% methanol at -20°C for at least 16 h
580 before hybridisation or immunohistochemistry. Immediately prior to use, brains were
581 rehydrated in 66/33% methanol and washed/equilibrated in PBST (3x10 min). Neuropils were
582 immunolabelled using anti-SYNORF1 antibody (3C11, Developmental Studies Hybridoma
583 Bank (DSHB)). For *E. pulchra* and *P. hawaiensis* brains immunohistochemistry followed [38], [39]
584 and (Supplementary Methods). HCR™RNA-FISH probes were designed and synthesised by
585 Molecular Instruments Inc, USA against user-supplied sequences (Supplementary Table 2).
586 HCR-FISH followed the manufacturer's protocol [40] with some minor alterations following [41]
587 (Supplementary Methods). To co-localise putative clock cells relative to major neuropils,
588 immunostaining with anti-SYNORF1 antibody was followed by HCR-FISH (Supplementary
589 Methods). Reference brains were generated from confocal image stacks of brains in which
590 neuropils were labelled with anti-SYNORF1 (Supplementary Methods).
591
592 **Time-course sampling design.**
593 To investigate clock gene expression pattern in the brain of *E. pulchra*, animals were collected
594 from Llanddona beach, Anglesey, UK, during spring high tides in October 2024 and loaded
595 into activity monitors. Prior to sampling, animals were maintained under 18 h: 6 h L:D cycle
596 for 24 hours. Animals showing peaks of swimming activity during the two subjective high
597 waters during this period were sampled every two hours, beginning at ZT7 (Supplementary
598 Figure 17a). To investigate daily clock gene expression pattern in the brain of *P. hawaiensis*,
599 animals were loaded into activity monitors and subjected to 12 h: 12 h LD cycle for 6 days as
600 described. Individuals showing significant 24-h rhythmicity in locomotor activity (as described)
601 over this entrainment period up to the day before sampling were marked for sampling. On the

602 day of sampling, marked animals were sampled every 2 hours, beginning at ZT1 and ending
603 at ZT25, for a total of 13 timepoints (Supplementary Figure 17b).
604
605 To investigate circatidal clock gene expression pattern in the brain of tidally entrained *P.*
606 *hawaiensis*, animals which have been subjected to tidal entrainment were loaded into activity
607 monitors as described. Sampling occurred every 3 hours, beginning at CT0 on the day after
608 monitor loading and ending at CT24, for a total of 9 timepoints (Supplementary Figure 17c).
609 Individuals were only sampled if they showed peaks of locomotor activity during the subjective
610 high tides preceding their sampling timepoint.
611
612 Dissected brains were processed for digital HCR-FISH as described. HCR-FISH probes used
613 for time -course experiments are described in Supplementary Table 10.
614
615 **Whole brain digital HCR-FISH**
616 For quantification of diffraction-limited spots [40], signal amplification with 60 nM of each hairpin
617 was performed for 1 h, followed by staining with 1 µg/mL DAPI (as above). Brains were
618 mounted in Prolong Glass Antifade Mountant (ThermoFisher #P36980). *E. pulchra* brains
619 were mounted with the posterior surface apposed to the coverslip whilst *P. hawaiensis* brains
620 were mounted with the anterior surface apposed. To minimise signal loss with imaging depth,
621 brains were compressed to within 40 µm by mounting the coverslips containing brains onto
622 spacers made from double-sided adhesive tape (Radio Spares #770-3422). An Andor BC43
623 CF benchtop microscope equipped with a 60x/1.42NA Plan Apochromat oil immersion
624 objective was used to image each brain with an optical section interval of 0.3 µm.
625
626 To prepare images for segmentation of cell groups enriched for expression of *per*, *cry2*, and/
627 or *Clk/ tim*, 2D maximum filters were applied to each HCR-FISH channel, followed by
628 summation of the filtered images across channels and 2D gaussian filtering. The resulting
629 images, together with the corresponding raw DAPI image as the auxiliary channel, were
630 subjected to segmentation using Cellpose [42] and a custom model (available at GitHub) trained
631 via the human-in-the-loop functionality of the Cellpose 2.0 graphical user interface [43]. The
632 resulting masks were manually curated as required in napari [44] and assigned to distinct cell
633 groups. For spot detection, images were deconvolved using ClearView™ Deconvolution with
634 10 iterations after being acquired in the Fusion software. RNA foci were then detected in
635 deconvolved images and assigned to cell groups using the RS-FISH ImageJ plugin [45].
636
637 **Statistical analyses**

Shapiro-Wilk test used to determine normal distribution of data, and Levene's test used to determine if the variances of all groups are equal. An overall time effect was tested by ANOVA for normally distributed data and by Kruskal-Wallis for non-normal datasets. Where this yielded a statistically significant effect, rhythmicity in the data was analysed further by JTK CYCLE [25] and RAIN [26] at 12-hour or 24-hour periods. JTK-cycle p-values are adjusted using Bonferroni's method, and RAIN p-values are adjusted using the adaptive Benjamini-Hochberg (default) method. Gene expression was considered rhythmic when ANOVA was significant, and both JTK CYCLE and RAIN were significant for the same period (12 hours or 24 hours).

References

1. Dunlap JC, Loros JJ, Decoursey PJ. *Chronobiology: biological timekeeping*. Sinauer (2004).

2. Naylor E. *Chronobiology of marine organisms*. Cambridge University Press (2010).

3. Hafker NS, Andreatta G, Manzotti A, Falciatore A, Raible F, Tessmar-Raible K. Rhythms and Clocks in Marine Organisms. *Ann Rev Mar Sci* **15**, 509-538 (2023).

4. Enright JT. Plasticity in an isopod's clockworks: shaking shapes form and affects phase and frequency. *Journal of Comparative Physiology A* **107**, 13-37 (1976).

5. Palmer JD. Dueling hypotheses: circatidal versus circalunidian battle basics--second engagement. *Chronobiol Int* **14**, 431-433 (1997).

6. Naylor E. Crab clockwork: the case for interactive circatidal and circadian oscillators controlling rhythmic locomotor activity of *Carcinus maenas*. *Chronobiol Int* **13**, 153-161 (1996).

7. Reppert SM, Weaver DR. Comparing Clockworks: Mouse versus Fly. *Journal of Biological Rhythms* **15**, 357-364 (2000).

8. Hardin PE, Panda S. Circadian timekeeping and output mechanisms in animals. *Curr Opin Neurobiol* **23**, 724-731 (2013).

9. Andreani TS, Itoh TQ, Yildirim E, Hwangbo DS, Allada R. Genetics of Circadian Rhythms. *Sleep Med Clin* **10**, 413-421 (2015).

10. Kwiatkowski ER, Rosenthal JJC, Emery P. Crosstalk between the circatidal and circadian clocks mediates behavioral adaptation to tidal patterns. *Curr Biol* **34**, 5239-5251 e5232 (2024).

11. Hastings MH. The Entraining Effect of Turbulence on the Circa-Tidal Activity Rhythm and Its Semi-Lunar Modulation in *Eurydice pulchra*. *J Mar Biol Assoc Uk* **61**, 151-160 (1981).

12. Zhang L*, et al.* Dissociation of circadian and circatidal timekeeping in the marine crustacean *Eurydice pulchra*. *Curr Biol* **23**, 1863-1873 (2013).

13. Kwiatkowski ER, Schnytzer Y, Rosenthal JJC, Emery P. Behavioral circatidal rhythms require Bmal1 in *Parhyale hawaiensis*. *Curr Biol* **33**, 1867-1882 e1865 (2023).

14. O'Neill JS*, et al.* Metabolic molecular markers of the tidal clock in the marine crustacean *Eurydice pulchra*. *Curr Biol* **25**, R326-327 (2015).

15. Hunt BJ, Mallon EB, Rosato E. In silico Identification of a Molecular Circadian System With Novel Features in the Crustacean Model Organism *Parhyale hawaiensis*. *Front Physiol* **10**, 1325 (2019).

16. Zhang L, Green EW, Webster SG, Hastings MH, Wilcockson DC, Kyriacou CP. Correction: The circadian clock gene bmal1 is necessary for co-ordinated circatidal rhythms in the marine isopod *Eurydice pulchra* (Leach). *PLoS Genet* **19**, e1011047 (2023).

17. Kenning M, Harzsch S. Brain anatomy of the marine isopod *Saduria entomon* Linnaeus, 1758 (Valvifera, Isopoda) with special emphasis on the olfactory pathway. *Front Neuroanat* **7**, 32 (2013).

18. Wittfoth C, Harzsch S, Wolff C, Sombke A. The "amphi"-brains of amphipods: new insights from the neuroanatomy of *Parhyale hawaiensis* (Dana, 1853). *Front Zool* **16**, 30 (2019).

19. Ramos AP, Gustafsson O, Labert N, Salecker I, Nilsson DE, Averof M. Analysis of the genetically tractable crustacean *Parhyale hawaiensis* reveals the organisation of a sensory system for low-resolution vision. *BMC Biol* **17**, 67 (2019).

20. Blau J, Young MW. Cycling vrille expression is required for a functional Drosophila clock. *Cell* **99**, 661-671 (1999).

21. Cyran SA*, et al.* vrille, Pdp1, and dClock form a second feedback loop in the Drosophila circadian clock. *Cell* **112**, 329-341 (2003).

22. Ito K*, et al.* A systematic nomenclature for the insect brain. *Neuron* **81**, 755-765 (2014).

23. Nagy D*, et al.* Peptidergic signaling from clock neurons regulates reproductive dormancy in *Drosophila melanogaster*. *PLoS Genet* **15**, e1008158 (2019).

24. Wilcockson DC, Zhang L, Hastings MH, Kyriacou CP, Webster SG. A novel form of pigment-dispersing hormone in the central nervous system of the intertidal marine isopod, *Eurydice pulchra* (leach). *J Comp Neurol* **519**, 562-575 (2011).

25. Hughes ME, Hogenesch JB, Kornacker K. JTK_CYCLE: An Efficient Nonparametric Algorithm for Detecting Rhythmic Components in Genome-Scale Data Sets. *Journal of Biological Rhythms* **25**, 372-380 (2010).

26. Thaben PF, Westermark PO. Detecting Rhythms in Time Series with RAIN. *Journal of Biological Rhythms* **29**, 391-400 (2014).

27. Zheng Y*, et al.* Neural function of Bmal1: an overview. *Cell Biosci* **13**, 1 (2023).

28. Beer K, Helfrich-Forster C. Model and Non-model Insects in Chronobiology. *Front Behav Neurosci* **14**, 601676 (2020).

29. Colizzi FS, Veenstra JA, Rezende GL, Helfrich-Forster C, Martinez-Torres D. Pigment-dispersing factor is present in circadian clock neurons of pea aphids and may mediate photoperiodic signalling to insulin-producing cells. *Open Biol* **13**, 230090 (2023).

30. Strauss J, Dircksen H. Circadian clocks in crustaceans: identified neuronal and cellular systems. *Front Biosci (Landmark Ed)* **15**, 1040-1074 (2010).

31. Takekata H, Numata H, Shiga S. The circatidal rhythm persists without the optic lobe in the mangrove cricket *Apteronemobius asahinai*. *J Biol Rhythms* **29**, 28-37 (2014).

32. Takekata H, Numata H, Shiga S, Goto SG. Silencing the circadian clock gene Clock using RNAi reveals dissociation of the circatidal clock from the circadian clock in the mangrove cricket. *J Insect Physiol* **68**, 16-22 (2014).

33. Tran D, Perrigault M, Ciret P, Payton L. Bivalve mollusc circadian clock genes can run at tidal frequency. *Proc Biol Sci* **287**, 20192440 (2020).

34. Geissmann Q, Garcia Rodriguez L, Beckwith EJ, Gilestro GF. Rethomics: An R framework to analyse high-throughput behavioural data. *PLOS ONE* **14**, e0209331 (2019).

35. Levine JD, Funes P, Dowse HB, Hall JC. Signal analysis of behavioral and molecular cycles. *BMC Neuroscience* **3**, 1 (2002).

36. Ruf T. The Lomb-Scargle Periodogram in Biological Rhythm Research: Analysis of Incomplete and Unequally Spaced Time-Series. *Biological Rhythm Research* **30**, 178-201 (1999).

37. Saver MA, Wilkens JL, Syed NI. In Situ and In Vitro Identification and Characterization of Cardiac Ganglion Neurons in the Crab, *Carcinus maenas*. *Journal of Neurophysiology* **81**, 2964-2976 (1999).

38. Ostrovsky A, Cachero S, Jefferis G. Clonal analysis of olfaction in Drosophila: immunochemistry and imaging of fly brains. *Cold Spring Harb Protoc* **2013**, 342-346 (2013).

39. Meissner GW*, et al.* DPX Mounting of Drosophila CNS (2018).

40. Choi HMT*, et al.* Third-generation *in situ* hybridization chain reaction: multiplexed, quantitative, sensitive, versatile, robust. *Development* **145**, dev165753 (2018).

41. Bruce HS, Jerz G., Kelly, S.R., McCarthy, J., Pomerantz, A., Senevirathne, G., Sherrard, A., Sun, D.A., Wolff, C., Patel, N.H. Hybridization Chain Reaction (HCR) In Situ Protocol V.1 *protocolsio*, (2021).

42. Stringer C, Wang T, Michaelos M, Pachitariu M. Cellpose: a generalist algorithm for cellular segmentation. *Nat Methods* **18**, 100-106 (2021).

43. Pachitariu M, Stringer C. Cellpose 2.0: how to train your own model. *Nature Methods* **19**, 1634-1641 (2022).

44. Sofroniew N*, et al.* napari: a multi-dimensional image viewer for Python (v0.5.0).). Zenodo (2024).

45. Bahry E*, et al.* RS-FISH: precise, interactive, fast, and scalable FISH spot detection. *Nature Methods* **19**, 1563-1567 (2022).

812 **Main Figures and Legends.**

813

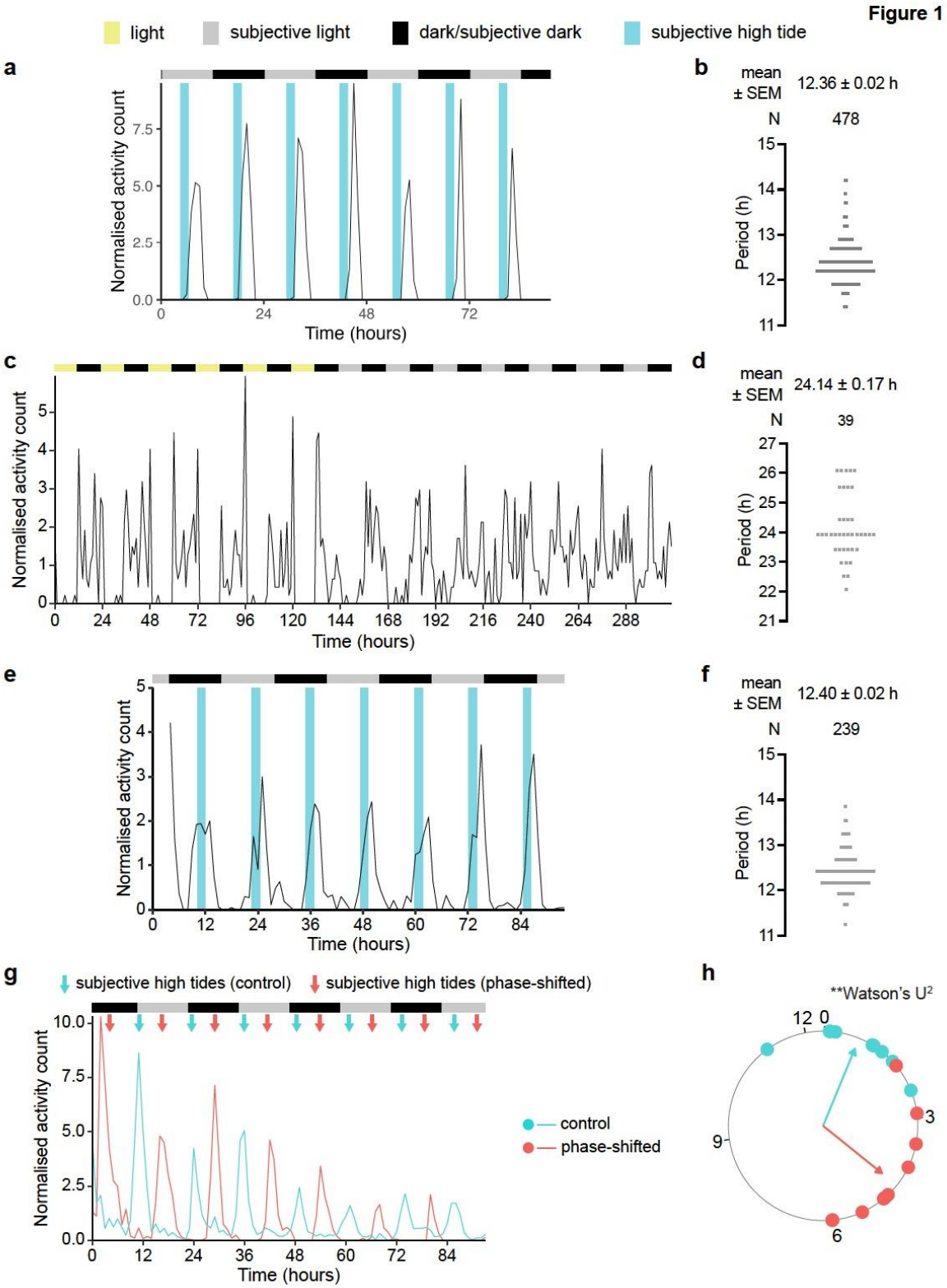

814

815 **Figure 1. Circatidal and circadian locomotor rhythms in *E. pulchra* and *P. hawaiensis*.**

816 **a** Beach-caught *E. pulchra* show robust circatidal swimming activity under free-running
817 conditions. Plot shows normalised swimming activity for an individual *E. pulchra* under DD.
818 Blue shadings indicate subjective high tides. See also **Supplementary Figure 1**.
819 **b** Individual periods of beach-caught *E. pulchra* swimming activity under DD. Mean (±S.E.M.)
820 is 12.36 ±0.02 h.
821 **c** Activity recording of individual laboratory-cultured *P. hawaiensis*, which had never been
822 subjected to tidal entrainment, showing more activity during the night when maintained under
823 12 h:12 h L:D cycle (yellow/black bars). When allowed to free-run under DD (grey/ black bars),
824 individual shows robust circadian locomotor activity with peaks in subjective night. See also
825 **Supplementary Figure 2**.
826 **d** Individual periods of circadian locomotor activity under DD of LD-entrained *P. hawaiensis*.
827 Mean (±S.E.M.) is 24.14 ±0.17 h.
828 **e** Activity recording of individual laboratory-cultured *P. hawaiensis* free-running under DD
829 (grey/ black bars), following entrainment to 2 h of agitation every 12.4 h. Blue bars indicate
830 time of subjective tidal agitation. See also **Supplementary Figure 3**.
831 **f** Individual periods of circatidal locomotor activity under DD of tidally entrained *P. hawaiensis*
832 Mean (±SEM) is 12.40 ±0.02 h.
833 **g** Activity recording of two individual laboratory-cultured *P. hawaiensis* free-running under DD
834 (black/ grey bars) following prior tidal entrainment at a period of 12.4 h (cyan, control) or 12.9
835 h (red, phase-shifted) over 6 days. Arrows indicate times of subjective tidal agitation. See
836 also **Supplementary Figure 3**.
837 **h** Circular plot on a 12.4 h timescale showing the phases of circatidal swimming of
838 individual animals from the control (cyan) and phase-shifted (red) tidal entrainment groups.
839 Arrowed lines indicate mean phase within each group ($\phi_{control}$ =0.77 ±0.33 h, $\phi_{phase\text{-}shifted}$ =4.44
840 ±0.42 h (mean ±SEM), Watson's U^2 test: U^2 =0.36, p <0.01, $N_{control}$ =9, $N_{phase\text{-}shifted}$ =10), and
841 length of arrowed lines indicates mean resultant length of the vector at each mean ($\rho_{control}$
842 =0.88, $\rho_{phase\text{-}shifted}$ =0.80). See also **Supplementary Figure 3**.
843

844

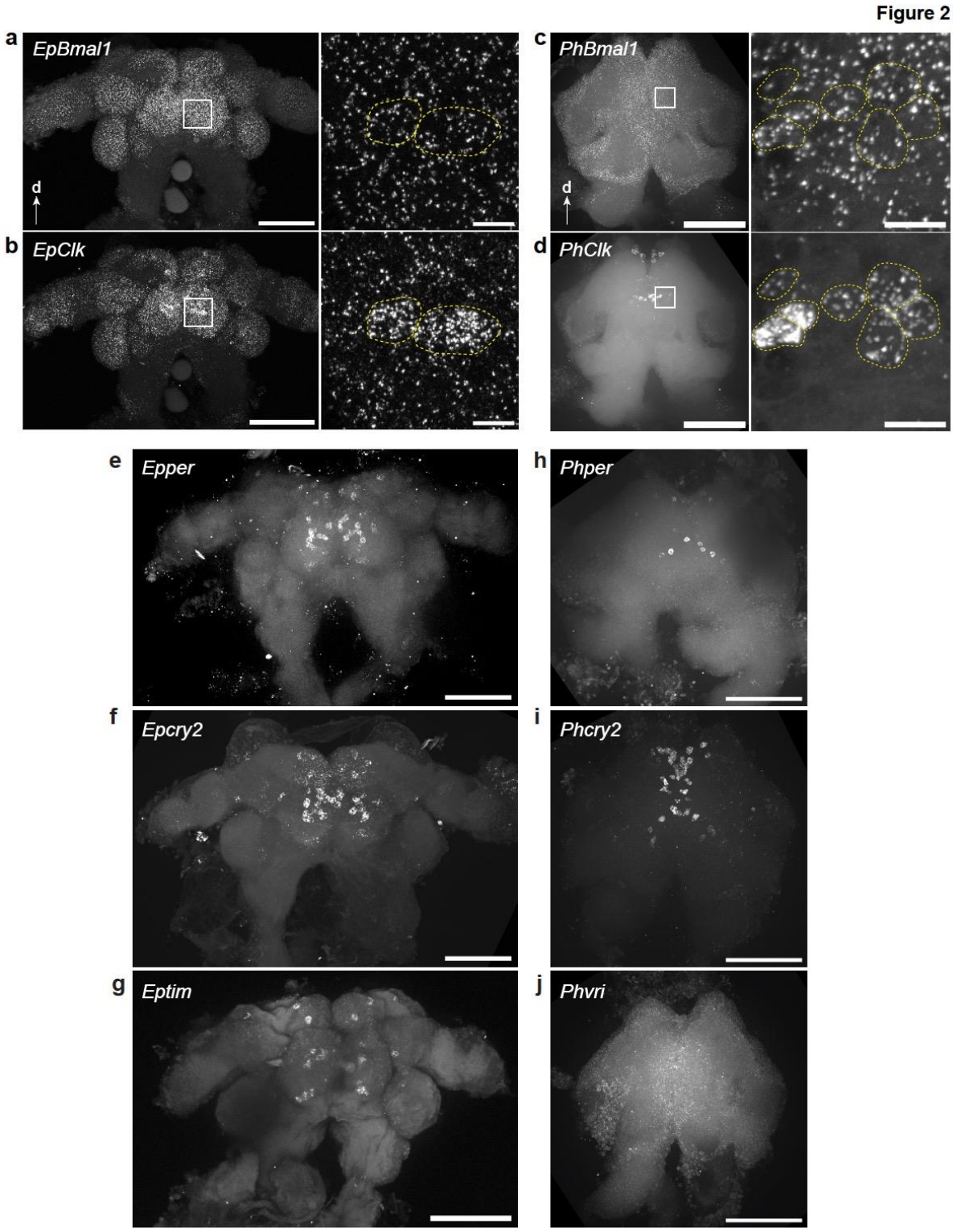

845

846 **Figure 2. Expression of circadian clock positive and negative regulators across the**
847 **brains of *E. pulchra* and *P. hawaiensis*.**

848 **a** Left panel: maximum intensity Z-projection of image stack of an entire *E. pulchra* brain
849 (posterior apposing coverslip) probed for circadian factor *EpBmal1* using HCR-FISH. Right

panel: maximum intensity Z-projection of two-cell-thick image stack (16 μm) from the boxed region of the brain in the left panel.

b As in **a**, probed for circadian factor, *EpClk*.

c Left panel: maximum intensity Z-projection of image stacks of a *P. hawaiensis* brain (anterior apposing coverslip) probed for circadian factor *PhBmal1*. Right panel: maximum intensity Z-projection of two-cell-thick image stacks (24 μm) from the boxed region of the brain in the left panels.

d As in **c**, probed for circadian factor, *PhClk*.

e, f, g Maximum intensity Z-projections of image stacks of *E. pulchra* brains (posterior apposing coverslip) probed for circadian clock repressors, *Epcry2, Epper* and *Eptim*, using HCR-FISH.

h, i, j Maximum intensity Z-projections of image stacks of *P. hawaiensis* brains (anterior apposing coverslip) probed for circadian clock repressors, *Phcry2* and *Phper* and secondary regulator *Phvri*. Scale bars: 100 μm.

Arrows indicate dorsal orientation. Yellow dotted outlines in **a- d** indicate cells in which *Clk* expression is enriched. Scale bars: 100 μm (**a-d:** left panels**, e-j**) and 10 μm (**a-d:** right panels).

868

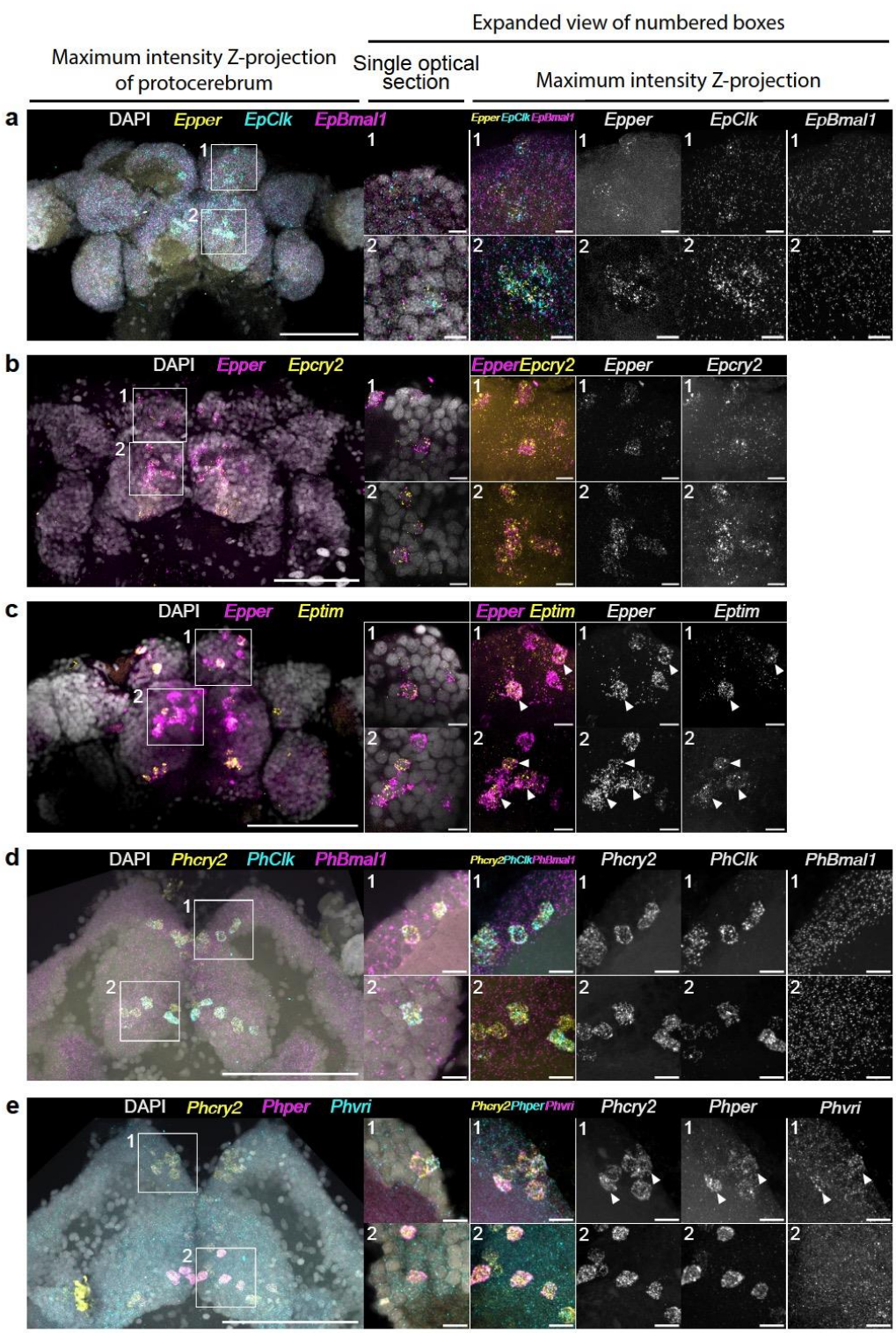

869

870 **Figure 3. Cellular co-expression of circadian clock genes in the brains of *E. pulchra***
871 **and *P. hawaiensis*.**

872 **a** Representative maximum intensity Z projections and single optical sections of *E. pulchra*
873 brain probed for *Epper*, *EpClk* and *EpBmal1* using HCR-FISH. Left: merged low-power (25x)

view of protocerebrum of *E. pulchra*, centre: merged high-power (40x) single optical sections in boxes labelled 1 and 2, right: single channel high-power maximum intensity Z projections. *EpBmal1* is widely and uniformly expressed in both putative clock cells and other cells across the brain, but it is not enriched in cells enriched for *EpClk*, whereas *Epper* is enriched in *EpClk*-enriched cells.

b As in **a** for *Epper* and *Epcry2*, expression of which is co-enriched in putative clock cells but not in other cells in the brain of *E. pulchra*.

c As in **a** for *Epper* and *Eptim*, of *Epper*-enriched cells (arrowheads) in *E. pulchra*.

d As in **a** but for *P. hawaiensis* brain probed for *PhBmal1*, *PhClk* and *Phcry2* using HCR-FISH. *PhBmal1* is widely and uniformly expressed in both putative clock cells and other cells across the brain, but it is not enriched in cells enriched for *PhClk*, whereas *Phcry2* is enriched in *PhClk*-enriched cells.

e As in **a** but for *P. hawaiensis* brain labelled for *Phcry2*, *Phper* and *Phvri*. *Phcry2* and *Phper* are co-enriched in putative clock cells, but not other cells in the brain, whilst *Phvri* expression is more widespread, with slight enrichment in some clock cells (arrowheads).

Scale bars: 100 μm (left-most panels), 10 μm (other panels).

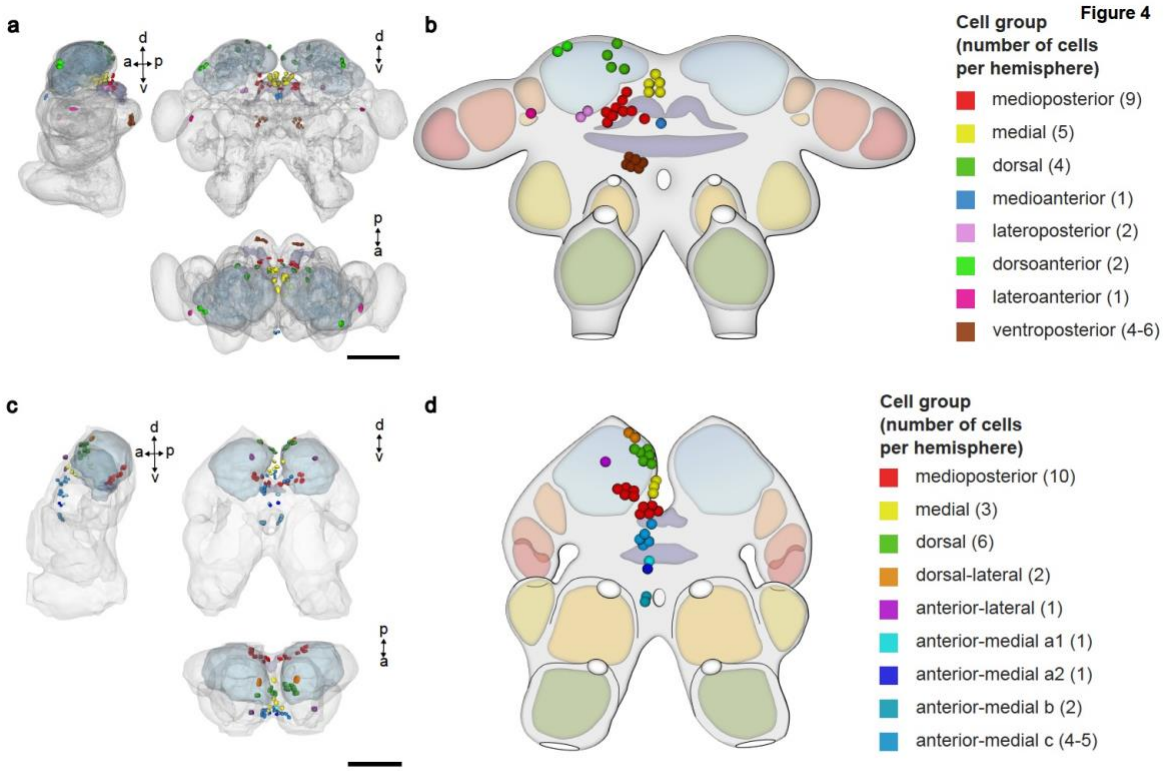

Figure 4. Distribution of cell clusters enriched for negative regulators *per* and *cry2* across the brains of *E. pulchra* and *P. hawaiensis*.

a Lateral, frontal and dorsal views of the *E. pulchra* reference brain model (from **Supplementary Figure 5a**) on to which somata enriched for expression of *Epper* and *Epcry2* are registered and segmented. Neuropils referred to in the main text to signpost putative clock cells are made translucent.

b Diagrammatic representation of the *E. pulchra* brain summarising the locations of cells co-enriched for *Epper* and *Epcry2*, based on the 3D reconstruction in **a**.

c Lateral, frontal and dorsal views of the *P. hawaiensis* reference brain model (from **Supplementary Figure 5c**) on to which somata enriched for expression of *Phper* and *Phcry2* are registered and segmented. Neuropils referred to in the main text to signpost putative clock cells are made translucent.

d Diagrammatic representation of the *P. hawaiensis* brain summarising the locations of cells co-enriched for *Phper* and *Phcry2*, based on the 3D reconstruction in **c**.

Compass markers in **a** and **c** show anterior (a), posterior (p), dorsal (d) and ventral (v) directions. Discrete cell groups are colour coded (see key). Cell numbers within each group (per hemisphere) in parenthesis. Scale bars: 100 µm.

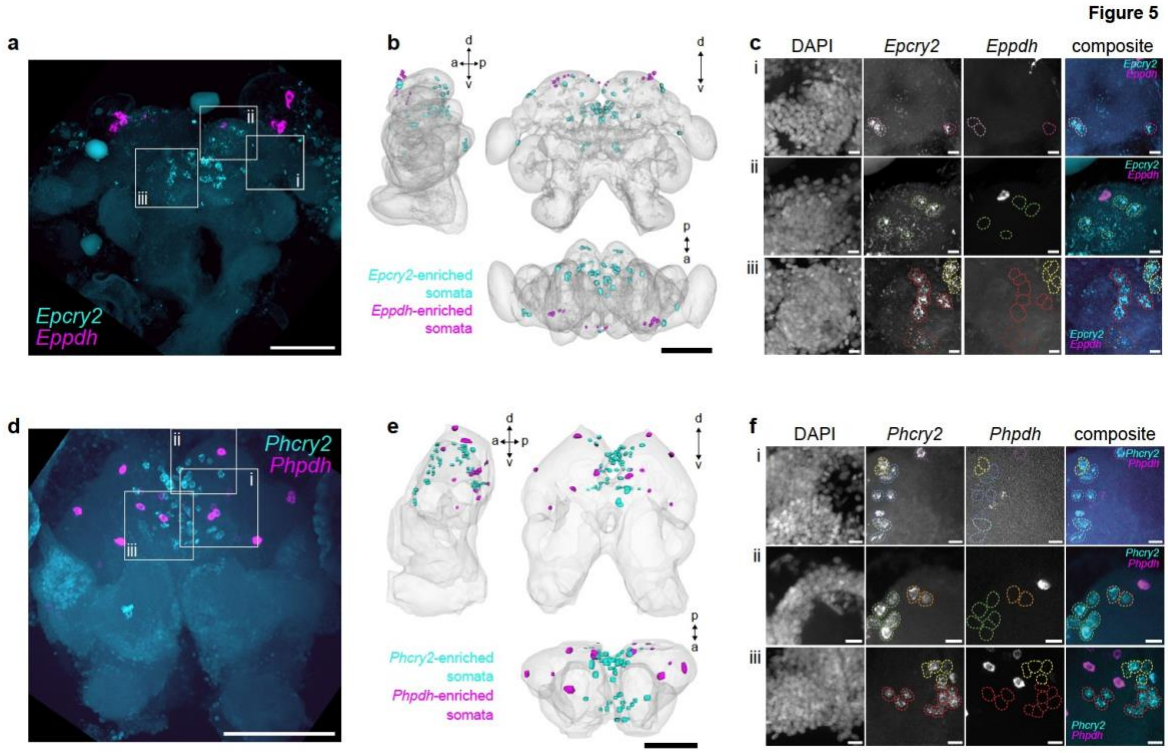

Figure 5. Relative distributions of cells expressing *pigment dispersing hormone* (*pdh*) and cells expressing *cry2* in the brains of *E. pulchra* or *P. hawaiensis*.

a Maximum intensity Z-projection of an *E. pulchra* brain probed for *Epcry2* (cyan) and *Eppdh* (magenta) using HCR-FISH.

b *E. pulchra* reference brain model onto which *Eppdh* and *Epcry2* channels were registered and somata enriched for either transcript was segmented.

c Maximum intensity Z-projections of the boxed regions in **a** (individual channels and composite), showing that none of the described putative clock cells express *Eppdh*.

d Maximum intensity projection of a *P. hawaiensis* brain probed for *Phcry2* and *Phpdh* using HCR-FISH.

e *P. hawaiensis* reference brain model onto which *Phpdh* and *Phcry2* channels were registered and somata enriched for either transcript was segmented.

f Maximum intensity Z-projections of the boxed regions in **d** (individual channels and composite), showing that none of the described putative clock cells express *Phpdh*.

Compass markers in **b** and **e** show anterior (a), posterior (p), dorsal (d) and ventral (v) directions. Dotted outlines in **c** and **f** are colour-coded according to the key in Figure 4 to indicate each cell group. Scale bars: 100 µm (**a, b, d, e**); 10 µm (**c, f**).

931

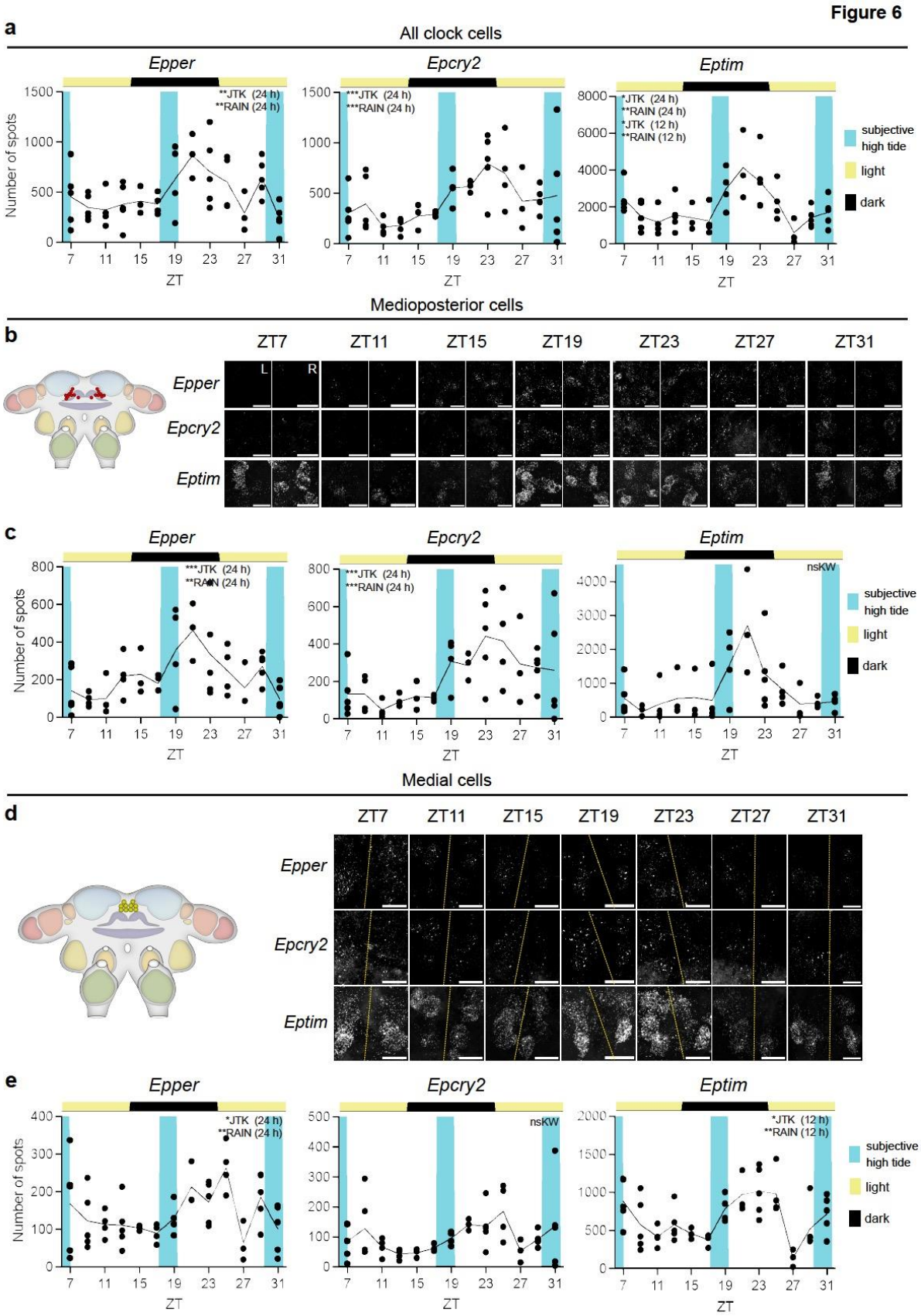
Figure 6
a
All clock cells
Epper
Epcry2
Eptim
Number of spots
**JTK (24 h)
**RAIN (24 h)
***JTK (24 h)
***RAIN (24 h)
*JTK (24 h)
**RAIN (24 h)
*JTK (12 h)
**RAIN (12 h)
ZT
subjective high tide
light
dark
Medioposterior cells
b
ZT7
ZT11
ZT15
ZT19
ZT23
ZT27
ZT31
L
R
c
nsKW
Medial cells
d
e

932

933

934 **Figure 6. Time course of expression of *per, tim and cry2* in cells of tidally rhythmic *E.***
935 ***pulchra* held on a LD cycle.**
936 **a** Profile of mean aggregate expression of *Epper, Epcry2* and *EpClk* across all cells plotted
937 across time in beach-caught animals held under LD. Each point is from one brain.
938 **b** Left: cartoon to show location of medioposterior cell group in the brain. Right: representative
939 maximum intensity Z-projections of *Epper*, *Epcry2* and *Eptim* expression in both hemispheres
940 (L: left, R: right) across ZT (individual HCR-FISH channels in rows). Scale bars: 20 µm.
941 **c** Profile of mean aggregate expression of *Eppler, Epcry2* and *EpClk* in medioposterior cell
942 group plotted across time in beach-caught animals held under LD. Each point is from one
943 brain.
944 **d, e** As **b** and **c** but for medial cells group. Yellow dashed lines: midlines. Scale bars: 10 µm.
945 Inset text in **c** and **e** indicate statistical tests (JTK-cycle and RAIN) performed to determine
946 rhythmicity following significant time effect by ANOVA or Kruskall-Wallis. p <0.001***, p
947 <0.01**, p ≤0.05*, p >0.05^{ns}. See also **Supplementary Figure 10** for other cell groups with
948 or without cycling clock gene expression. For statistics and data shown in this figure, refer to
949 **Supplementary Table 2**.
950

951

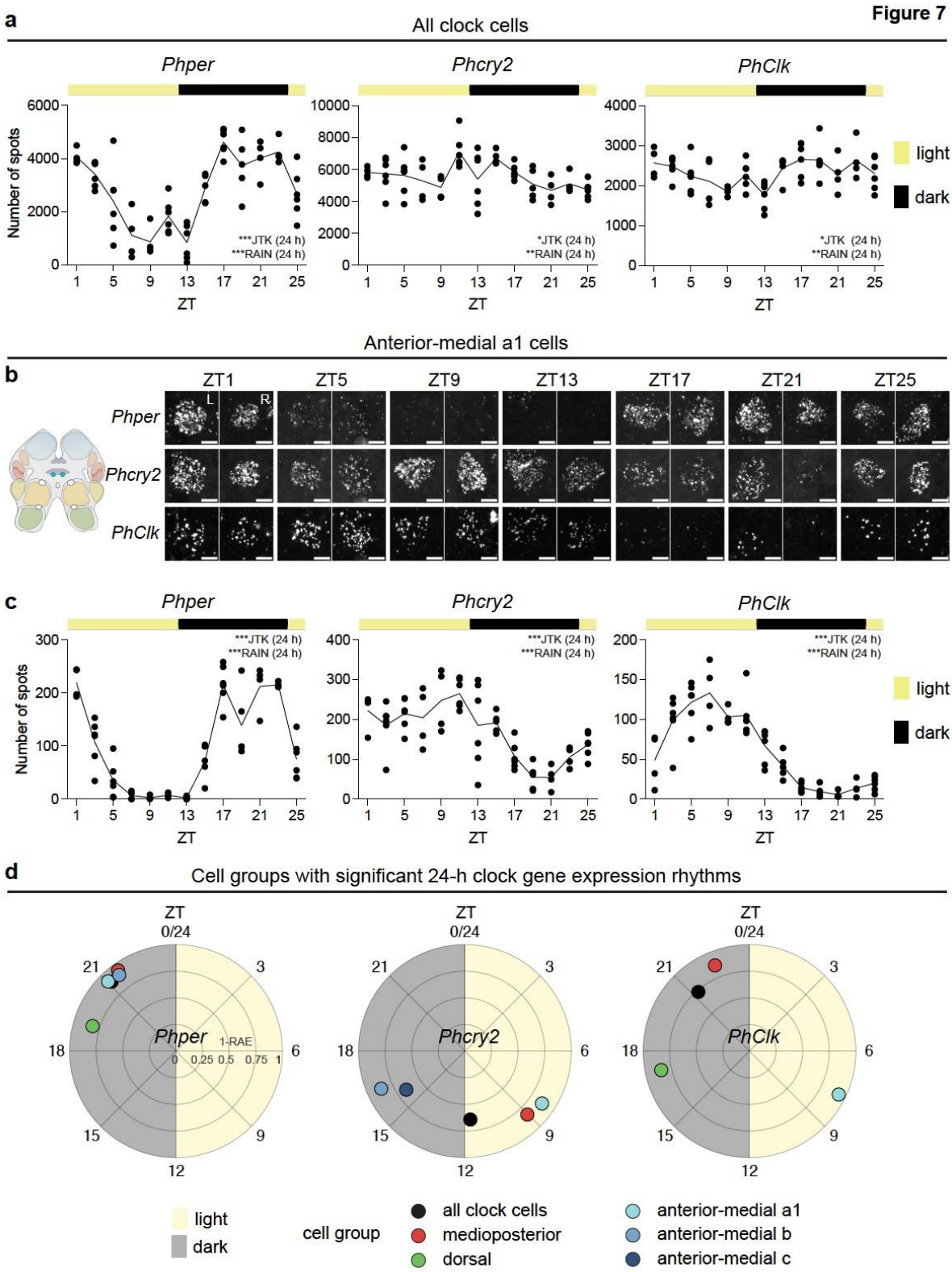
Figure 7
a
All clock cells
Phper
Phcry2
PhClk
Number of spots
ZT
***JTK (24 h)
***RAIN (24 h)
*JTK (24 h)
**RAIN (24 h)
light
dark
Anterior-medial a1 cells
b
ZT1
ZT5
ZT9
ZT13
ZT17
ZT21
ZT25
L
R
c
d
Cell groups with significant 24-h clock gene expression rhythms
ZT
0/24
1-RAE
cell group
all clock cells
medioposterior
dorsal
anterior-medial a1
anterior-medial b
anterior-medial c

952

953

954 **Figure 7. Time course of expression of *per, cry2* and *Clk* in cells of *P. hawaiensis***
955 **synchronised to the LD cycle.**
956 **a** Profile of mean aggregate expression of *Phper, Phcry2* and *PhClk* across all cells plotted
957 across time in animals entrained to, and sampled under, a 12 h:12 h LD cycle. Each point is
958 from one brain.
959 **b** Left: cartoon to show location of anterior-medial a1 cell group in the brain. Right:
960 representative maximum intensity Z-projections of *Phper*, *Phcry2* and *PhClk* expression in
961 both hemispheres (L: left, R: right) across ZT (individual HCR-FISH channels in rows). Scale
962 bars: 5 µm.
963 **c** Plots of mean transcript abundance, quantified as the number of FISH spots, across daily
964 time for *Phper* (left), *Phcry2* (middle) and *PhClk* (right).
965 **d** Circular plots of peak expression of *Phper*, *Phcry2* and *PhClk* across cell groups with
966 significant 24-h clock gene expression rhythms. RAE, relative amplitude error.
967 Inset text in **a** and **c** indicate statistical tests (JTK-cycle and RAIN) performed to determine 24-
968 hour rhythmicity. $p < 0.001$***, $p < 0.01$**, $p \leq 0.05$*, $p > 0.05^{ns}$. See also **Supplementary Figure**
969 **11** for other cell groups with 24-h cycling in clock gene expression, and **Supplementary**
970 **Figure 12** for cell groups with no evidence of 24-h clock gene expression rhythm. For statistics
971 and data shown in this figure, refer to **Supplementary Table 3**.
972

973

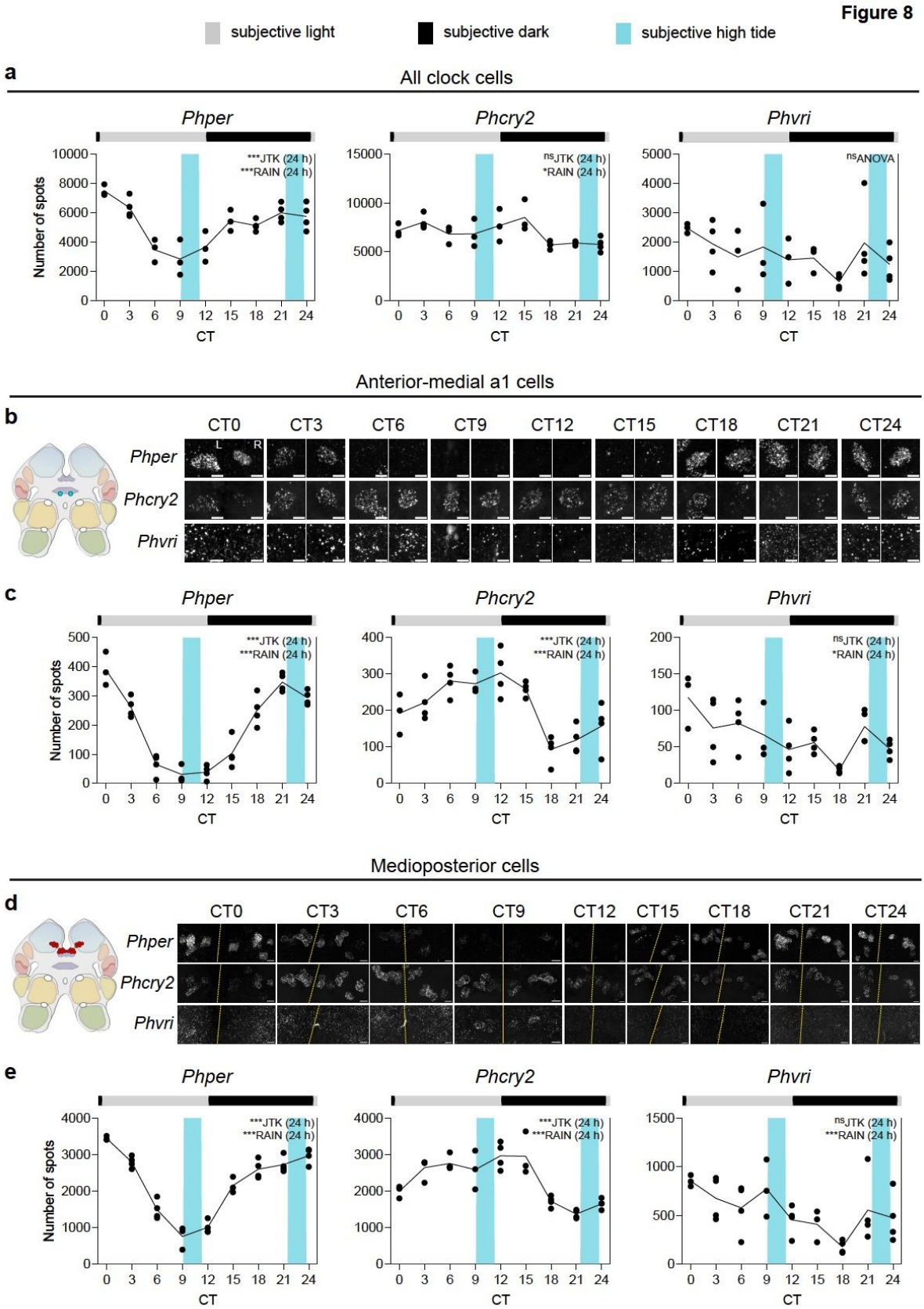
Figure 8
subjective light
subjective dark
subjective high tide
a
All clock cells
Phper
Phcry2
Phvri
Number of spots
CT
***JTK (24 h)
***RAIN (24 h)
nsJTK (24 h)
*RAIN (24 h)
nsANOVA
Anterior-medial a1 cells
b
CT0
CT3
CT6
CT9
CT12
CT15
CT18
CT21
CT24
L
R
c
Medioposterior cells
d
e

974

975

Figure 8. Free-running clock gene expression rhythms in tidally entrained *P. hawaiensis* (tidal phase θ).

a Profile of mean aggregate expression of *Phper, Phcry2* and *Phvri* across all putative clock cells plotted across time in tidally entrained animals sampled under DD. Each point is from one brain.

b Left: cartoon to show location of anterior-medial a1 cell group in the brain. Right: representative maximum intensity Z-projections of *Phper*, *Phcry2* and *Phvri* expression in both hemispheres (L: left, R: right) across CT (individual HCR-FISH channels in rows). Scale bars: 5 µm.

c Plots of mean transcript abundance, quantified as the number of FISH spots, across CT for *Phper* (left), *Phcry2* (middle) and *Phvri* (right). Each point is from one brain.

d, e As in **b** and **c** for medioposterior cells. Yellow dashed lines: midlines. Scale bars: 10 µm. Inset text in **a**, **c**, **d** and **e** indicate statistical tests (JTK-cycle and RAIN) performed to determine 24-h rhythmicity with the tested periods in parentheses. $p < 0.001^{***}$, $p < 0.01^{**}$, $p \leq 0.05^{*}$, $p > 0.05^{ns}$. See also **Supplementary Figures 14-15** for other cell groups with 24-hour cycling in clock gene expression for the experiments with tidal phase θ +1.2 h and θ –5.4 h, respectively. For statistics shown in this figure, refer to **Supplementary Table 4**.

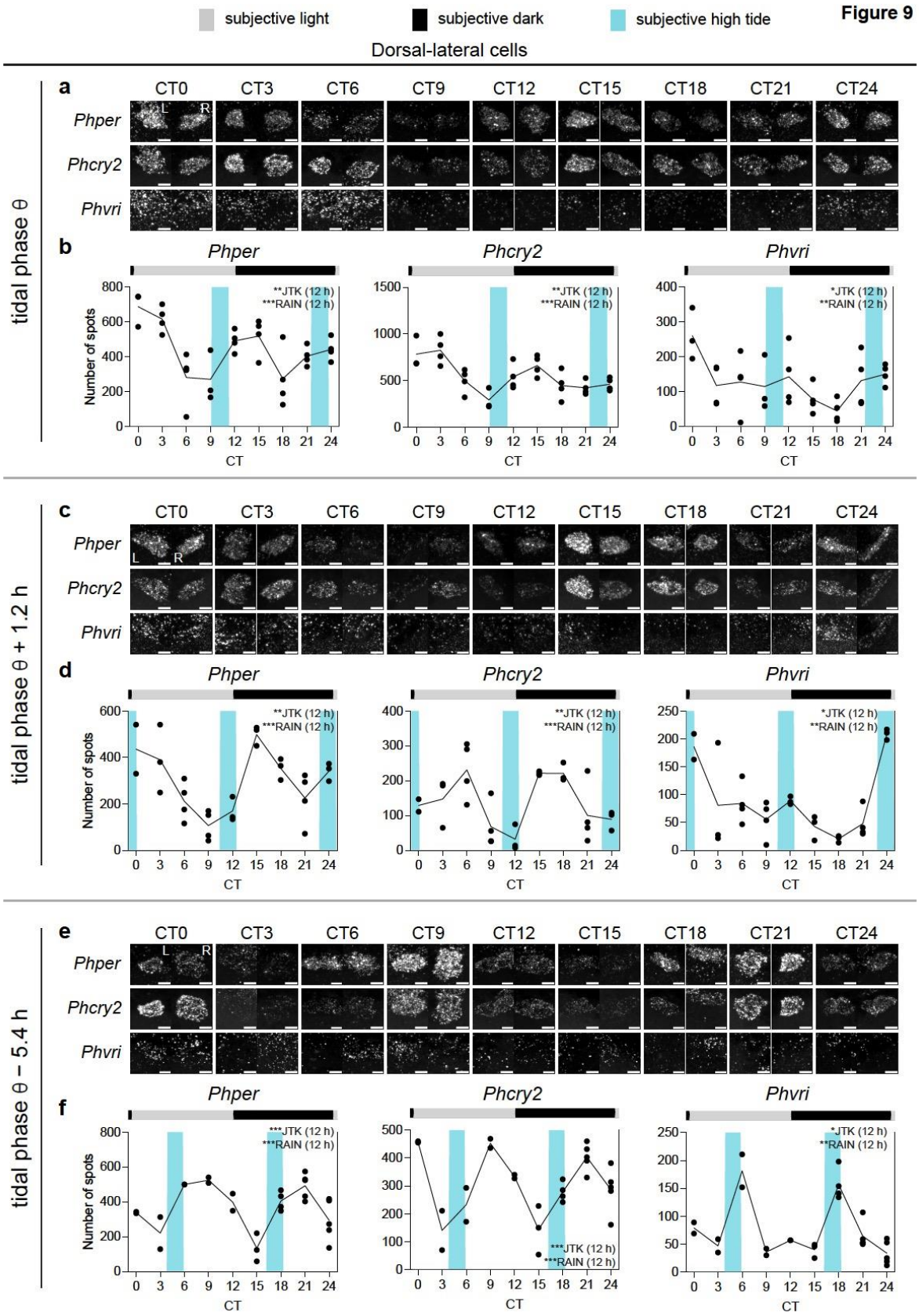
subjective light
subjective dark
subjective high tide
Figure 9
Dorsal-lateral cells
tidal phase θ
tidal phase θ + 1.2 h
tidal phase θ – 5.4 h
a
b
c
d
e
f
CT0
CT3
CT6
CT9
CT12
CT15
CT18
CT21
CT24
Phper
Phcry2
Phvri
L
R
Number of spots
CT
**JTK (12 h)
***RAIN (12 h)
*JTK (12 h)
**RAIN (12 h)
***JTK (12 h)
***RAIN (12 h)

997 **Figure 9**. **Circatidal rhythms of expression of *Phper*, *Phcry2* and *Phvri* in dorsal-lateral**
998 **cells in the brain of tidally entrained *P. hawaiensis*.**
999 **a** Representative maximum intensity Z-projections of *Phper*, *Phcry2* and *Phvri* expression in
1000 both hemispheres (L: left, R: right) across CT (individual HCR-FISH channels in rows). Scale
1001 bars: 5 µm.
1002 **b** Plots of mean transcript abundance, quantified as the number of FISH spots, across
1003 circadian time for *Phper* (left), *Phcry2* (middle) and *Phvri* (right) (blue shadings: subjective high
1004 water). Each point is from one brain.
1005 **c**, **d** As in **a** and **b** for animals entrained to a tidal cycle delayed, relative to the LD cycle, by
1006 1.2 hours.
1007 **e, f** As in **a** and **b** for animals entrained to a tidal cycle advanced, relative to the LD cycle, by
1008 5.4 hours.
1009 Inset text in **b**, **d** and **f** indicate statistical tests (JTK-cycle and RAIN) performed to determine
1010 rhythmicity, with the tested periods in parentheses. p <0.001***, p< 0.01**, p ≤0.05*, p >0.05^{ns}.
1011 For statistics and data of FISH time-course experiments on tidally entrained animals, refer to
1012 **Supplementary Table 4, 5 and 6** (tidal phases θ, +1.2 h and –5.4 h).
1013

1014

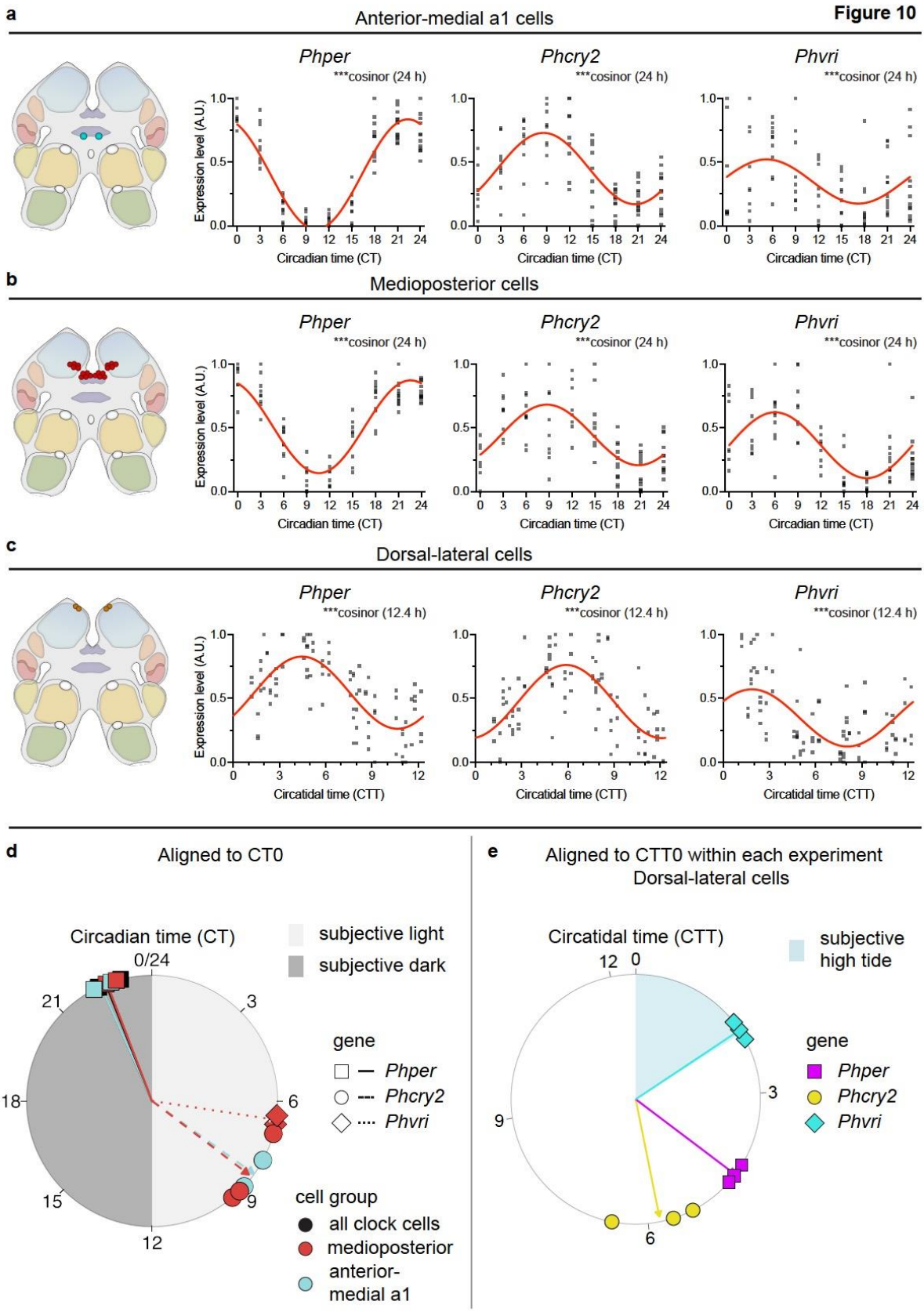

1015

1016

1017 **Figure 10. Summary analysis of circatidal and circadian rhythms of clock gene**
1018 **expression in dorsal-lateral, anterior-medial a1 and medioposterior cell groups of *P.***
1019 ***hawaiensis* exhibiting circatidal activity rhythms.**
1020 **a** Cartoon to show location of the anterior-medial a1 cell group in the brain (left) and scatter
1021 plot of aggregate expression of *Phper* (left), *Phcry2* (middle) and *Phvri* (right) across three
1022 independent experiments registered to subjective circadian time (Circadian Time, CT =0). Red
1023 lines indicate 24-h cosinor fits.
1024 **b** As in **a** for medioposterior cells.
1025 **c** Cartoon to show location of the dorsal-lateral cell group in the brain (left) and scatter plot of
1026 aggregate expression of *Phper* (left), *Phcry2* (middle) and *Phvri* (right) across three
1027 independent experiments registered to subjective high tide (Circatidal Time, CTT =0). Red
1028 lines indicate 12.4-h cosinor fits. Inset text in **a-c** indicate statistical significance of cosinor fit.
1029 p <0.001***.
1030 **d** Circular plot of circadian peak expression phase of *Phper*, *Phcry2* and *Phvri* in selected
1031 rhythmic cell groups of *P. hawaiensis* exhibiting circatidal activity rhythms. Each colour-shape
1032 combination represents data from across N =3 experiments (except for medioposterior-*Phvri*
1033 combination, of which only 2 out of 3 experiments reported significant 24-h rhythmicity).
1034 Arrowed lines indicate mean phase for each gene-cell group combination, and length of
1035 arrowed lines indicates mean resultant length of the vector at each mean.
1036 **e** Circular plots of circatidal peak expression phase of *Phper*, *Phcry2* and *Phvri* in the dorsal-
1037 lateral cells of *P. hawaiensis* exhibiting circatidal activity rhythms, with the circatidal acrophase
1038 aligned to CTT0 within each individual experiment. Arrowed lines indicate mean phase for
1039 each gene-cell group combination, and length of arrowed lines indicates mean resultant length
1040 of the vector at each mean. For mean phase and mean vector lengths for each gene-cell
1041 group combination in **d** and **e**, see **Supplementary Table 7**.
1042
1043

Supplementary materials: Figures, Tables, Results, Methods and References.

Supplementary Figures and Legends

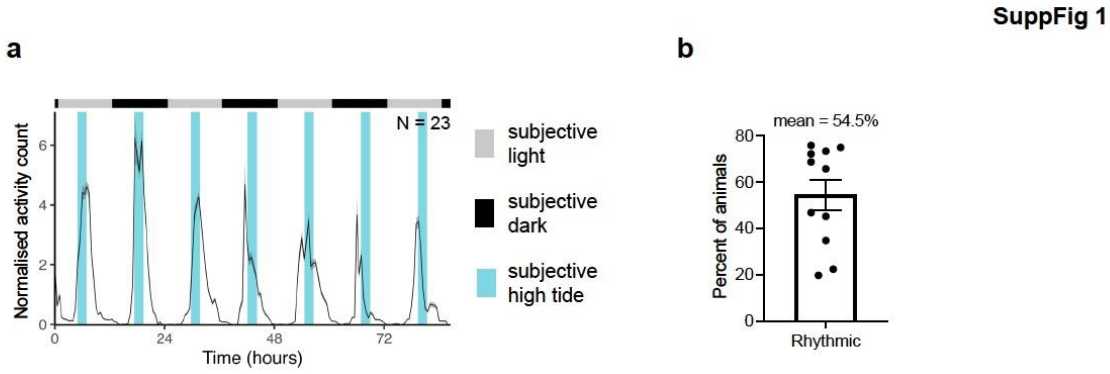

Supplementary Figure 1. Details of circatidal locomotor activity for *E. pulchra*.

a Beach-caught *E. pulchra* show robust circatidal swimming activity under free-running conditions. Plot shows the mean ±SEM normalised swimming activity for a group of *E. pulchra* under DD (N =23).

b Percentage of animals showing rhythmic swimming behaviour from 11 independent experiments, representing 11 beach collections from 2022 to 2024. Error bar indicates SEM.

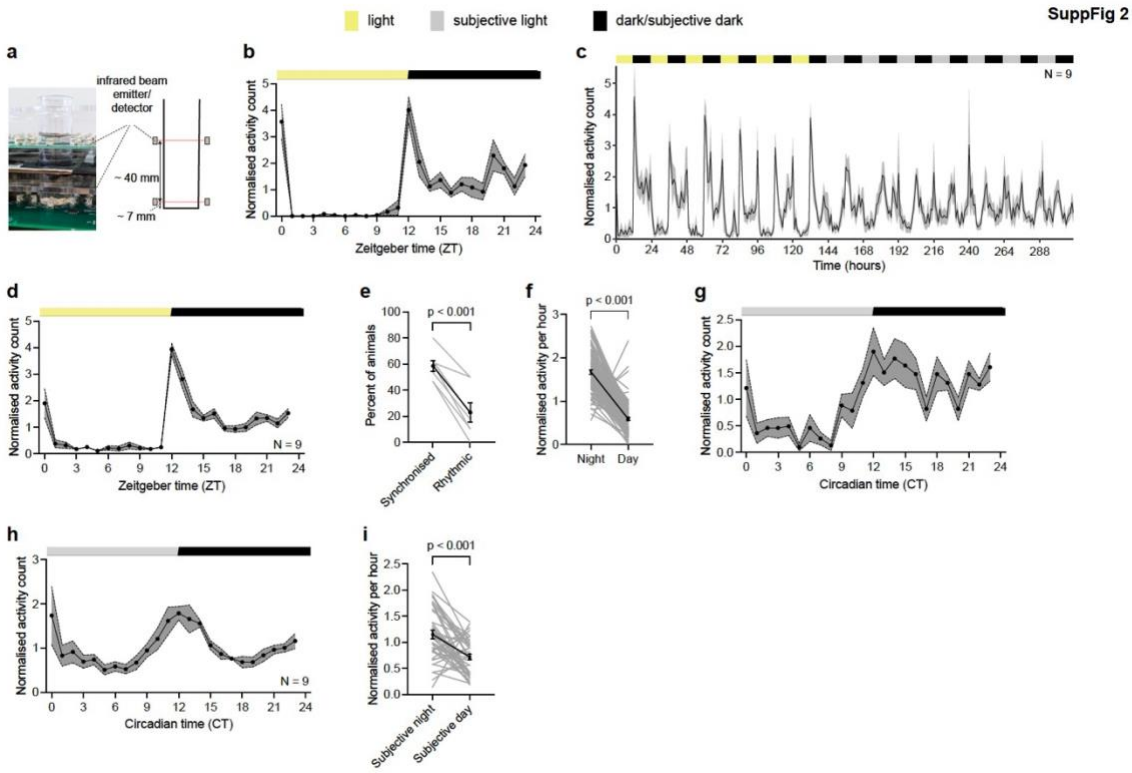

Supplementary Figure 2. Laboratory-cultured *P. hawaiensis* show circadian activity rhythms after entrainment to LD cycle.

a Activity-recording apparatus used two LAM25 infrared beam emitter/ detector arrays stacked over each other to capture locomotor activity of individual *P. hawaiensis* both at the substrate level (all locomotion) and within the water column (swimming).

b Mean daily profile for the individual from **Figure 1c** showing its higher activity during night-time, as well as peaks of activity during light transitions. Shaded area indicates ±SEM.

c Mean normalised locomotor activity profile for all circadian rhythmic *P. hawaiensis* under LD (yellow/ black bars) and then DD (grey/ black bars) from the same experiment as the individual in **Figure 1c** (N =9). Shaded area indicates ±SEM.

d Aggregate daily profile for circadian rhythmic *P. hawaiensis* from **c**, showing their prior LD-synchronised activity was higher during night-time. Shaded area indicates mean ±SEM.

e Percentage of animals showing daily or circadian rhythmic activity under LD cycles and subsequent DD, respectively. Data from 7 independent experiments (N =189) indicating that circadian rhythmicity is detected in ~50% of *P. hawaiensis* that were rhythmic under the preceding LD cycle (paired *t*-test: t =7.37, df =6, p <0.001, Cohen's d =2.784). Filled black circles indicate mean and error bars indicate SEM.

f *P. hawaiensis* synchronised to the LD cycle are more active during the night than during the day (7 independent experiments, N =105, Wilcoxon signed rank test: $|W|$ =5267, $p < 0.001$, rank biserial correlation =0.95). Filled black circles indicate mean and error bars indicate SEM.

g Mean circadian profile for the individual from **Figure 1c** showing its higher activity over periods of subjective night. Shaded area indicates ±SEM.

h Aggregate circadian profile for the group of rhythmic animals from **c**, showing that *P. hawaiensis* are more active during subjective night. Shaded area indicates mean ±SEM.

i *P. hawaiensis* which show a circadian activity rhythm are more active during subjective night (7 independent experiments, N =41, Wilcoxon signed rank test: $|W|$ =595, $p < 0.001$, rank biserial correlation =0.69). Filled black circles indicate mean and error bars indicate SEM.

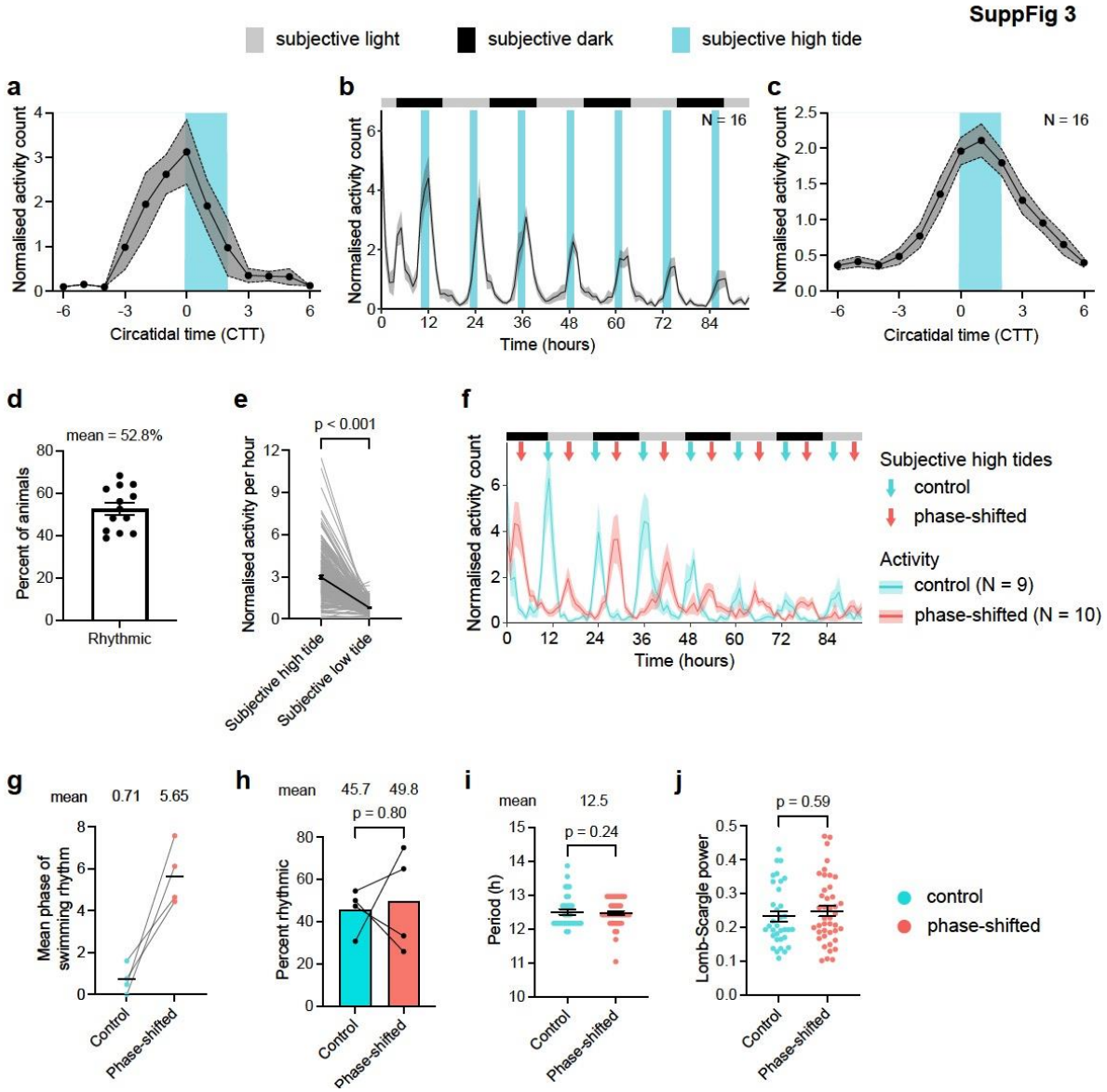

Supplementary Figure 3. Laboratory-cultured *P. hawaiensis* show circatidal activity rhythms after entrainment to a tidal cycle of 2 hours of mechanical agitation every 12.4 hours simulating high water.

a Mean activity profile for the individual from **Figure 1e** showing activity peak coincides with subjective high tide (blue shadings). Shaded area indicates ±SEM.

b Mean normalised swimming activity profile for all circatidal rhythmic *P. hawaiensis* under DD (grey/ black bars) from the same experiment as the individual in **Figure 1e** (N =16). Blue shadings are anticipated tidal agitation, shaded area indicates ±SEM.

c Aggregate activity profile for circatidally rhythmic animals from **b** (N =16), showing that tidally entrained *P. hawaiensis* are more active during subjective high water. Blue shadings are anticipated tidal agitation, shaded area indicates ±SEM.

d Percentage of animals showing a circatidal rhythm in swimming activity after tidal entrainment by agitation. Data from 13 independent experiments (N =456). Error bars indicate SEM.

e Circatidally rhythmic *P. hawaiensis* have higher swimming activity during times of subjective high tide under DD (13 independent experiments, N =239, Wilcoxon signed rank test: $|W|$ =27748, p <0.001, rank biserial correlation =0.97). Filled black circles indicate mean and error bars indicate SEM.

f Mean normalised swimming activity profile for circatidally rhythmic control (12.4 h agitation) and phase-shifted (12.9 h agitation) *P. hawaiensis* under DD (grey/ black bars) from the same phase-shift experiment as the individuals in Figure 1G ($N_{control}$ =9, $N_{phase\text{-}shifted}$ =10). Coloured arrows are anticipated tidal agitation for the control and phase-shifted groups, shaded area indicates ±SEM.

g Mean phase of swimming rhythm of *P. hawaiensis* after tidal entrainment by agitation under control and phase-shifted conditions, with the subjective high tide onset of control animals defined as phase =0 (4 independent experiments, $N_{control}$ =34, $N_{phase\text{-}shifted}$ =42). Horizontal lines indicate mean phase within each group.

h Percentage of *P. hawaiensis* showing a circatidal rhythm in swimming activity after tidal entrainment by agitation under control and phase-shifted conditions (4 independent experiments, $N_{control}$ =73, $N_{phase\text{-}shifted}$ =93, paired *t*-test: t =0.27, df =3, p =0.80, n.s., Cohen's d =0.136). Bars indicate mean within each group.

i Period of circatidal activity rhythm of *P. hawaiensis* after tidal entrainment by agitation under control and phase-shifted conditions (4 independent experiments, $N_{control}$ =34, $N_{phase\text{-}shifted}$ =42, Kolmogorov-Smirnov test: D =0.238, p =0.24, n.s.). Horizontal lines indicate mean phase within each group, and error bars indicate SEM.

j Power of circatidal rhythm reported as by Lomb-Scargle periodogram of *P. hawaiensis* after tidal entrainment by agitation under control and phase-shifted conditions (4 independent experiments, $N_{control}$ =34, $N_{phase\text{-}shifted}$ =42, Kolmogorov-Smirnov test: D =0.1779, p =0.59, n.s.). Horizontal lines indicate mean phase within each group, and error bars indicate SEM.

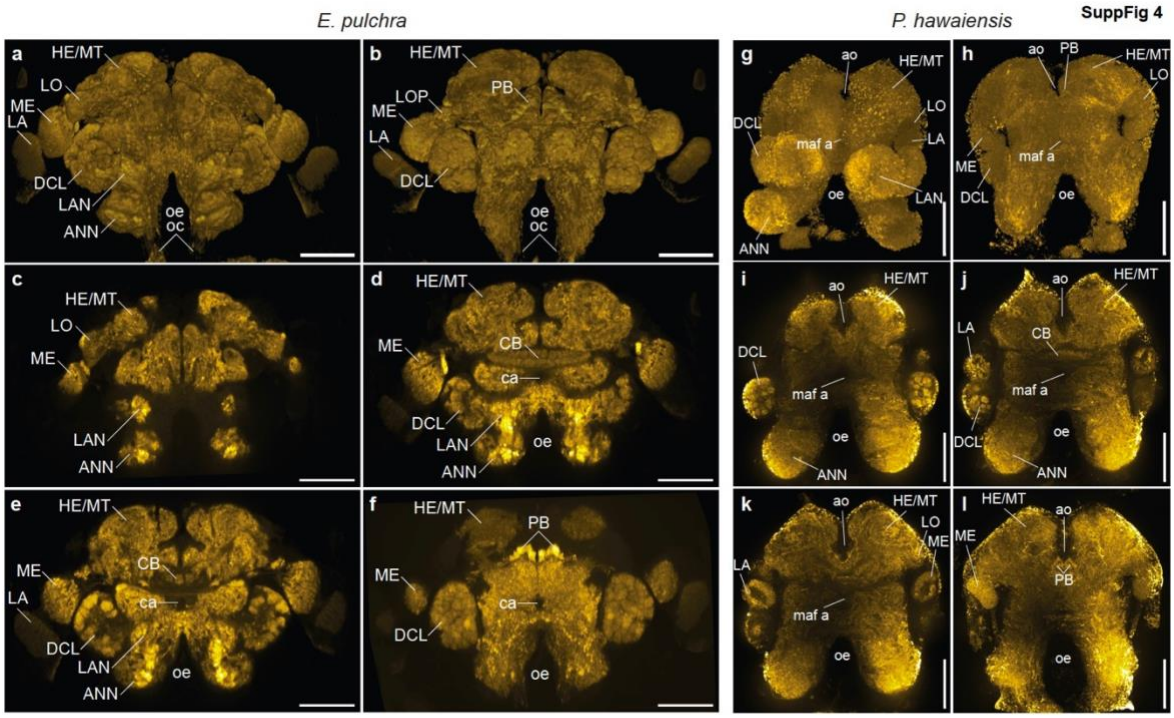

Supplementary Figure 4. Overview of representative *E. pulchra* and *P. hawaiensis* brains, immunostained with anti-SYNORF to highlight the neuropils.

a Anterior view of a *E. pulchra* brain (3D volume projection), with optic lobes, deutocerebral chemosensory lobes, antenna neuropils and hemi-ellipsoid body/medulla terminalis complexes are visible on the anterior surface of the brain.

b Posterior view of a *E. pulchra* brain (3D volume projection). The optic lobes, deutocerebral chemosensory lobes and hemi-ellipsoid body/medulla terminalis complexes are visible on the posterior surface. The protocerebral bridge appears as a distinct arch-like structure under the hemi-ellipsoid body/medulla terminalis complexes.

c-e Selected optical sections of a *E. pulchra* brain from anterior to posterior, showing locations of distinct neuropils throughout the depth of the brain. The optic lobes span the anterior-posterior axis, with the lobula constrained to the anterior aspect (**c**), and the medulla and lamina (**d**, **e**) occupying the medial and posterior aspects. The cigar-shaped central body is at its most expansive towards the middle of the brain.

f Maximum intensity Z-projection through the protocerebral bridge of a *E. pulchra* brain.

g Anterior view of a *P. hawaiensis* brain (3D volume projection), with parts of the optic lobes (lamina and lobula), deutocerebral chemosensory lobes, antenna neuropils and hemi-ellipsoid body/medulla terminalis complexes are visible on the anterior surface of the brain.

h Posterior view of a *P. hawaiensis* brain (3D volume projection). Parts of the optic lobes (medulla and lobula), deutocerebral chemosensory lobes and hemi-ellipsoid body/medulla terminalis complexes are visible on the posterior surface. As in *E. pulchra,* the protocerebral bridge of *P. hawaiensis* is located posteriorly under the hemi-ellipsoid body/medulla terminalis complexes.

i-k Selected optical sections of a *P. hawaiensis* brain from anterior to posterior, showing locations of distinct neuropils throughout the depth of the brain. The hemi-ellipsoid body/medulla terminalis complexes and the foramina accommodating two of the brain arteries, the anterior aorta and myoarterial formation a, are visible throughout the thickness of the brain. The former also constitute the most dorsal neuropils of the brain. The deutocerebral chemosensory lobes are located anterior to the rest of the optic lobes (**i**, **j**). The lamina is the most anteriorly positioned optic neuropils (**j**), followed almost simultaneously by the medulla and lobula (**k**). The sausage-shaped central body is at its most expansive towards the middle of the brain (**j**).

l Maximum intensity Z-projection through the protocerebral bridge of a *P. hawaiensis* brain.

Abbreviations: ANN, antenna 2 neuropil; ao, anterior aorta; ca, cerebral artery; CB, central body; DCL, deutocerebral chemosensory lobe; HE/MT, hemi-ellipsoid body/medulla terminalis; LA, lamina; LAN, lateral antenna 1 neuropil; LO, lobula; LOP, lobula plate; maf a, myoarterial formation a; ME, medulla; oc, oesophageal connective; oe, oesophageal foramen; PB, protocerebral bridge. Scale bars*:* 100 μm.

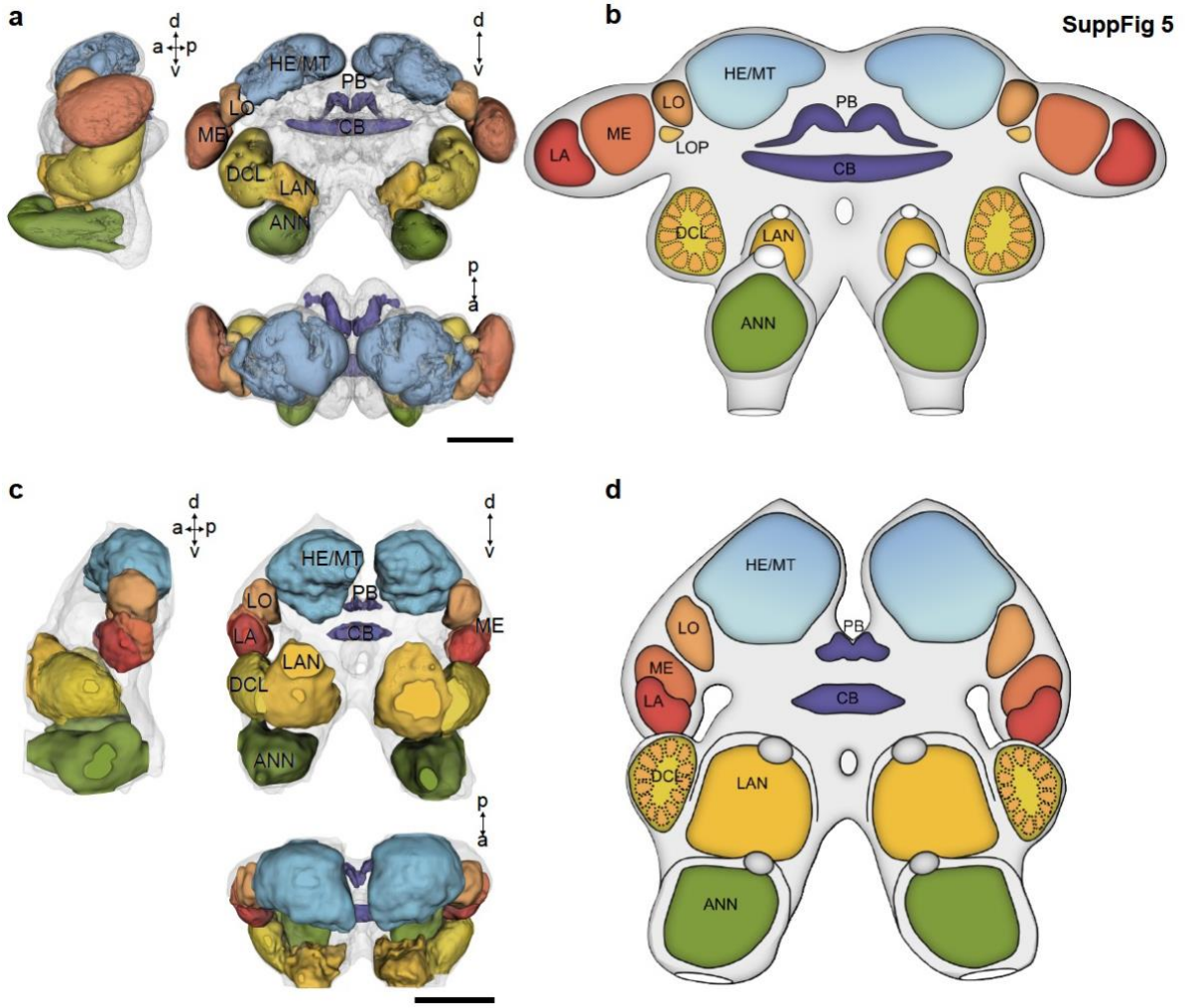

Supplementary Figure 5. Gross anatomy of *E. pulchra* and *P. hawaiensis* brains revealed by anti-SYNORF1 immunostaining, registered to refence brain.

a Lateral, anterior and dorsal views of the *E. pulchra* surface-rendered 3D average reference brain, with major neuropils demarcated. See also Supplementary Video 1.

b Diagrammatic representation of the of *E. pulchra* brain, based on **a**.

c Lateral, anterior and dorsal views of *P. hawaiensis* surface-rendered 3D average reference brain with major neuropils demarcated. See also Supplementary Video 2.

d Diagrammatic representation of the *P. hawaiensis* brain, based on **c**.

Compass markers in **a** and **c** show anterior (a), posterior (p), dorsal (d) and ventral (v) directions.

Abbreviations: ANN antenna 2 neuropil, CB central body, DCL deutocerebral chemosensory lobe, HE/MT medulla terminalis/ hemi-ellipsoid body, LA lamina, LAL lateral accessory lobe, LAN lateral antenna 1 neuropil, LO lobula, LOP lobula plate, ME medulla, PB protocerebral bridge. Scale bars: 100 µm.

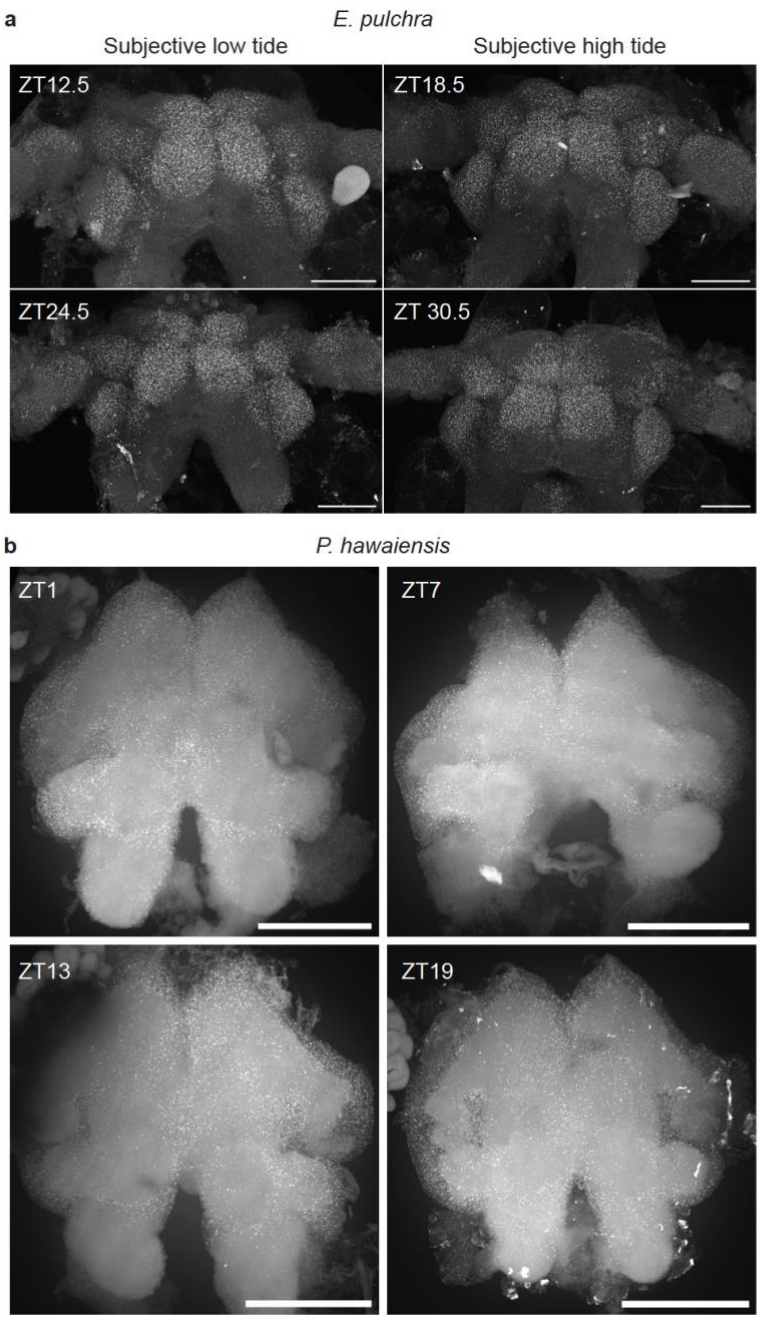

SuppFig 6

Supplementary Figure 6. Cellular expression of *Bmal1* in brains of *E. pulchra* and *P. hawaiensis* brains across time.

a Maximum intensity Z-projections of representative brains (posterior apposing coverslip) from field-collected *E. pulchra* sampled under 14 h: 10 h LD cycle and then probed for *EpBmal1* using HCR-FISH.

b Maximum intensity Z-projections of representative *P. hawaiensis* brains (anterior apposing coverslip) sampled under 12 h: 12 h LD cycle and then probed for *PhBmal1* using HCR-FISH.

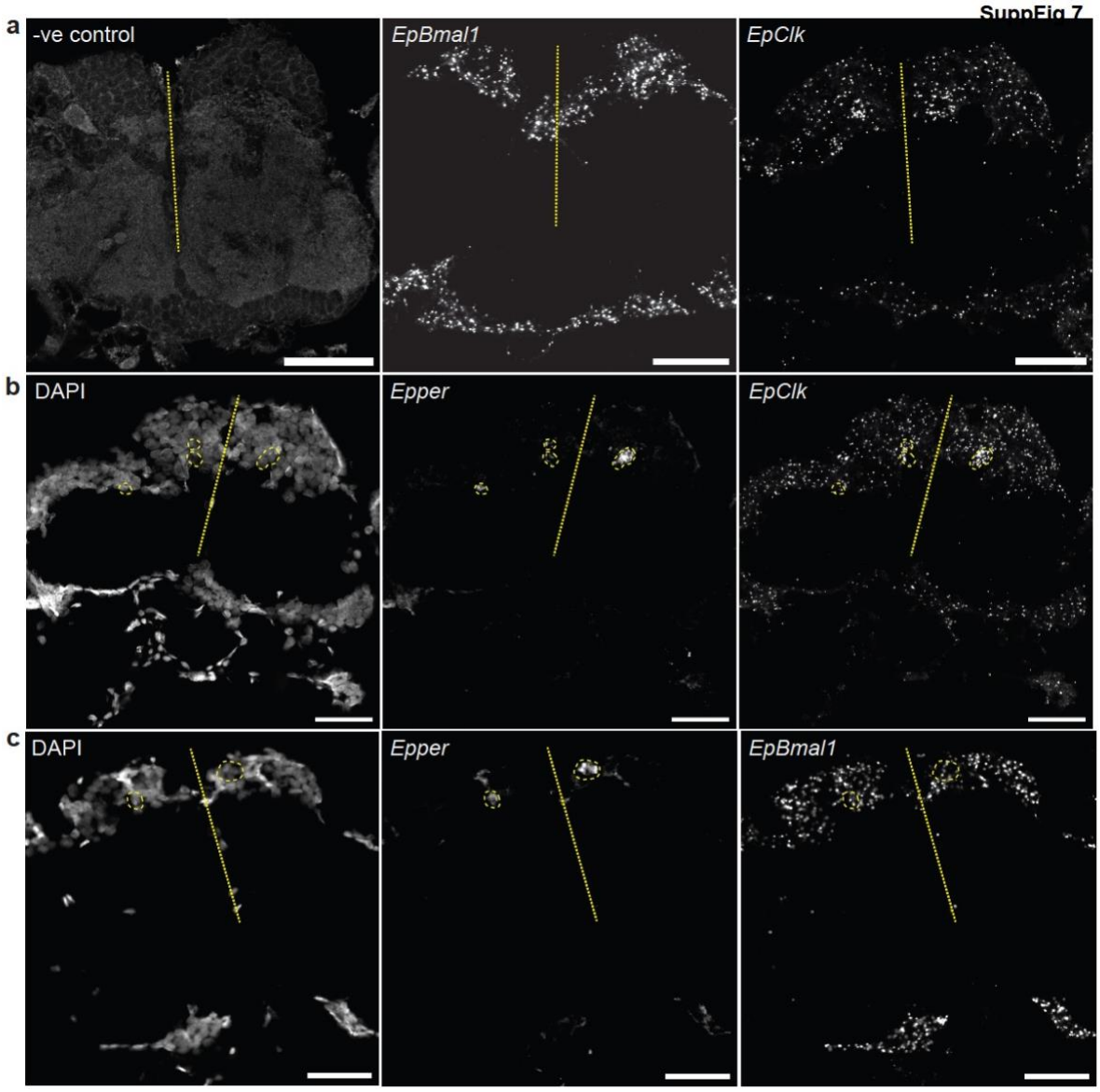

Supplementary Figure 7. Expression of circadian clock genes in *E. pulchra* brain sections detected using RNAScope™.

a Representative image (single optical section) of *E. pulchra* brain sections probed for negative control (left), *EpBmal1* (middle) and *EpClk* (right).

b Representative image (single optical section) of a *E. pulchra* brain section stained with DAPI (left) and probed for *Epper* (middle) and *EpClk* (right).

c As in **b** for *Epper* and *EpBmal1*.

Yellow dashed outlines indicate cells enriched for *Epper* and *EpClk* expression. Yellow dotted lines indicate midlines. Scale bars: 10 μm.

SuppFig 8

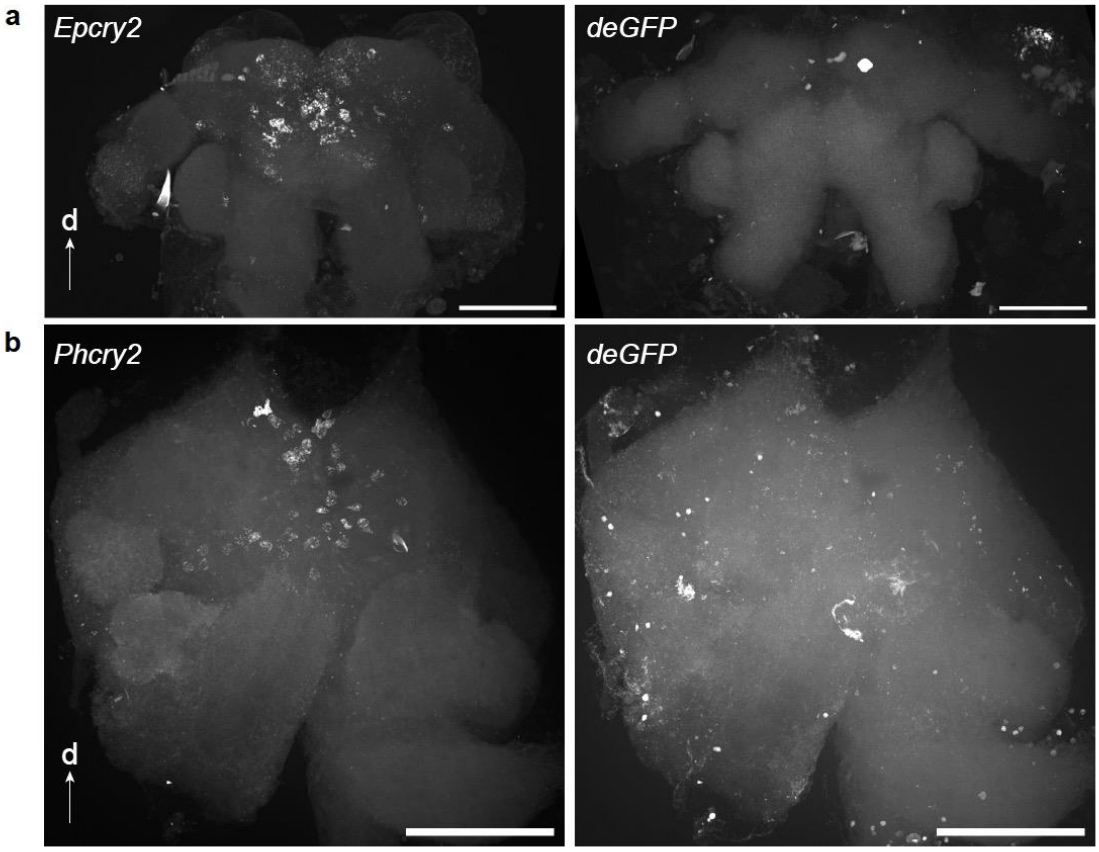

Supplementary Figure 8. HCR-FISH negative control.

a Representative maximum intensity Z-projection of *E. pulchra* brains (posterior apposing coverslip) labelled for *Epcry2* (left) as a positive signal and the negative control probe *deGFP* (right).

b Representative maximum intensity Z-projection of a *P. hawaiensis* brain (anterior apposing coverslip) co-labelled for *Phcry2* as a positive signal (left) and the negative control probe *deGFP* (right).

Scale bars: 100 µm. Arrows indicates dorsal orientation.

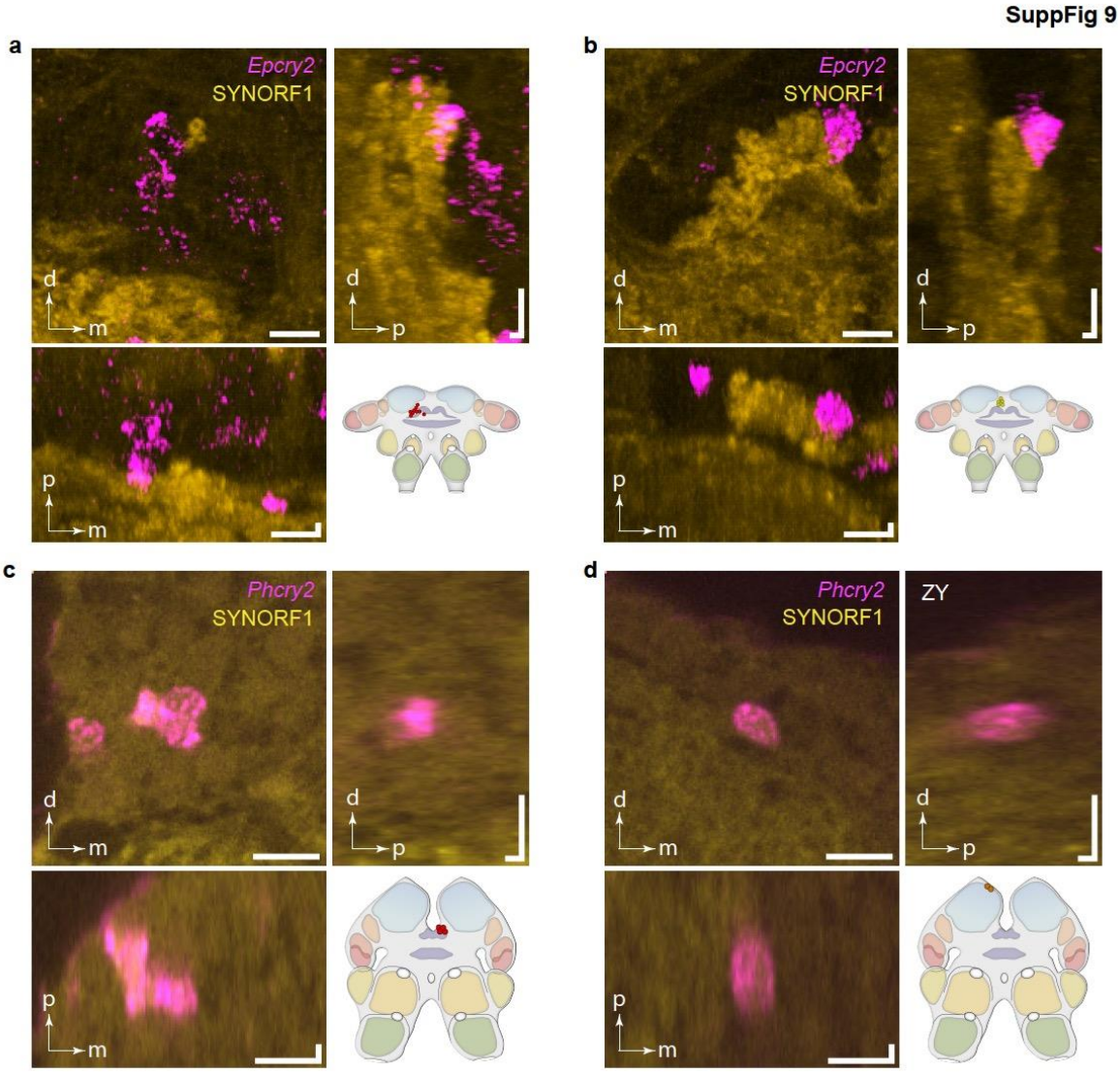

Supplementary Figure 9. Representative orthogonal views of brains co-labelled with anti-synorf (IHC) and *cry2* (HCR-FISH).

a Orthogonal views showing *Phcry2* enrichment in four medioposterior cells of a *E. pulchra* brain co-stained with anti-SYNORF1. Cartoon shows location of these cells.

b As in **a** but for the medial cells.

c Orthogonal views showing *Phcry2* enrichment in four medioposterior cells of a *P. hawaiensis* brain co-stained with anti-SYNORF1. Cartoon shows location of these cells.

d As in **c** but for the two dorsal-lateral cells.

Horizonal (and vertical) scale bars: 10 µm.

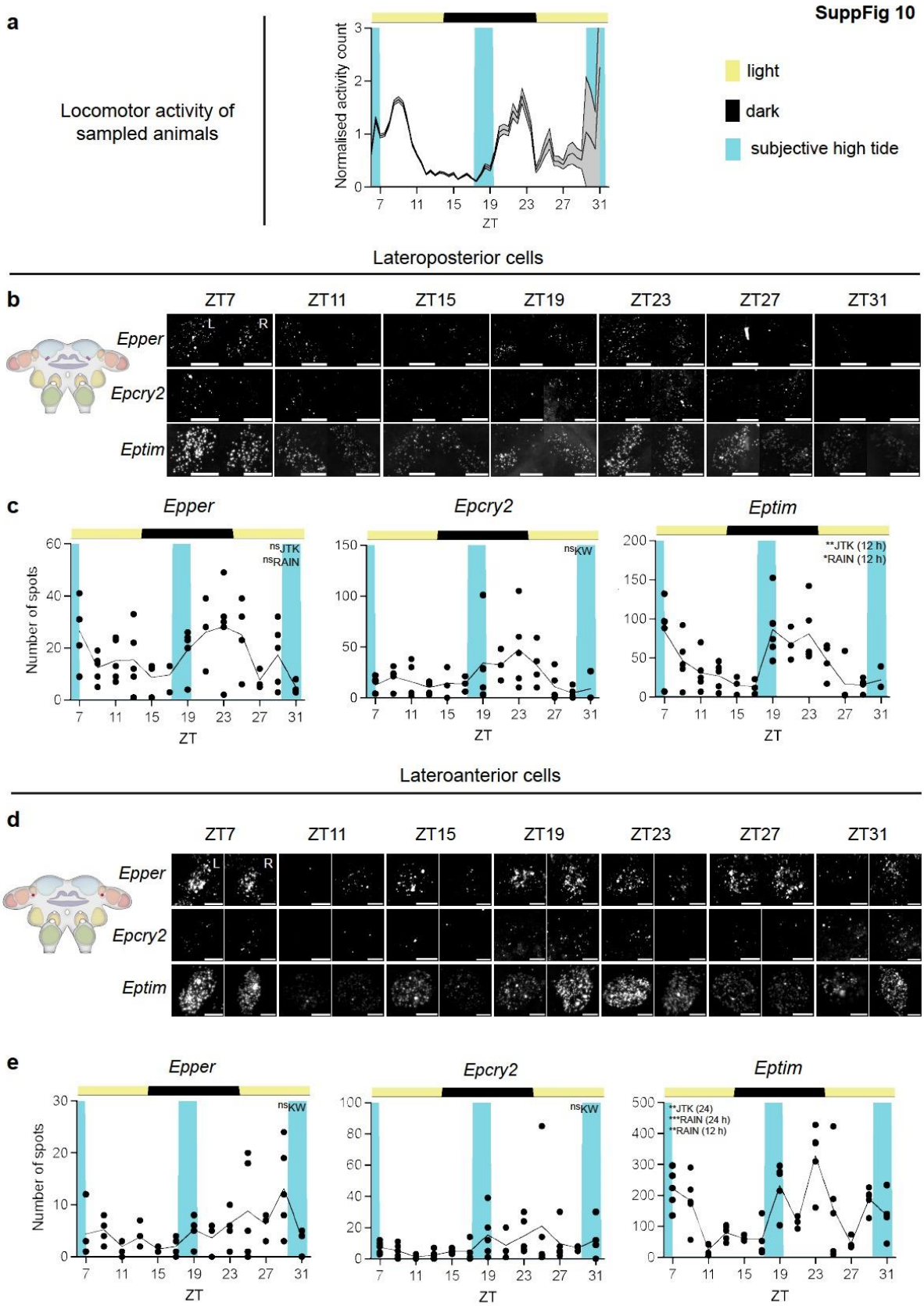
SuppFig 10
a
Locomotor activity of sampled animals
Normalised activity count
ZT
light
dark
subjective high tide
Lateroposterior cells
b
ZT7
ZT11
ZT15
ZT19
ZT23
ZT27
ZT31
Epper
Epcry2
Eptim
L
R
c
Epper
Epcry2
Eptim
Number of spots
ZT
nsJTK
nsRAIN
nsKW
**JTK (12 h)
*RAIN (12 h)
Lateroanterior cells
d
e
**JTK (24)
***RAIN (24 h)
**RAIN (12 h)

SuppFig 10

Dorsal cells

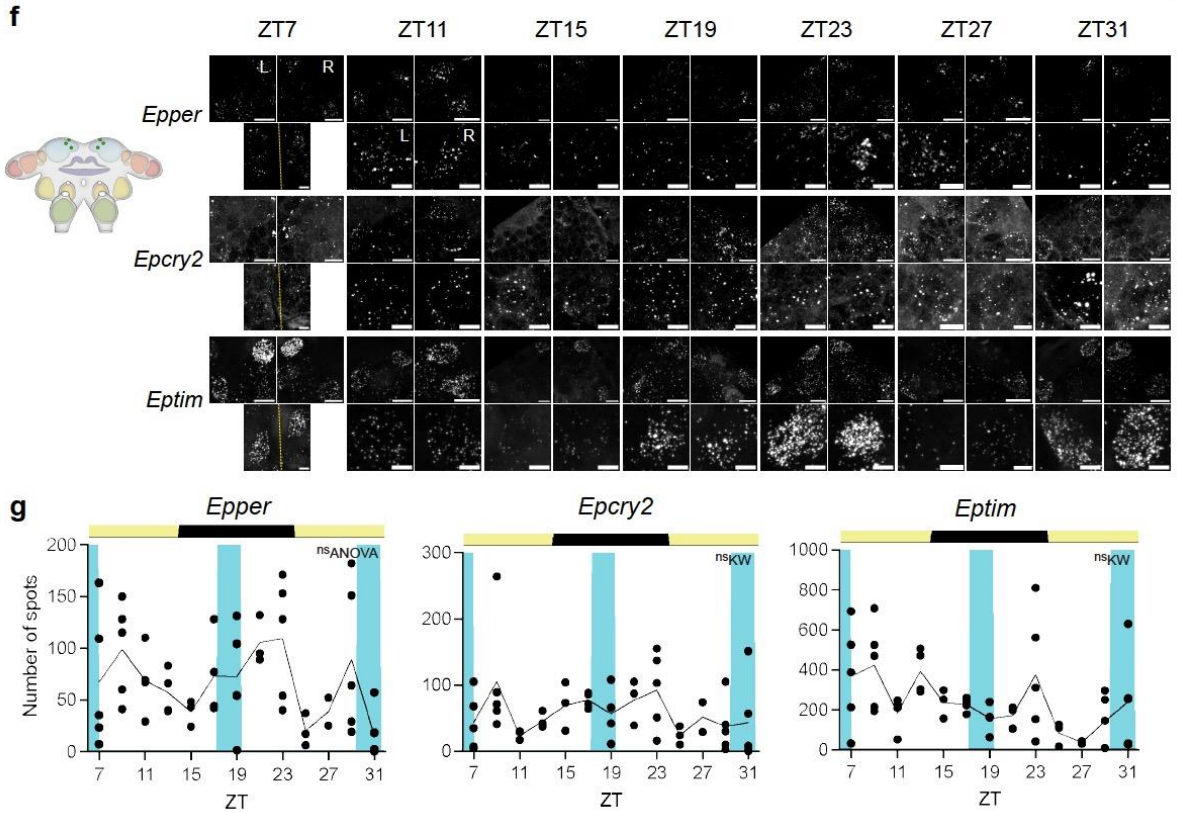

Large dorsal cells

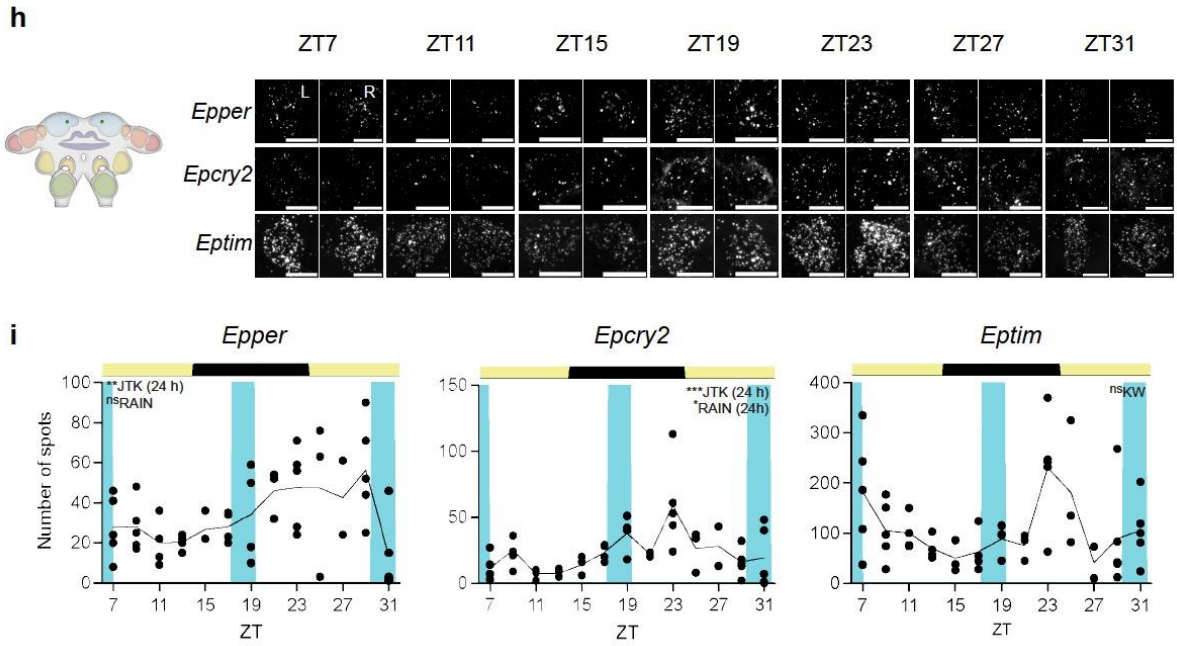

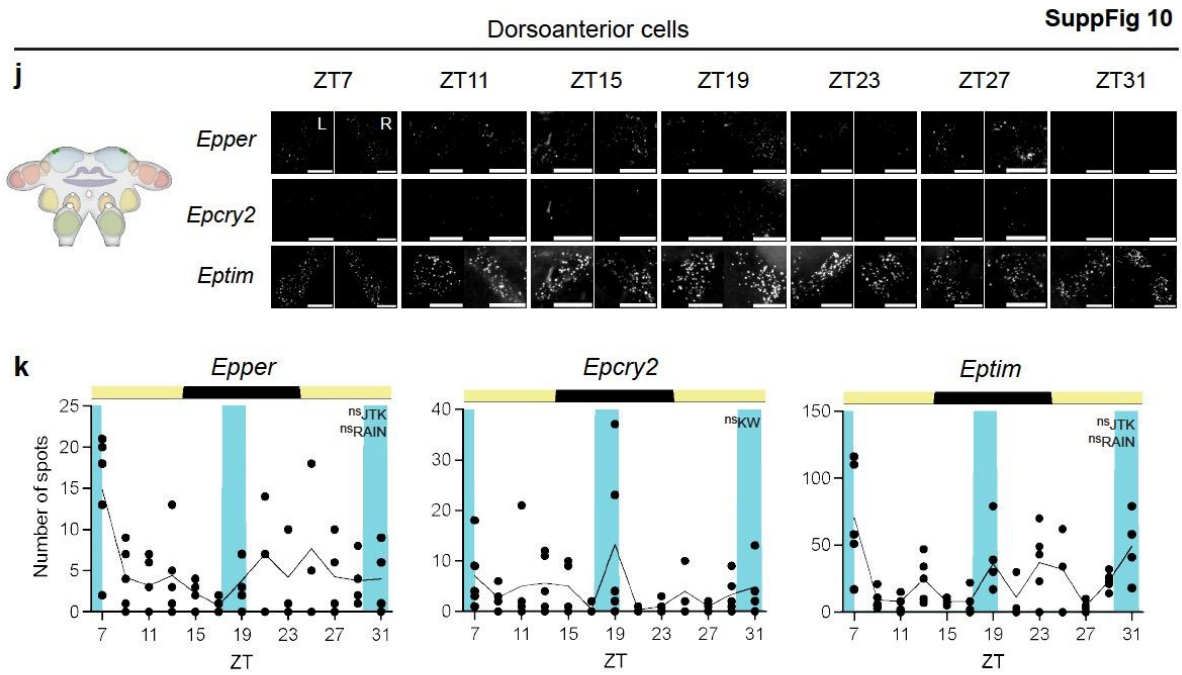

Supplementary Figure 10. Time course of expression of *per, cry2* and *tim* in cells of tidally rhythmic *E. pulchra* held on a LD cycle.

a Normalised swimming activity of beach-caught *E. pulchra* used in the HCR-FISH time-course showed peak activity just after expected HW under LD (16 h:8 h). Plots shows normalised locomotor activity (mean ±SEM) of harvested animals over the sampling interval (initial group size at start of harvest at ZT7 =65).

b Left: Cartoon to show location of lateroposterior cell group in the brain and Right: representative maximum intensity Z-projections of *Epper*, *Epcry2* and *Eptim* expression in lateroposterior cells in both hemispheres (L: left, R: right, yellow dashed lines: midlines) across ZT (individual HCR-FISH channels in rows).

c. Plots of mean transcript abundance, quantified as the number of FISH spots, across ZT for *Epper* (left), *Epcry2* (middle) and *Eptim* expression (right) in the lateroposterior cells. Each point is from one brain.

d, e As in **b, c** for lateroanterior cells.

f, g As in **b, c** for dorsal cells.

h, i As in **b, c** for large dorsal cells.

j, k As in **b, c** for dorsoanterior cells.

Inset text in **c**, **e**, **g, i** and **k** indicate statistical tests performed to determine variation of gene expression with time and/or rhythmicity, with the tested periods (if any) in parentheses. p <0.001***, p <0.01**, p ≤0.05*, p >0.05^{ns}. For statistics shown in this figure, refer to Supplementary Table 2. Scale bars: 10 µm (**b**, **d**, **f** (upper row)), 5 µm (**f** (lower row), **h**, **j**).

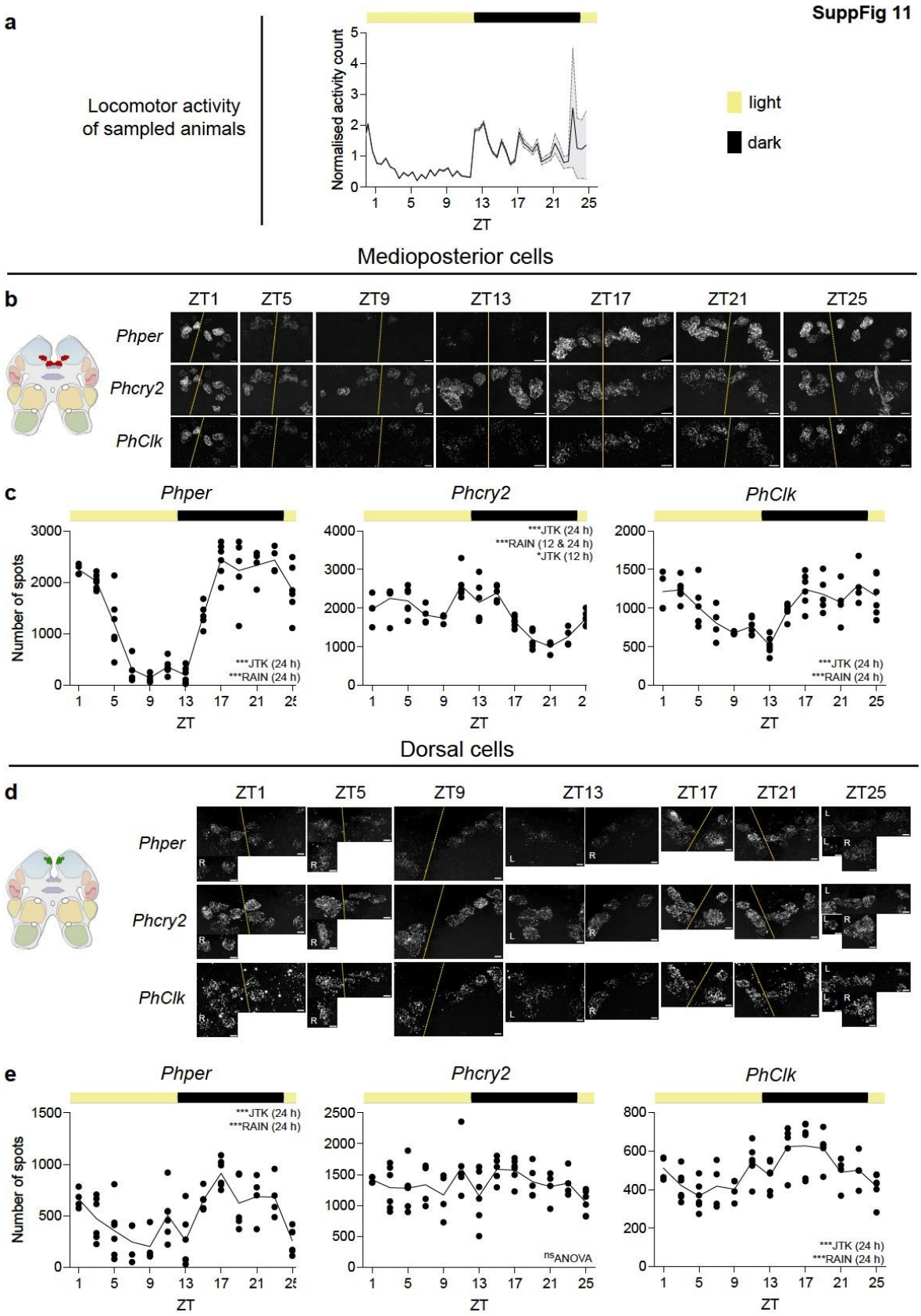
SuppFig 11
a
Locomotor activity
of sampled animals
Normalised activity count
ZT
light
dark
Medioposterior cells
b
ZT1
ZT5
ZT9
ZT13
ZT17
ZT21
ZT25
Phper
Phcry2
PhClk
c
Phper
Phcry2
PhClk
Number of spots
***JTK (24 h)
***RAIN (24 h)
***RAIN (12 & 24 h)
*JTK (12 h)
ZT
Dorsal cells
d
e
nsANOVA

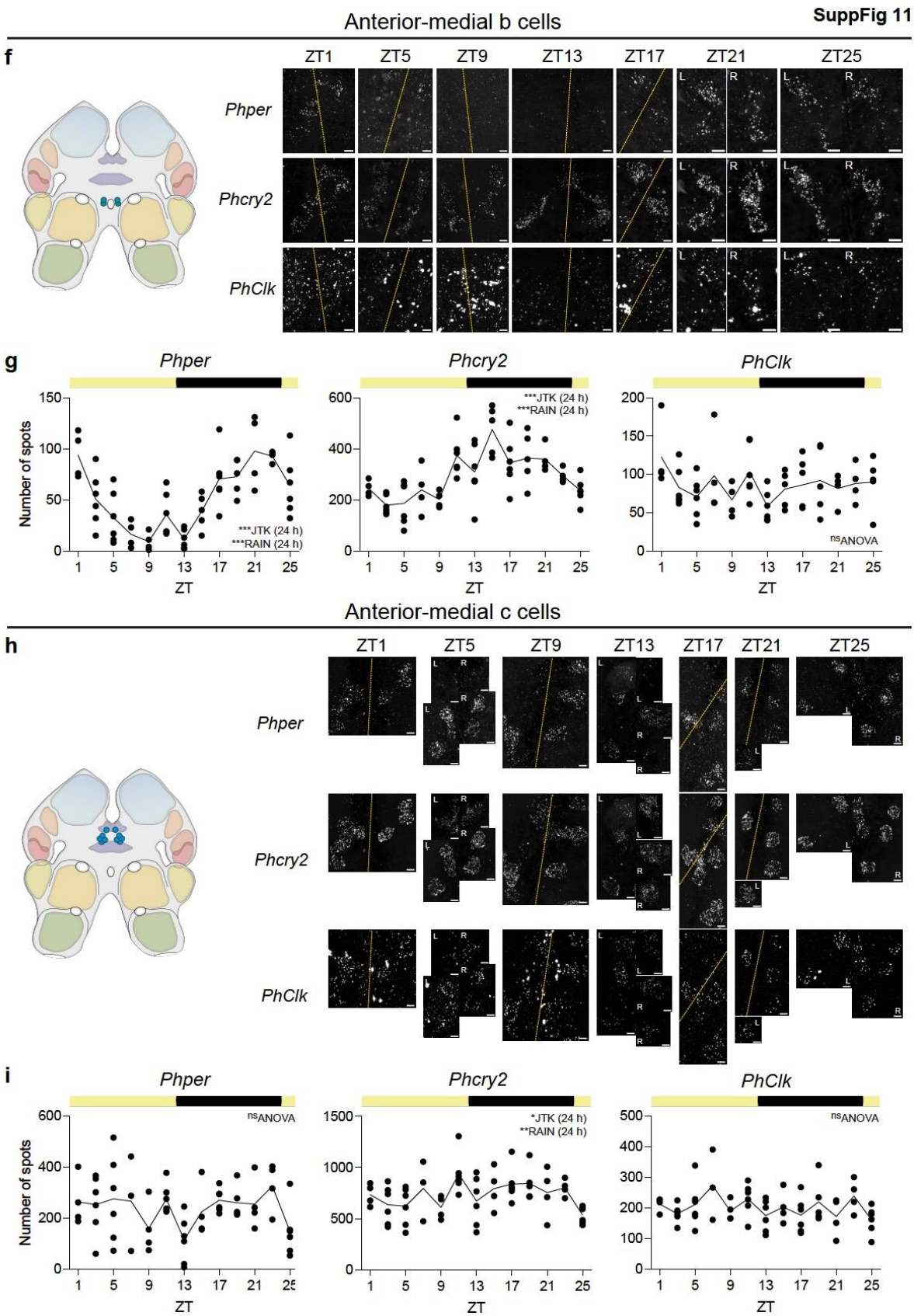

Supplementary Figure 11. Time course of rhythmic expression of *per, cry2* and *Clk* in cells of *P. hawaiensis* synchronised to the LD cycle.

a Normalised swimming activity of *P. hawaiensis* used in the HCR-FISH time-course showed a daily activity rhythm synchronised to the LD cycle. Plots shows mean activity with SEM (shading) of harvested animals over the sampling interval (initial group size at start of harvest at ZT1 =79).

b Left: Cartoon to show location of medioposterior cell group in the brain and Right: representative maximum intensity Z-projections of *Phper*, *Phcry2* and *PhClk* expression in the medioposterior cells of both hemispheres (L: left, R: right, yellow dashed lines: midlines) across ZT (individual HCR-FISH channels in rows).

c Plots of mean transcript abundance, quantified as the number of FISH spots, across ZT for *Phper* (left), *Phcry2* (middle) and *PhClk* (right) in the medioposterior cells. Each point is from one brain.

d, **e** As in **b**, **c** for dorsal cell group.

f, **g** As in **b**, **c** for anterior-medial b cell group.

h, **i** As in **b**, **c** for anterior-medial c cell group.

Inset text in **c**, **e**, **g** and **i** indicate statistical tests performed to determine variation of gene expression with time and/or rhythmicity, with the tested periods (if any) in parentheses. $p < 0.001$***, $p < 0.01$**, $p \leq 0.05$*, $p > 0.05^{ns}$. Scale bars: 10 µm (**b**), 5 µm (**d**, **f**, **h**). For statistics shown in this figure, refer to Supplementary Table 3.

SuppFig 12

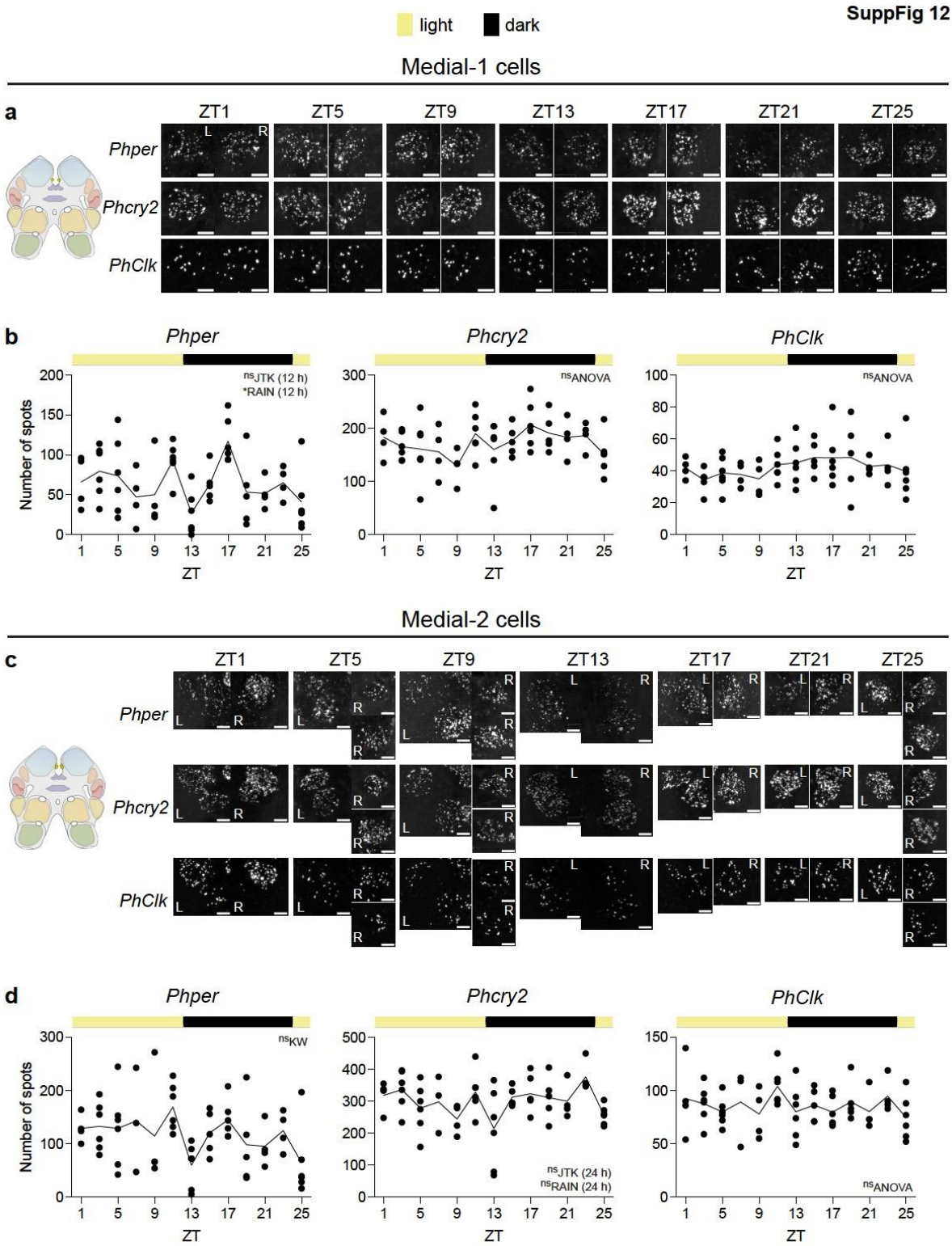
light
dark
Medial-1 cells
a
ZT1
ZT5
ZT9
ZT13
ZT17
ZT21
ZT25
Phper
Phcry2
PhClk
L
R
b
Phper
Phcry2
PhClk
Number of spots
ZT
nsJTK (12 h)
*RAIN (12 h)
nsANOVA
nsANOVA
Medial-2 cells
c
ZT1
ZT5
ZT9
ZT13
ZT17
ZT21
ZT25
Phper
Phcry2
PhClk
d
Phper
Phcry2
PhClk
Number of spots
ZT
nsKW
nsJTK (24 h)
nsRAIN (24 h)
nsANOVA

Dorsal-lateral cells

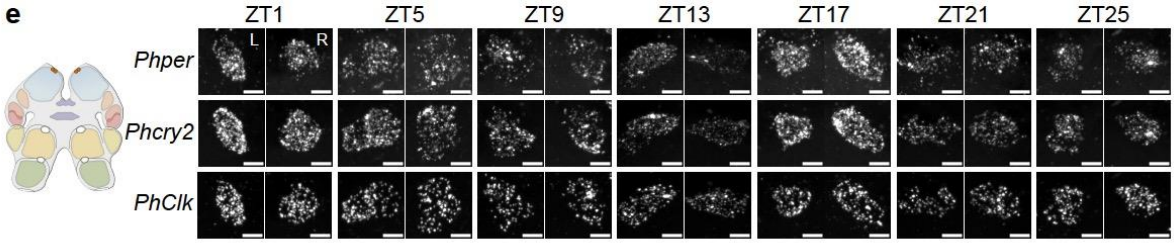

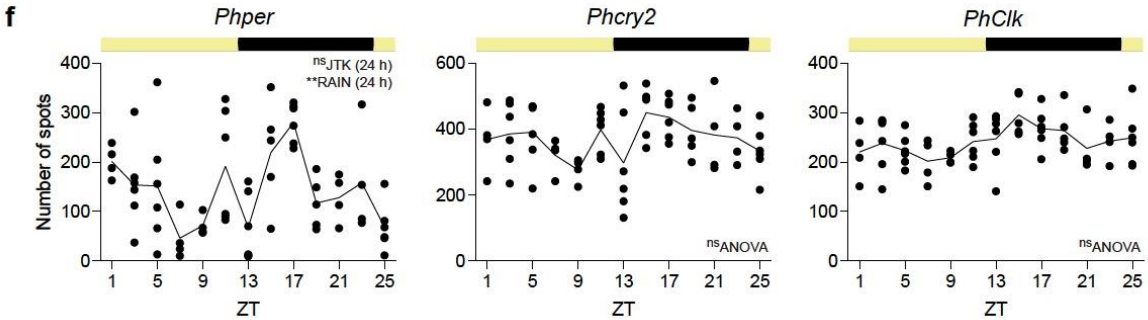

Anterior-lateral cells

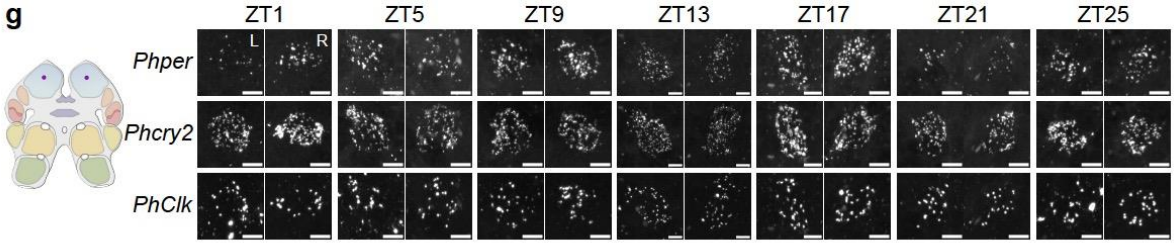

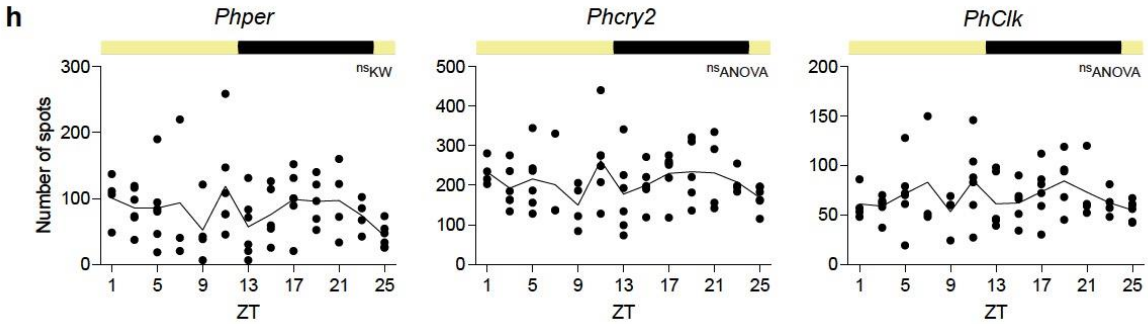

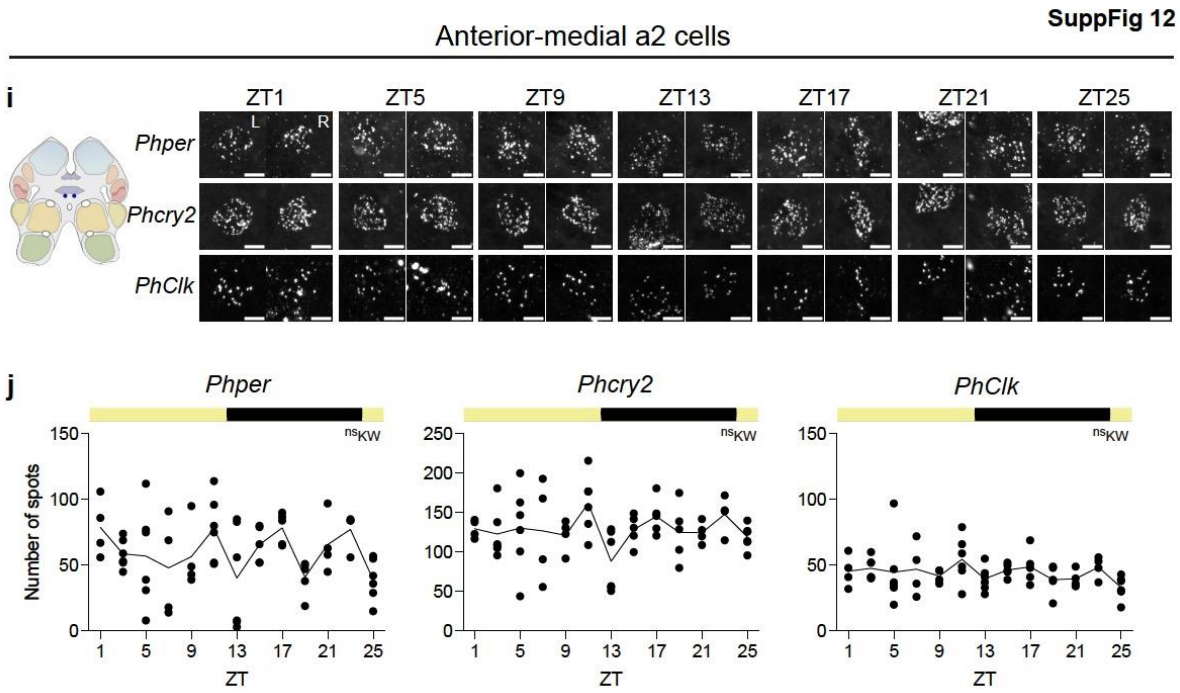

Supplementary Figure 12. Time course of non-rhythmic expression of *per, cry2* and *Clk* in cells of *P. hawaiensis* synchronised to the LD cycle.

a Left: Cartoon to show location of medial-1 cell group in the brain and Right: representative maximum intensity Z-projections of *Phper*, *Phcry2* and *PhClk* expression in the medial-1 cells from both hemispheres (L: left, R: right, yellow dashed lines: midlines) across ZT (individual HCR-FISH channels in rows).

b Plots of mean transcript abundance, quantified as the number of FISH spots, across ZT for *Phper* (left), *Phcry2* (middle) and *PhClk* (right) in the medial-1 cells. Each point is from one brain.

c, **d** As in **a**, **b** for medial-2 cell group.

e, **f** As in **a**, **b** for dorsal-lateral cell group.

g, **h** As in **a**, **b** for anterior-lateral cell group.

i, **j** As in **a**, **b** for anterior-medial a2 cell group.

Inset text in **b**, **d**, **f**, **h** and **j** indicate statistical tests performed to determine variation of gene expression with time and/or rhythmicity, with the tested periods (if any) in parentheses. $p<0.001$***, $p<0.01$**, $p\leq0.05$*, $p>0.05^{ns}$. KW: Kruskal-Wallis test. For statistics shown in this figure, refer to Supplementary Table 3. Scale bars: 5 µm.

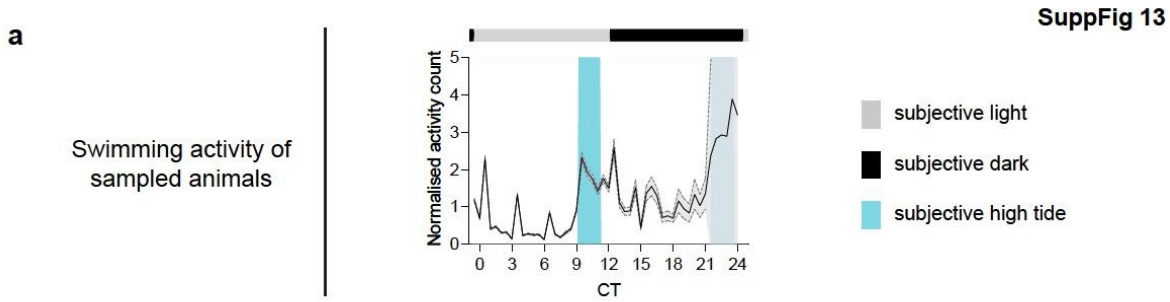

Supplementary Figure 13. Free-running activity of tidally entrained *P. hawaiensis* (tidal phase θ).

a Normalised swimming activity of *P. hawaiensis* used in the HCR-FISH time-course showed a circatidal activity rhythm synchronised to the prior agitation cycle. Plots shows mean activity with SEM (shading) of harvested animals over the sampling interval (initial group size at start of harvest at CT0 =37).

SuppFig 14

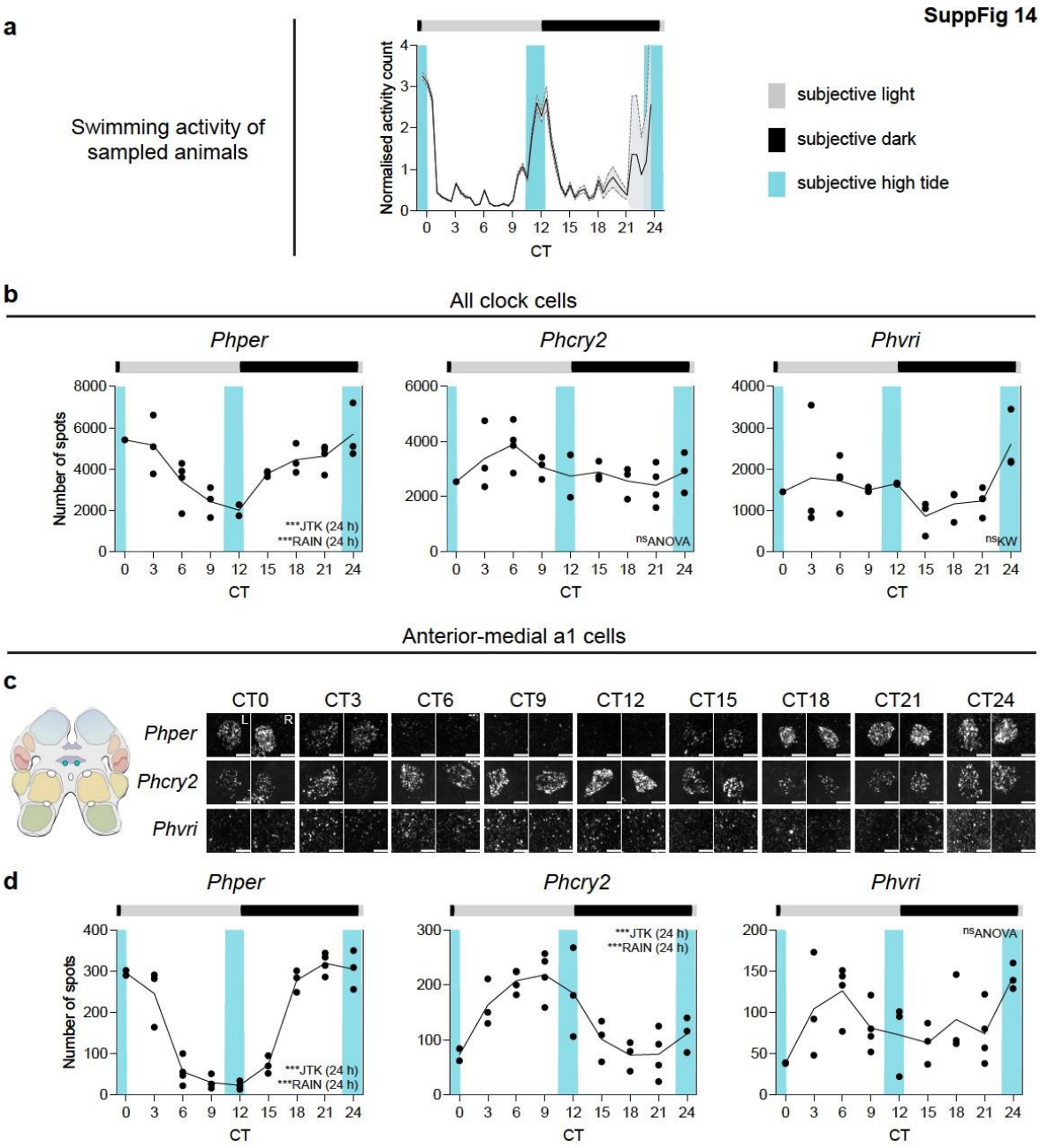
a
Swimming activity of sampled animals
Normalised activity count
CT
subjective light
subjective dark
subjective high tide
b
All clock cells
Phper
Phcry2
Phvri
Number of spots
***JTK (24 h)
***RAIN (24 h)
nsANOVA
nsKW
CT
Anterior-medial a1 cells
c
CT0
CT3
CT6
CT9
CT12
CT15
CT18
CT21
CT24
L
R
Phper
Phcry2
Phvri
d
Phper
Phcry2
Phvri
Number of spots
***JTK (24 h)
***RAIN (24 h)
nsANOVA
CT

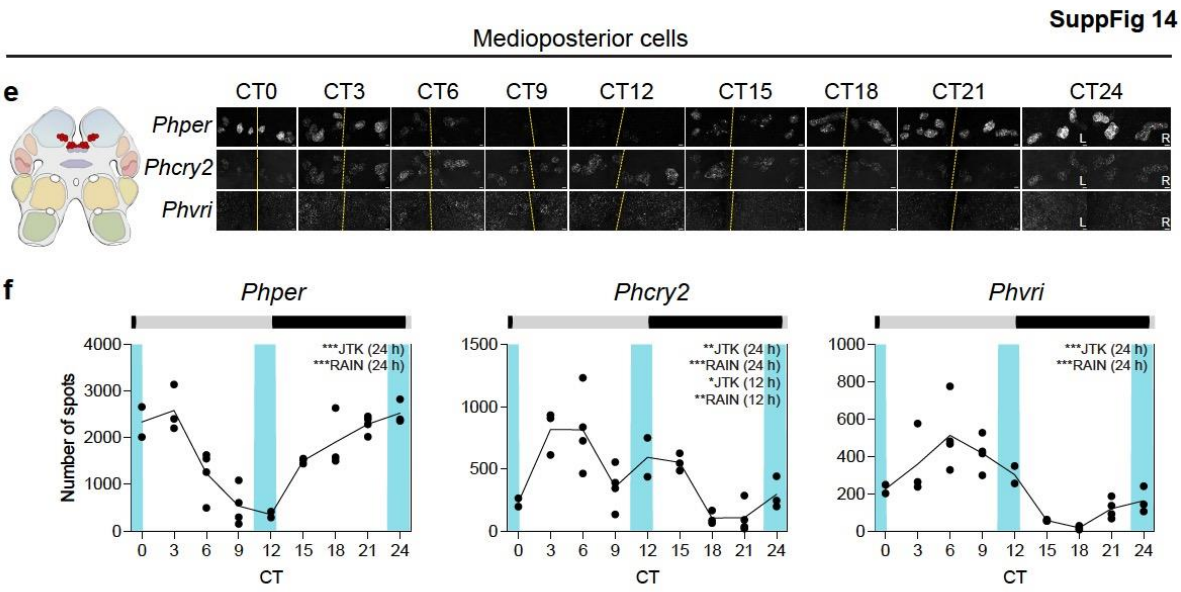

Supplementary Figure 14. Free-running clock gene expression rhythms in tidally entrained *P. hawaiensis* (tidal phase θ + 1.2 h).

a Normalised swimming activity of *P. hawaiensis* used in the HCR-FISH time-course showed a circatidal activity rhythm synchronised to the prior agitation cycle. Plots shows mean activity with SEM (shading) of harvested animals over the sampling interval (initial group size at start of harvest at CT0 =35.

b Profile of mean aggregate expression of *Phper, Phcry2* and *Phvri* across all cells plotted across time in tidally entrained animals sampled under DD. Each point is from one brain.

c Left: Cartoon to show location of anterior-medial a1 in the brain and Right: representative maximum intensity Z-projections of *Phper*, *Phcry2* and *Phvri* expression in the anterior-medial a1 cells from both hemispheres (L: left, R: right, yellow dashed lines: midlines) across CT (individual HCR-FISH channels in rows).

d Plots of mean transcript abundance, quantified as the number of FISH spots, across CT for *Phper* (left), *Phcry2* (middle) and *Phvri* (right) in the anterior-medial a1 cells. Each point is from one brain.

e, **f** As in **c**, **d** for medioposterior cell group.

Inset text in **b**, **d** and **f** indicate statistical tests performed to determine variation of gene expression with time and/or rhythmicity, with the tested periods (if any) in parentheses. p <0.001***, p <0.01**, p ≤0.05*, p >0.05^{ns}. KW: Kruskal-Wallis test. For statistics shown in this figure, refer to Supplementary Table 5. Scale bars: 5 µm (**c**), 10 µm (**e**).

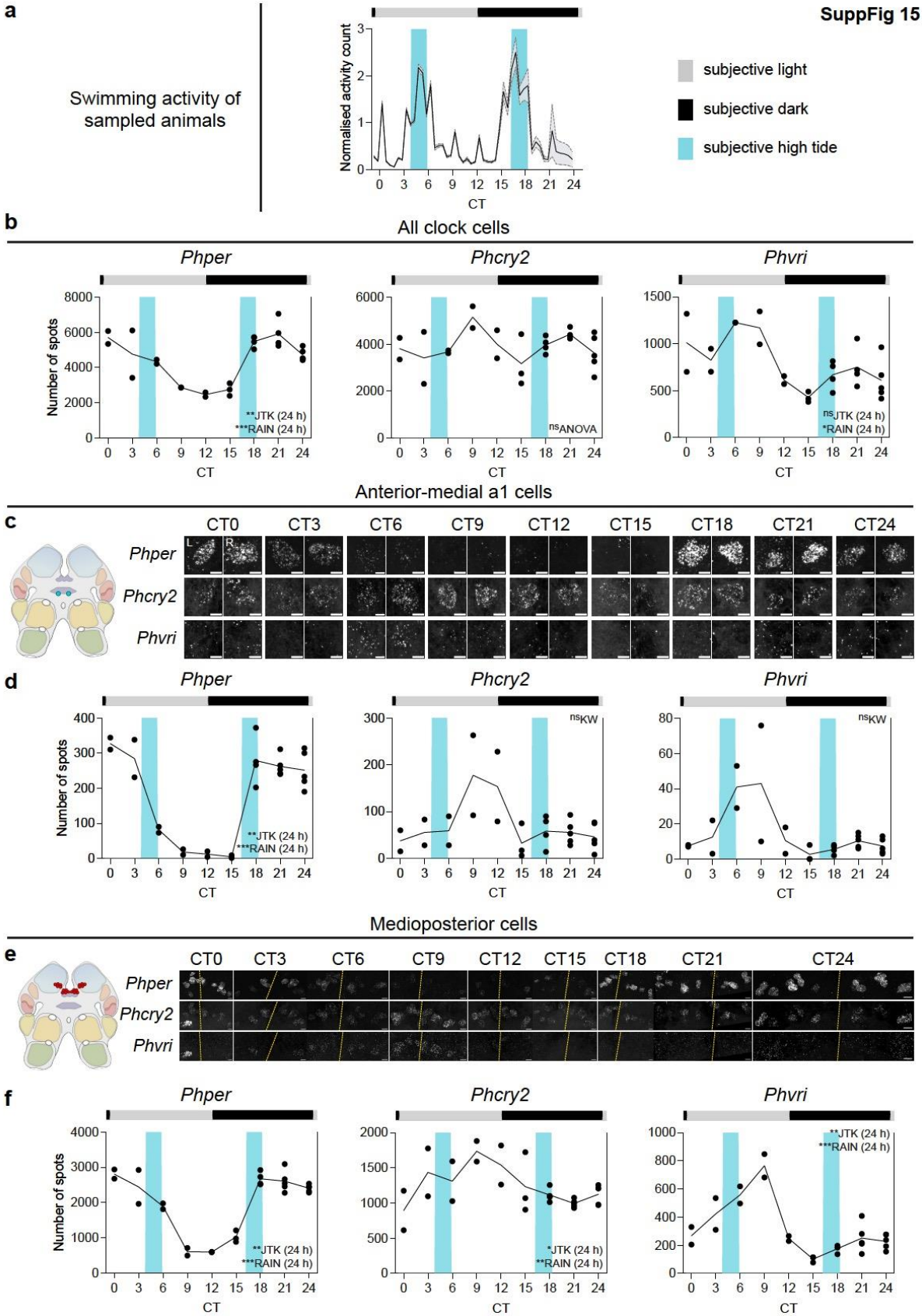
SuppFig 15
a
Swimming activity of sampled animals
Normalised activity count
CT
subjective light
subjective dark
subjective high tide
b
All clock cells
Phper
Phcry2
Phvri
Number of spots
**JTK (24 h)
***RAIN (24 h)
nsANOVA
nsJTK (24 h)
*RAIN (24 h)
Anterior-medial a1 cells
c
CT0
CT3
CT6
CT9
CT12
CT15
CT18
CT21
CT24
L
R
d
nsKW
Medioposterior cells
e
f
*JTK (24 h)
**RAIN (24 h)

Supplementary Figure 15. Free-running clock gene expression rhythms in tidally entrained *P. hawaiensis* (tidal phase θ +5.4 h).

a Normalised swimming activity of *P. hawaiensis* used in the HCR-FISH time-course showed a circatidal activity rhythm synchronised to the prior agitation cycle. Plots shows mean activity with SEM (shading) of harvested animals over the sampling interval (initial group size at start of harvest at CT0 =35).

b Profile of mean aggregate expression of *Phper, Phcry2* and *Phvri* across all cells plotted across time in tidally entrained animals sampled under DD. Each point is from one brain.

c Left: Cartoon to show location of anterior-medial a1 cells in the brain and Right: representative maximum intensity Z-projections of *Phper*, *Phcry2* and *Phvri* expression in the anterior-medial a1 cells from both hemispheres (L: left, R: right, yellow dashed lines: midlines) across CT (individual HCR-FISH channels in rows).

d Plots of mean transcript abundance, quantified as the number of FISH spots, across CT for *Phper* (left), *Phcry2* (middle) and *Phvri* (right) in the anterior-medial a1 cells. Each point is from one brain.

e, **f** As in **c**, **d** for medioposterior cell group.

Inset text in **b**, **d** and **f** indicate statistical tests performed to determine variation of gene expression with time and/or rhythmicity, with the tested periods (if any) in parentheses. $p < 0.001$***, $p < 0.01$**, $p \leq 0.05$*, $p > 0.05^{ns}$. KW: Kruskal-Wallis test. For statistics shown in this figure, refer to Supplementary Table 6. Scale bars: 5 µm (**c**), 10 µm (**e**).

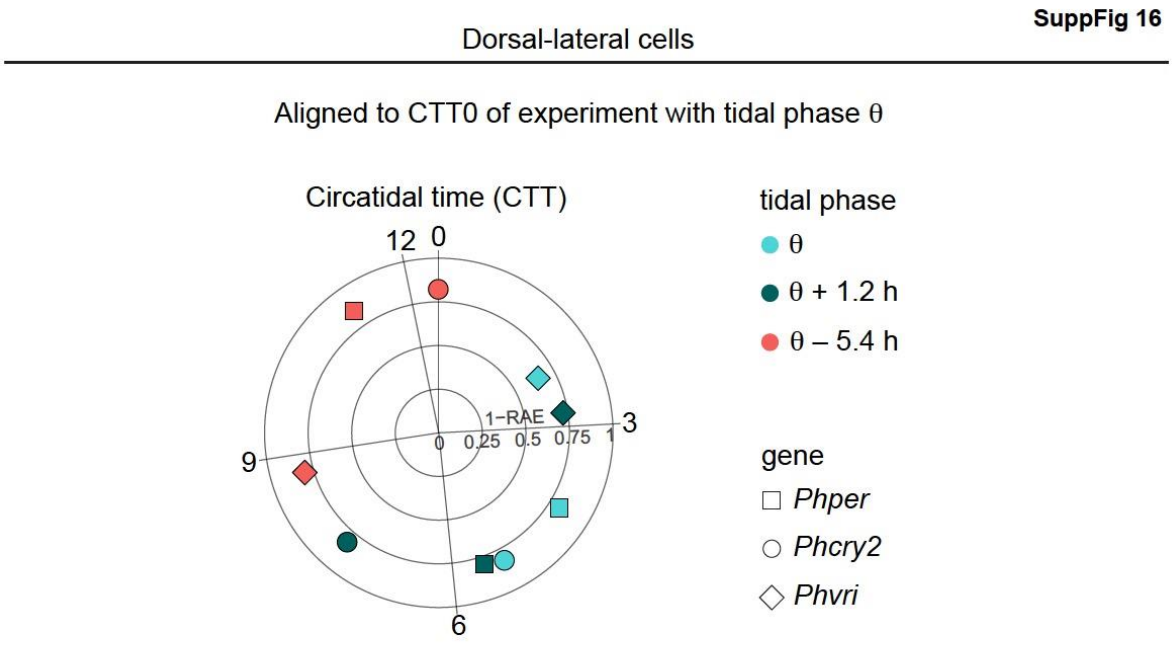

Supplementary Figure 16. Acrophase of free-running clock gene expression pattern in the dorsal lateral cells of *P. hawaiensis* entrained to tidal cycles of different phase. Circular plots of phase of circatidal peak expression of *Phper*, *Phcry2* and *Phvri* in the dorsal-lateral cells of *P. hawaiensis* exhibiting circatidal activity rhythms. The phase of each experiment is aligned to circatidal time (CTT) =0 of the experiment with tidal phase θ. Each colour represents an individual experiment at each of different phases (total N =3 X 3). RAE: relative amplitude error.

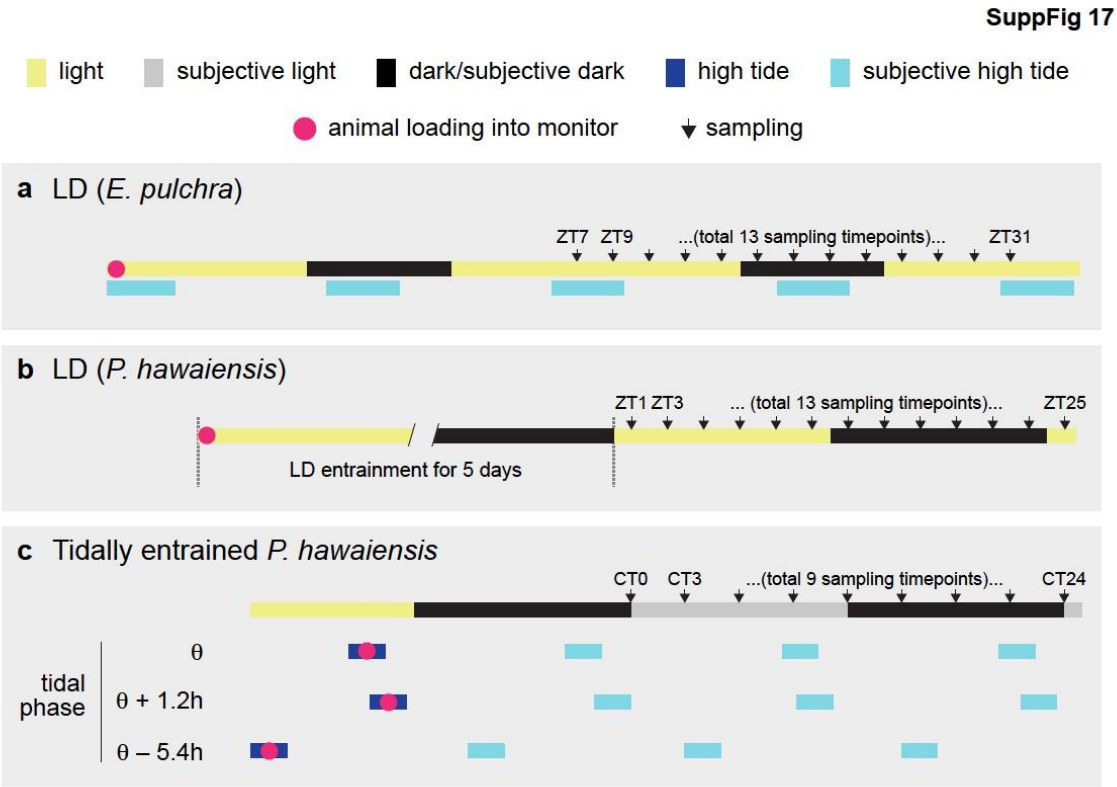

Supplementary Figure 17. HCR-FISH time-course design.

a Field-caught *E. pulchra* were loaded into activity monitors and maintained under 16 h: 8 h LD cycles. At ZT7 on the day after loading, animals showing circatidal rhythmicity in their swimming activity were sampled every 2 hours, for a total of 13 timepoints.

b Laboratory-cultured *P. hawaiensis* that had never been tidally entrained were loaded into activity monitors and maintained under 12 h: 12 h LD cycles for 5 days. Animals showing 24-h rhythmicity over the 5-day LD entrainment period were sampled every 2 hours beginning at ZT1 on day 6, for a total of 13 timepoints.

c Laboratory-cultured *P. hawaiensis* which had been subjected to tidal cycles of mechanical agitations were loaded into activity monitors whilst being shaken. At CT0 on the day after loading, animals showing peaks in activity coinciding with the subjective high tide during the night before were sampled every 3 hours, for a total of 9 timepoints.

Time-course design is also described in Supplementary Table 10.

Supplementary Table 1. Summary of cell groups enriched for *per* and *cry* expression in *E. pulchra* and *P. hawaiensis*.

E. pulchra				***P. hawaiensis***		
Cell group	# of cells	Anatomical location		Cell group	# of cells	Anatomical location
Medioposterior	18	rPBp		Medioposterior	20	rPBp
Medial	10	rPBdp		Medial	6	rPBp
Dorsal	8	rHE/MTp		Dorsal	12	rHE/MTd
Medioanterior	2	rMPa		Dorsal-lateral	4	rHE/MTd
Lateroposterior	4	rMTp		Anterior-lateral	2	rHE/MTa
Dorsoanterior	4	rHE/MTa		Anterior-medial a1	2	rMPa
Lateroanterior	2	rLOva		Anterior-medial a2	2	rMPa
Ventroposterior	8-12	rMPp		Anterior-medial b	4	rMPa
				Anterior-medial c	8-10	rMPa

Supplementary Table 2. Statistical tests for all gene-cell group combinations for the HCR-FISH time-course experiment of tidally active, beach-caught *E. pulchra* under LD. Effect size quantified as eta squared. Related to Figure 6 and Supplementary Figure 10. KW: Kruskal-Wallis test.

Gene	Cell group	Significant variation with time					24-h rhythmicity		12-h rhythmicity	
		Test	df	Test statistic	p-value	Effect size	JTK_cycle	RAIN	JTK_cycle	RAIN
Epper	all clock cells	ANOVA	12	2.590	0.011	0.425	0.003	0.001	1.000	0.852
	dorsal	ANOVA	12	1.718	0.100	0.346				
	dorsoanterior	ANOVA	12	2.346	0.020	0.390	0.602	1.000	0.943	1.000
	large-dorsal	ANOVA	12	2.090	0.041	0.391	0.003	0.192	1.000	1.000
	lateroanterior	KW	12	20.792	0.054	0.187				
	lateroposterior	ANOVA	12	2.200	0.030	0.386	0.459	1.000	1.000	0.999
	medial	ANOVA	12	2.617	0.011	0.428	0.022	0.003	1.000	0.711
	medioposterior	ANOVA	12	2.522	0.014	0.431	<0.001	0.001	1.000	0.990
Epcry2	all clock cells	KW	12	24.662	0.017	0.301	<0.001	<0.001	1.000	0.747
	dorsal	KW	12	16.606	0.165	0.118				
	dorsoanterior	KW	12	14.737	0.256	0.061				
	large-dorsal	KW	12	26.095	0.010	0.361	<0.001	0.017	1.000	0.996
	lateroanterior	KW	12	18.405	0.104	0.133				
	lateroposterior	KW	12	19.553	0.076	0.176				
	medial	KW	12	19.532	0.076	0.179				
	medioposterior	ANOVA	12	2.563	0.013	0.435	<0.001	<0.001	1.000	0.886

Supplementary Table 2. Continued.

Gene	Cell group	Significant variation with time					24-h rhythmicity		12-h rhythmicity	
		Test	df	Test statistic	p-value	Effect size	JTK_cycle	RAIN	JTK_cycle	RAIN
Eptim	all clock cells	KW	12	26.588	0.009	0.347	0.034	0.009	0.034	0.008
	dorsal	KW	12	19.182	0.084	0.184				
	dorsoanterior	KW	12	30.541	0.002	0.412	0.539	0.545	0.169	0.050
	large-dorsal	KW	12	17.331	0.138	0.137				
	lateroanterior	KW	12	40.436	<0.001	0.592	0.005	0.001	0.092	0.002
	lateroposterior	KW	12	31.599	0.002	0.456	0.556	1.000	0.009	0.042
	medial	KW	12	29.999	0.003	0.429	0.170	0.028	0.046	0.005
	medioposterior	KW	12	20.747	0.054	0.219				

Supplementary Table 3. Statistical tests and cosinor analysis (with defined periods of 24-h whenever appropriate) for all gene-cell group combinations for the HCR-FISH time-course experiment of *P. hawaiensis* synchronised to and sampled under LD. Related to Figure 7 and Supplementary Figure 11-12. Effect size quantified as eta squared. Phase derived from cosinor fit is corrected to Circadian Time (CT) =0. KW: Kruskal-Wallis test; RAE: relative amplitude error.

Gene	Cell group	Significant variation with time					24-h rhythmicity		12-h rhythmicity		Cosinor fit	
		Test	df	Test statistic	p-value	Effect size	JTK_cycle	RAIN	JTK_cycle	RAIN	phase	RAE
Phper	all clock cells	ANOVA	12	14.28	<0.001	0.764	<0.001	<0.001	1	0.250	21.14	0.11
	medioposterior	KW	12	54.45	<0.001	0.801	<0.001	<0.001	1	0.515	21.62	0.07
	medial-1	KW	12	24.66	0.017	0.239	1	0.868	1	0.014		
	medial-2	KW	12	20.18	0.064	0.157						
	dorsal-lateral	ANOVA	12	3.973	<0.001	0.474	0.103	0.003	1	0.051		
	dorsal	ANOVA	12	6.225	<0.001	0.585	<0.001	<0.001	1	0.193	19.11	0.18
	anterior-lateral	KW	12	13.09	0.363	0.021						
	anterior-medial a1	KW	12	57.04	<0.001	0.850	<0.001	<0.001	1	0.717	21.05	0.09
	anterior-medial a2	KW	12	20.94	0.051	0.172						
	anterior-medial b	ANOVA	12	9.073	<0.001	0.673	<0.001	<0.001	1	0.791	21.55	0.11
	anterior-medial c	ANOVA	12	1.697	0.095	0.285						
Phcry2	all clock cells	KW	12	26.16	0.010	0.267	0.05	0.001	1	0.019	11.70	0.36
	medioposterior	ANOVA	12	12.40	<0.001	0.737	<0.001	<0.001	0.014	<0.001	9.03	0.16
	medial-1	ANOVA	12	1.233	0.286	0.218						
	medial-2	ANOVA	12	2.057	0.037	0.322	1	0.951	1	0.989		
	dorsal-lateral	ANOVA	12	1.501	0.153	0.254						
	dorsal	ANOVA	12	1.792	0.074	0.289						
	anterior-lateral	ANOVA	12	0.9371	0.518	0.178						
	anterior-medial a1	KW	12	41.79	<0.001	0.562	<0.001	<0.001	1	0.219	8.28	0.12
	anterior-medial a2	KW	12	15.15	0.233	0.061						
	anterior-medial b	ANOVA	12	6.574	<0.001	0.598	<0.001	<0.001	1	0.580	16.39	0.14
	anterior-medial c	ANOVA	12	2.203	0.026	0.341	0.049	0.009	1	0.034	15.78	0.34

Supplementary Table 3. Continued.

Gene	Cell group	Significant variation with time					24-h rhythmicity		12-h rhythmicity		Cosinor fit	
		Test	df	Test statistic	p-value	Effect size	JTK_cycle	RAIN	JTK_cycle	RAIN	phase	RAE
PhClk	all clock cells	ANOVA	12	2.626	0.008	0.374	0.022	0.001	1	0.251	21.28	0.26
	medioposterior	ANOVA	12	7.723	<0.001	0.636	<0.001	<0.001	1	0.085	22.54	0.13
	medial-1	ANOVA	12	0.6906	0.753	0.135						
	medial-2	ANOVA	12	0.812	0.637	0.158						
	dorsal-lateral	ANOVA	12	1.426	0.184	0.244						
	dorsal	KW	12	31.68	0.002	0.371	<0.001	<0.001	1	0.831	17.19	0.15
	anterior-lateral	ANOVA	12	0.7788	0.669	0.152						
	anterior-medial a1	ANOVA	12	23.71	<0.001	0.843	<0.001	<0.001	1	0.743	7.73	0.07
	anterior-medial a2	KW	12	14.58	0.265	0.050						
	anterior-medial b	ANOVA	12	1.300	0.246	0.227						
	anterior-medial c	ANOVA	12	1.353	0.219	0.241						

Supplementary Table 4. Statistical tests and cosinor analysis (with defined periods of 24-h and/or 12.4-h, whenever appropriate) for all gene-cell group combinations for the HCR-FISH time-course experiment of *P. hawaiensis* entrained to tidal phase θ. Related to Figures 8-9, Supplementary Figure 13 and Supplementary Table 7. Effect size quantified as eta squared. Phase derived from cosinor fit is corrected to Circadian Time (CT) =0 or Circatidal Time (CTT) =0, as appropriate. KW: Kruskal-Wallis test; RAE: relative amplitude error.

Gene	Cell group	Significant variation with time					24-h rhythmicity		12-h rhythmicity		Cosinor fit	
		Test	df	Test statistic	p-value	Effect size	JTK_cycle	RAIN	JTK_cycle	RAIN	phase	RAE
Phper	all clock cells	ANOVA	8	11.99	<0.001	0.813	<0.001	<0.001	0.299	0.083	22.33	0.16
	medioposterior	ANOVA	8	62.35	<0.001	0.954	<0.001	<0.001	0.381	0.262	22.32	0.07
	medial-1	ANOVA	8	1.031	0.441	0.256						
	medial-2	ANOVA	8	1.180	0.353	0.291						
	dorsal-lateral	ANOVA	8	6.584	<0.001	0.678	1	0.034	0.006	<0.001	4.20	0.18
	dorsal	ANOVA	8	1.962	0.099	0.406						
	anterior-lateral	ANOVA	8	1.090	0.403	0.267						
	anterior-medial a1	ANOVA	8	43.95	<0.001	0.934	<0.001	<0.001	0.388	0.793	22.31	0.06
	anterior-medial a2	ANOVA	8	2.157	0.068	0.408						
	anterior-medial b	ANOVA	8	2.253	0.059	0.429						
	anterior-medial c	ANOVA	8	1.856	0.125	0.426						
Phcry2	all clock cells	ANOVA	8	3.942	0.005	0.589	0.441	0.023	0.087	0.004		
	medioposterior	ANOVA	8	15.13	<0.001	0.835	<0.001	<0.001	0.059	0.002	9.35	0.14
	medial-1	ANOVA	8	1.387	0.252	0.316						
	medial-2	KW	8	8.827	0.357	0.036						
	dorsal-lateral	ANOVA	8	6.866	<0.001	0.687	1	0.086	0.002	<0.001	5.26	0.18
	dorsal	ANOVA	8	1.391	0.252	0.326						
	anterior-lateral	ANOVA	8	0.7758	0.628	0.205						
	anterior-medial a1	ANOVA	8	9.814	<0.001	0.758	<0.001	<0.001	0.930	0.567	8.86	0.14
	anterior-medial a2	ANOVA	8	0.4122	0.903	0.117						
	anterior-medial b	ANOVA	8	1.501	0.209	0.333						
	anterior-medial c	KW	8	7.572	0.476	−0.021						

Supplementary Table 4. Continued.

Gene	Cell group	Significant variation with time					24-h rhythmicity		12-h rhythmicity		Cosinor fit	
		Test	df	Test statistic	p-value	Effect size	JTK_cycle	RAIN	JTK_cycle	RAIN	phase	RAE
Phvri	all clock cells	ANOVA	8	1.348	0.273	0.329						
	medioposterior	ANOVA	8	2.796	0.024	0.482	0.057	<0.001	0.582	0.299		
	medial-1	ANOVA	8	0.7772	0.626	0.206						
	medial-2	ANOVA	8	0.9382	0.505	0.246						
	dorsal-lateral	ANOVA	8	2.770	0.024	0.470	0.623	0.003	0.025	0.003	2.11	0.35
	dorsal	ANOVA	8	0.7326	0.662	0.203						
	anterior-lateral	ANOVA	8	0.5677	0.794	0.159						
	anterior-medial a1	ANOVA	8	3.428	0.009	0.523	0.441	0.022	1	0.923		
	anterior-medial a2	ANOVA	8	1.220	0.328	0.281						
	anterior-medial b	ANOVA	8	1.603	0.176	0.348						
	anterior-medial c	ANOVA	8	0.8998	0.535	0.265						

Supplementary Table 5. Statistical tests and cosinor analysis (with defined periods of 24-h and/ or 12.4-h, whenever appropriate) for all gene-cell group combinations for the HCR-FISH time-course experiment of *Parhyale hawaiensis* entrained to tidal phase θ +1.2 h. Related to Figure 9, Supplementary Figure 14 and Supplementary Table 7. Effect size quantified as eta squared. Phase derived from cosinor fit is corrected to Circadian Time (CT) =0 or Circatidal Time (CTT) =0, as appropriate. KW: Kruskal-Wallis test; RAE: relative amplitude error.

Gene	Cell group	Significant variation with time					24-h rhythmicity		12-h rhythmicity		Cosinor fit	
		Test	df	Test statistic	p-value	Effect size	JTK_cycle	RAIN	JTK_cycle	RAIN	phase	RAE
Phper	all clock cells	ANOVA	8	4.899	0.003	0.697	<0.001	<0.001	1	<0.001	23.03	0.17
	medioposterior	ANOVA	8	12.96	<0.001	0.845	<0.001	<0.001	0.772	0.462	22.90	0.11
	medial-1	ANOVA	8	0.5012	0.84	0.182						
	medial-2	ANOVA	8	0.4058	0.902	0.160						
	dorsal-lateral	ANOVA	8	7.212	<0.001	0.743	0.232	0.003	0.016	<0.001	4.53	0.21
	dorsal	ANOVA	8	0.7518	0.648	0.273						
	anterior-lateral	ANOVA	8	1.982	0.109	0.468						
	anterior-medial a1	ANOVA	8	49.29	<0.001	0.952	<0.001	<0.001	1	0.753	22.17	0.06
	anterior-medial a2	ANOVA	8	1.732	0.152	0.410						
	anterior-medial b	KW	8	16.20	0.040	0.304	0.232	0.003	0.772	0.106		
	anterior-medial c	ANOVA	8	1.101	0.414	0.370						
Phcry2	all clock cells	ANOVA	8	1.266	0.323	0.373						
	medioposterior	ANOVA	8	7.967	<0.001	0.770	0.005	<0.001	0.023	0.001	7.01	0.24
	medial-1	ANOVA	8	0.6999	0.688	0.237						
	medial-2	ANOVA	8	1.522	0.222	0.417						
	dorsal-lateral	ANOVA	8	4.908	0.002	0.663	1	0.215	0.016	<0.001	6.58	0.18
	dorsal	ANOVA	8	0.9256	0.522	0.316						
	anterior-lateral	ANOVA	8	0.5485	0.805	0.196						
	anterior-medial a1	ANOVA	8	6.807	<0.001	0.731	<0.001	<0.001	1	0.773	7.88	0.13
	anterior-medial a2	ANOVA	8	1.667	0.168	0.400						
	anterior-medial b	ANOVA	8	2.880	0.026	0.535	0.222	0.014	1	0.460		
	anterior-medial c	ANOVA	8	0.4578	0.867	0.196						

Supplementary Table 5. Continued.

Gene	Cell group	Significant variation with time					24-h rhythmicity		12-h rhythmicity		Cosinor fit	
		Test	df	Test statistic	p-value	Effect size	JTK_cycle	RAIN	JTK_cycle	RAIN	phase	RAE
Phvri	all clock cells	KW	8	13.08	0.109	0.299						
	medioposterior	KW	8	24.10	0.002	0.847	<0.001	<0.001	1	0.815	6.44	0.12
	medial-1	ANOVA	8	0.5257	0.822	0.189						
	medial-2	ANOVA	8	0.3815	0.916	0.152						
	dorsal-lateral	KW	8	18.13	0.02	0.507	0.245	<0.001	0.032	0.001	1.79	0.28
	dorsal	KW	8	13.35	0.100	0.334						
	anterior-lateral	ANOVA	8	1.553	0.208	0.408						
	anterior-medial a1	ANOVA	8	2.132	0.081	0.460						
	anterior-medial a2	ANOVA	8	1.460	0.233	0.369						
	anterior-medial b	KW	8	20.20	0.010	0.610	0.173	0.01	1	0.569		
	anterior-medial c	ANOVA	8	3.369	0.020	0.642	0.460	0.082	0.772	0.092		

Supplementary Table 6. Statistical tests and cosinor analysis (with defined periods of 24-h and/ or 12.4-h, whenever appropriate) for all gene-cell group combinations for the HCR-FISH time-course experiment of *P. hawaiensis* entrained to tidal phase θ – 5.4 h. Related to Figure 9, Supplementary Figure 15 and Supplementary Table 7. Effect size quantified as eta squared. Phase derived from cosinor fit is corrected to Circadian Time (CT) =0 or Circatidal Time (CTT) =0, as appropriate. KW: Kruskal-Wallis test; RAE: relative amplitude error.

Gene	Cell group	Significant variation with time					24-h rhythmicity		12-h rhythmicity		Cosinor fit	
		Test	df	Test statistic	p-value	Effect size	JTK_cycle	RAIN	JTK_cycle	RAIN	phase	RAE
Phper	all clock cells	KW	8	19.98	0.010	0.705	0.002	<0.001	0.627	0.25	22.32	0.16
	medioposterior	KW	8	20.39	0.009	0.689	0.002	<0.001	1	0.879	22.57	0.11
	medial-1	KW	8	11.56	0.172	0.223						
	medial-2	KW	8	7.392	0.495	-0.036						
	dorsal-lateral	ANOVA	8	7.469	<0.001	0.768	1	0.277	<0.001	<0.001	4.40	0.15
	dorsal	ANOVA	8	1.808	0.145	0.460						
	anterior-lateral	KW	8	11.99	0.152	0.234						
	anterior-medial a1	ANOVA	8	23.67	<0.001	0.913	0.005	<0.001	0.829	0.654	22.73	0.12
	anterior-medial a2	KW	8	6.759	0.563	−0.073						
	anterior-medial b	ANOVA	8	1.912	0.121	0.096						
	anterior-medial c	KW	8	9.893	0.273	0.111						
Phcry2	all clock cells	ANOVA	8	1.544	0.215	0.421						
	medioposterior	ANOVA	8	2.537	0.048	0.530	0.016	0.001	1	0.84	9.06	0.23
	medial-1	ANOVA	8	1.497	0.234	0.428						
	medial-2	ANOVA	8	0.8941	0.542	0.296						
	dorsal-lateral	ANOVA	8	8.943	<0.001	0.799	0.758	0.085	<0.001	<0.001	5.59	0.18
	dorsal	KW	8	13.51	0.096	0.324						
	anterior-lateral	ANOVA	8	4.823	0.003	0.694	1	0.203	<0.001	<0.001	3.93	0.17
	anterior-medial a1	KW	8	10.06	0.261	0.114						
	anterior-medial a2	KW	8	12.26	0.14	0.251						
	anterior-medial b	ANOVA	8	1.129	0.391	0.334						
	anterior-medial c	ANOVA	8	2.131	0.090	0.501						

Supplementary Table 6. Continued.

Gene	Cell group	Significant variation with time					24-h rhythmicity		12-h rhythmicity		Cosinor fit	
		Test	df	Test statistic	p-value	Effect size	JTK_cycle	RAIN	JTK_cycle	RAIN	phase	RAE
Phvri	all clock cells	ANOVA	8	4.368	0.005	0.673	0.331	0.014	0.198	0.095		
	medioposterior	ANOVA	8	16.67	<0.001	0.881	0.002	<0.001	0.627	0.203	6.71	0.17
	medial-1	ANOVA	8	1.722	0.169	0.463						
	medial-2	KW	8	3.99	0.858	−0.236						
	dorsal-lateral	ANOVA	8	16.35	<0.001	0.879	1	0.229	0.05	0.007	1.93	0.20
	dorsal	ANOVA	8	1.421	0.257	0.401						
	anterior-lateral	KW	8	9.894	0.273	0.111						
	anterior-medial a1	KW	8	11.42	0.179	0.190						
	anterior-medial a2	ANOVA	8	1.708	0.168	0.446						
	anterior-medial b	ANOVA	8	0.9457	0.505	0.296						
	anterior-medial c	ANOVA	8	1.696	0.171	0.444						

Supplementary Table 7. Circular statistics of gene-cell group combinations that show statistically significant rhythmicity (at 24-h or 12-h) across 3 HCR-FISH time-course experiments of tidally entrained *P. hawaiensis*. Related to Figure 10, Supplementary Figures 13-15, Supplementary Tables 4-6.

Gene	Cell group	Mean phase	Mean vector length	Number of experiments
Circadian oscillators				
Phper	All clock cells	22.56	1.00	3
	Medioposterior	22.60	1.00	3
	Anterior-medial a1	22.40	1.00	3
Phcry2	Medioposterior	8.48	0.96	3
	Anterior-medial a1	8.37	0.99	2
Phvri	Medioposterior	6.58	1.00	2
Circatidal oscillators				
Phper	Dorsal-lateral	4.38	1.00	3
Phcry2		5.81	0.96	3
Phvri		1.94	1.00	3

Supplementary Table 8. The targets, hairpin identities and lot numbers of the HCR-FISH primary probes used to generate the data described in this study.

Probe/target genes	NCBI accession #	Probe hairpin	Number of probe pairs	Lot number	Relevant figure(s)
EpBmal1	KC885968.1	B3	20	PRP939	Fig. 2-3, Supp. Fig. 6
EpBmal1 additional	KC885968.1	B3	40	RTA402	Fig. 2-3, Supp. Fig. 6
EpClk 1-9	KC885973.1	B1	40	RTA400	Fig. 2-3
EpClk 1-9 additional	KC885973.1	B1	29	RTE285	Fig. 2-3
Epcry2	KC885970.1	B1	20	RTA399	Fig. 2-3, 5, Supp. Fig. 8
Epcry2	KC885970.1	B3	20	RTO453	Fig. 6, Supp. Fig. 10
Epper	KC885967.1	B2	20	RTO454	Fig. 2-3, 6, Supp. Fig. 10
Eptim	KC885969.1	B1	20	PRP937	Fig. 2-3, 6, Supp. Fig. 10
Eppdh	GQ380440.1	B4	9	RTE284	Fig. 5
PhBmal1	Not applicable. Sequences from Hunt, Mallon & Rosato (2019)	B1	38	RTC080	Fig. 2-3, Supp. Fig. 6
Phpdh		B1	12	RTF908	Fig. 5
Phper		B1/B2	30	RTK407/RTC082	Fig. 2-3, 7-9, Supp. Fig. 11-15
PhClk-fragment 1		B2	40	RTG497	Fig. 2-3, 7, Supp. Fig. 11-12
PhClk-fragment 2		B2	28	RTG498	Fig. 2-3, 7, Supp. Fig. 11-12
Phcry2		B3	30	RTC083	Fig. 2-3, 5, 7-9, Supp. Fig. 8-9, 11-15
Phvri		B4	20	RTC086	Fig. 2-3, 9, Supp. Fig. 14-15
Phvri-30-probe-pairs		B4	30	RTI933	Fig. 8-9, Supp. Fig. 13
deGFP	Not applicable. Sequence provided by Molecular Instruments Inc.	B1	12	RTA210	Supp. Fig. 8
deGFP		B2	12	PRQ740	Supp. Fig. 8

Supplementary Table 9. The names, hairpin identities and lot numbers of the RNAScope technology FISH probes

Probe/target gene	**NCBI accession #**	**Amplifier**	**ACD cat number**
Epper-C4	KC885967.1	C4	578211-C4
EpClk5-C1	KC885973.1	C1	578151-C1
Epcry2-C1	KC885970.1	C1	1039411-C1
Eptim-C3	KC885969.1	C3	1099401-C3
EpBmal1-C2	KC885968.1	C2	578191-C2
-ve control			

*negative control probe is designed against the DapB gene of *Bacillus subtilis* strain

Supplementary Table 10. FISH time-course designs for investigating clock gene expression rhythms. Related to Supplementary Figure 17.

Experiment	Sampling condition	First sampling time-point	*N* total animals sampled	Sampling interval	1st subjective high tide onset during sampling	HCR-FISH primary probes	HCR-FISH hairpins (AF: AlexaFluor)	Relevant figures/tables
14h:10h LD-maintained *E. pulchra*								
LD (*E. pulchra*) (Supp. Fig. 17a)	LD	ZT7	65	2	ZT18.4	*Eptim*-B1, *Epper*-B2, *Epcry2*-B3	B1-AF647, B2-AF546, B3-AF488	Fig. 6, Supp. Fig. 10, Supp. Table 2
12h:12h LD-synchronised *P. hawaiensis*								
LD (*P. hawaiensis*) (Supp. Fig. 17b)	LD	ZT1	79	2	N.A.	*Phper*-B1, *PhClk*-fragment1-B2, *PhClk*-fragment2-B2, *Phcry2*-B3	B1-AF647, B2-AF546, B4-AF647	Fig. 7, Supp. Figs. 11-12, Supp. Table 3
Tidally entrained *P. hawaiensis* (Supp. Fig. 17c)								
θ	DD	CT0	37	3	CT9.2	*Phper*-B2, *Phcry2*-B3, *Phvri*-30-probe-pairs-B4	B2-AF546, B3-AF488, B4-AF647	Fig. 8-9, Supp. Fig. 13, Supp. Table 4
θ + 1.2h	DD	CT0	35	3	CT10.4	*Phper*-B2, *Phcry2*-B3, *Phvri*-B4	B2-AF647, B3-AF488, B4-AF546	Fig. 9, Supp. Fig. 14, Supp. Table 5
θ – 5.4h	DD	CT0	35	3	CT3.8	*Phper*-B2, *Phcry2*-B3, *Phvri*-B4	B2-AF647, B3-AF488, B4-AF546	Fig. 9, Supp. Fig. 15, Supp. Table 6

Supplementary results

Neuropils of *E. pulchra*.

In *E. pulchra*, the optic neuropils comprise lamina (LA), medulla (ME), and lobula (LO). The ME is proximal to the LA and distal to the LO. Ventral to the LO is a small unidentified neuropil. The optic neuropils are distal to the lateral protocerebrum (LP), which comprises the medulla terminalis (MT) and hemi-ellipsoid body (HE). These neuropils are poorly demarcated, and we did not attempt to determine the borders of each, segmenting them as a contiguous complex (HE/MT). The median protocerebrum (MP) comprises a large central body (CB) and protocerebral bridge (PB). The CB extends across the width of the brain and appears to be layered. Ventral to the protocerebrum is the deutocerebrum comprising the deutocerebral chemosensory lobes (DCL) and lateral antenna 1 neuropil (LAN). The DCL are lateral to the brain and comprise numerous olfactory glomeruli. Medial of the DCL is the LAN and ventral of this is antenna 2 neuropil (ANN) within the tritocerebrum. We also identified lateral accessory lobes (LAL) and nodules (NOD), and the medial antenna 1 neuropil (MAN). For *P. hawaiensis* we confirmed the anatomy of Whittforth et al. [1] and identified all major neuropils in our refence brain, which correspond closely with those we describe in *E. pulchra*. See also Supplementary Figures 4-5 and Supplementary Videos 1-2.

Supplementary Video 1

Reference brain of *E. pulchra* revealed by anti-SYNORF1 immunostaining and neuroanatomy of putative clock cell groups revealed by co-immuno-HCR-FISH staining.

Related to Figure 4a and Supplementary Figure 5a.

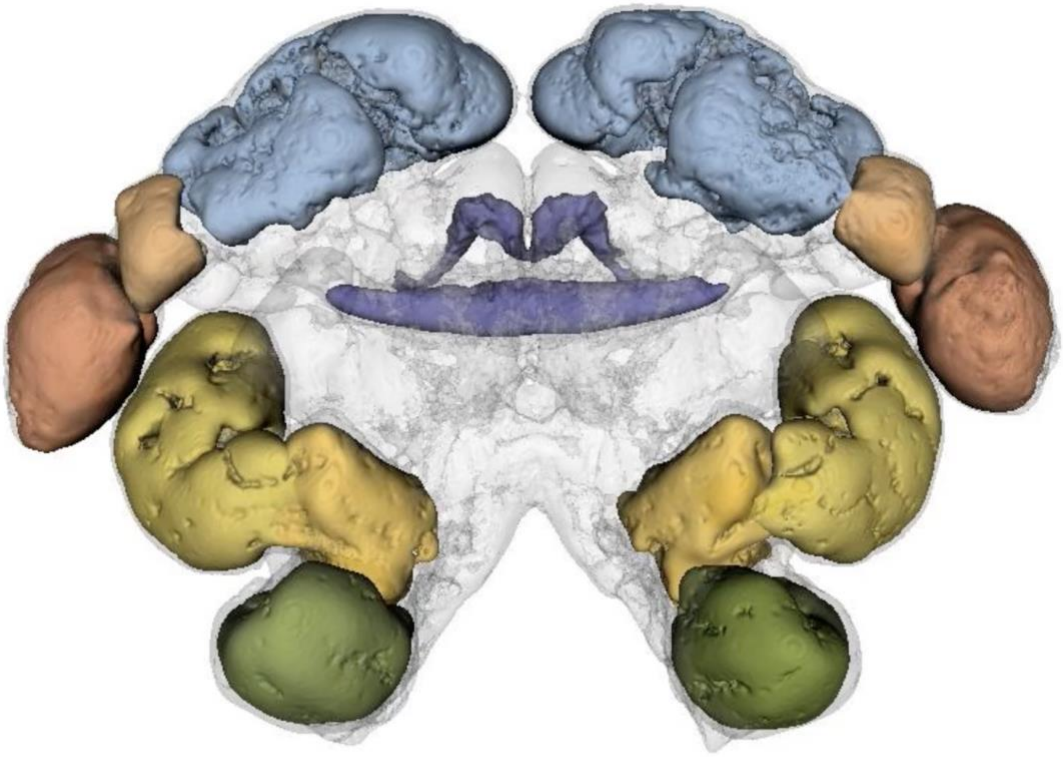

Supplementary Video 2

Reference brain of *P. hawaiensis* revealed by anti-SYNORF1 immunostaining and neuroanatomy of putative clock cell groups revealed by co-immuno-HCR-FISH staining.

Related to Figure 4c and Supplementary Figure 5 c.

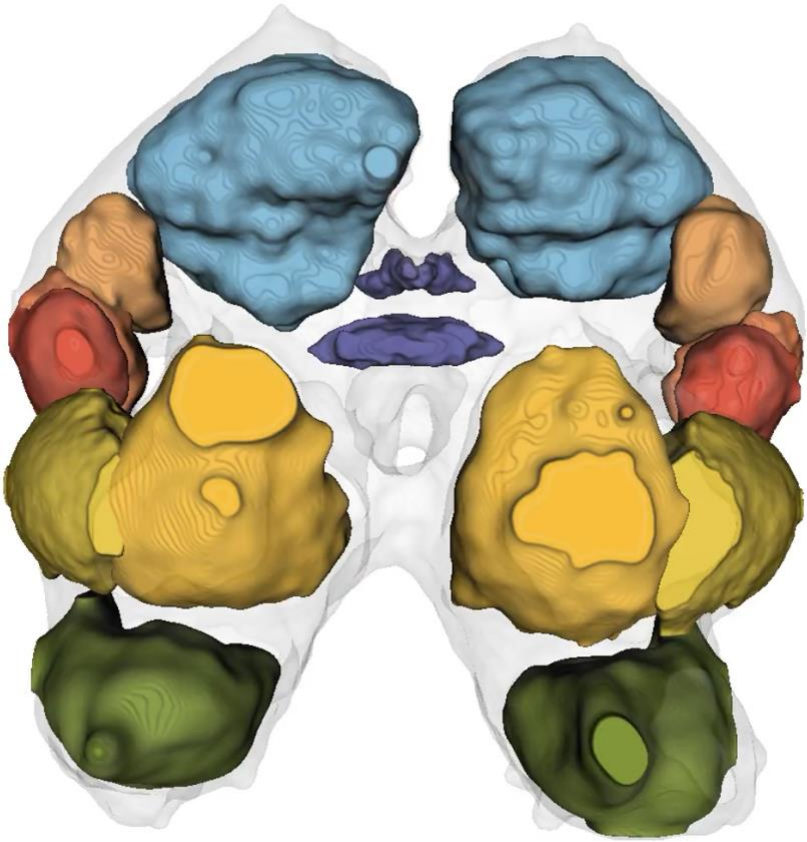

Supplementary methods

Immunostaining

For immunolabelling of *E. pulchra* brains with anti-SYNORF1, after rehydration to PBST, brains were washed in PTx (PBS supplemented with 0.1% Triton X-100), permeabilised in detergent solution (50 mM Tris-HCl pH 7.5, 150 mM NaCl, 1 mM EDTA pH 8, 1% SDS, 0.5% Tween-20) for 30 min at room temperature (Bruce et al. 2021) and then incubated with 1:50 anti-SYNORF1 in PTx containing 5% normal goat serum (NGS) overnight at room temperature, followed by 5 days at 4°C, with rotation. After extensive washing in PTx, brains were incubated with anti-mouse Alexa 488 (ThermoFisher #A-21141) at 1:1000 in PTx containing 5% NGS for 3 days at 4°C, with rotation. After extensive washing with PTx, nuclei were stained with 0.1 µg/mL DAPI int PTx for 1h. Brains were then bridge-mounted in RapiClear 1.49 (SunJin Lab Optical Clearing Innovation, #RC149001) using No. 2 thickness coverslips to maintain 3D morphology. For *P. hawaiensis*, brains were incubated in blocking buffer (1x PBS, 0.5% Tween-20, 5% NGS, 1% bovine serum albumin) containing 1:50 anti-SYNORF1 for 3 days at 4°C with gentle shaking, followed by extensive washing in PTw (PBS supplemented with 0.5% Tween-20) and incubation in secondary antiserum F(ab')2-goat anti-mouse IgG-Alexa Fluor 488 (ThermoFisher #A-11017) or Alexa Fluor Plus 555 (ThermoFisher #A48287) at 1:250 made in blocking buffer for 2 days at 4°C with gentle agitation. Nuclei were stained with 0.1 µg/mL DAPI for 30 min prior to final washing in PTw and preparations mounted in DPX (Sigma Aldrich #06522) according to [2].

Reference brains

Whole-mount brain samples used for generating reference brains and describing the neuroanatomy of putative clock cells were imaged on a Nikon CSU-W1 spinning disk confocal microscope equipped with a 25x/1.05NA silicone oil CFI Plan Apochromat Lambda S objective and a Prime 95B 22mm sCMOS camera. To make an *E. pulchra* reference brain, two sex-specific references were made by registering and then averaging 7 male brains to one male "seed" brain and 6 female brains to a female "seed" brain. These sex-specific references were then averaged to generate a final intersex reference brain (an average of 15 brains) used for all subsequent analyses. For *P. hawaiensis*, 10 male brains were registered and then averaged to a seed brain to generate a reference brain. Registration and averaging were done using: https://github.com/jefferislab/MakeAverageBrain [3] [4]. Briefly, Computational Morphometry Toolkit (CMTK) was used to register image stacks against a seed image stack; first with a rigid and then a non-rigid registration [5, 6]. Image stacks of brains with co-immuno-RNA-FISH labelling of neuropils and circadian clock genes (*per*/ *cry2*/ *tim*) were registered to

101 reference brains based on the anti-SYNORF1 signal. Three-dimensional surface models of
102 neuropils were based on reference brains and generated using the Segmentation Editor in
103 3DSlicer software (www.slicer.org). 3D surface models of putative clock cells were based on
104 circadian clock gene HCR-FISH labelling (*Epcry2* or *Phcry2*) in an image stack registered to
105 the reference brain and using the Segmentation Editor in 3DSlicer.
106
107 ***HCR-FISH***
108 For HCR-FISH, rehydrated brains were permeabilised in detergent solution for 30 min at room
109 temperature, and equilibrated in pre-warmed probe hybridisation buffer for 30 min at 37°C.
110 Brains were then incubated in probe hybridisation solution containing 10 nM of each primary
111 probe set for 2 days (*E. pulchra*) or 3 days (*P. hawaiensis*) at 37°C. For *P. hawaiensis*, 1:1000
112 murine RNase inhibitor (NEB #M0314L) was added to the probe hybridisation buffer. Signal
113 amplification with 60 nM fluorescently tagged hairpins was allowed to proceed for 2 days,
114 followed by staining with 0.1 µg/mL DAPI in 5x SSC supplemented with 0.5% Tween-20 (30
115 min) during one of the final washing steps. *E. pulchra* brains were bridge-mounted using No.
116 1.5 thickness coverslips in RapiClear 1.49 whilst *P. hawaiensis* brains were dehydrated and
117 mounted in DPX according to [2]. The target genes used for probe design, their accession
118 numbers, and the Molecular Instruments probe lot numbers and concentrations used are listed
119 in Supplementary Tables 8. For experiments investigating co-expression of clock genes, a
120 40x/1.3NA Plan Fluorite oil immersion objective was used to image with an optical section
121 interval of 1 µm.
122
123 For co-immuno-RNA-FISH staining, following rehydration and permeabilization in detergent
124 solution, *E. pulchra*, brains were incubated with 1:50 anti-SYNORF1 in PTx containing 1.6
125 U/µL RNaseOUT™ ribonuclease inhibitor (Invitrogen #10777019) overnight at room
126 temperature, followed by 3 days at 4°C, with rotation. After extensive washing in PTx, brains
127 were incubated with anti-mouse Alexa 488 (ThermoFisher #A-21141) at 1:1000 in PTx
128 containing RNase inhibitor for 2 days at 4°C, with rotation. After washing in PTx/w, brains
129 were fixed in 4% PFA (in PBS) for 1 hour at room temperature. After washing in PTx/w, the
130 neuropil-stained brains were processed for HCR-FISH as above and mounted as described
131 above. *P. hawaiensis* brains were washed in PTw and subjected to one-step immunostaining
132 [7] by incubating in PTw containing pre-mixed 1:250 murine RNase inhibitor, 1:50 anti-
133 SYNORF1, 3.33 ng/µL Fab goat anti-mouse IgG-Alexa Fluor 488 (Jackson ImmunoResearch
134 #115-547-003) for 2 days at room temperature.
135
136 **RNAscope methods for formalin-fixed, paraffin-wax embedded *E.pulchra* brains**

137

138 *E. pulchra* brains were dissected in ice-chilled crustacean saline [8] and fixed immediately in
139 10% normal buffered formalin (10%) overnight (16h) at RT. After fixing, brains were washed
140 extensively in PBS, dehydrated through an ethanol series (50%, 70%, 80%, 90%, 95%,
141 100%), cleared in xylene (1h at RT) and infiltrated in molten wax (Leica Paraplast Plus®, Leica
142 Biosystems, Sheffield UK) 3x, each for 1h, before embedding in wax such that the brains could
143 be mounted for frontal sections to be cut. Serial sections (6µm) were cut on a standard wax
144 microtome and mounted on Superfrost™ Plus (Thermo Fisher, UK). After drying, sections
145 were baked at 60°C for 2h to adhere fully to the slides. Slides were de-waxed in clean xylene
146 and taken to water through an ethanol series before drying at 60C for 1h. Following
147 preparation, manufacturer's instructions were followed exactly, except that target retrieval was
148 done in 700 mL Target Retrieval buffer in a 1L beaker, for 15 minutes at 98-104°C, over a hot-
149 plate. Protease Plus was applied for 30 minutes at 40°C. Signal amplification was done using
150 Opal™ fluors (Opal 520 and Opal 570). All reagents and kit components were as
151 recommended by ACD Biotechne (Abingdon, Oxford, UK. RNAscope® Multiplex Fluorescent
152 Reagent Kit v2 Assay). Target probes were designed by ACD Biotechne and probe details
153 provided in Supplementary Tables 9. Negative control probes were supplied by ACD
154 Biotechne and are designed against the *DapB2* gene of *Bacillus subtilis.* Following
155 hybridisation and amplification, sections were counterstained with DAPI provided with the kit
156 and mounted under Vectashield® Antifade mounting fluid (Vector Laboratories, supplied by
157 2B Scientific, Oxford, UK). Images were captured on a Leica SP8 confocal microscope at
158 1µm z-stack intervals and using Leica LAX proprietary software. Images were re-sized,
159 cropped and adjusted for brightness and contrast using ImageJ software.

160

161

Supplementary References

1. Wittfoth C, Harzsch S, Wolff C, Sombke A. The "amphi"-brains of amphipods: new insights from the neuroanatomy of *Parhyale hawaiensis* (Dana, 1853). *Front Zool* **16**, 30 (2019).

2. Meissner GW*, et al.* DPX Mounting of Drosophila CNS (2018).

3. Costa M, Manton JD, Ostrovsky AD, Prohaska S, Jefferis GS. NBLAST: Rapid, Sensitive Comparison of Neuronal Structure and Construction of Neuron Family Databases. *Neuron* **91**, 293-311 (2016).

4. Bates AS*, et al.* The natverse, a versatile toolbox for combining and analysing neuroanatomical data. *Elife* **9**, (2020).

5. Jefferis GSXE*, et al.* Comprehensive Maps of Drosophila Higher Olfactory Centers: Spatially Segregated Fruit and Pheromone Representation. *Cell* **128**, 1187-1203 (2007).

6. Rohlfing T, Maurer CR, Jr. Nonrigid image registration in shared-memory multiprocessor environments with application to brains, breasts, and bees. *IEEE Trans Inf Technol Biomed* **7**, 16-25 (2003).

7. Wang S. Single Molecule RNA FISH (smFISH) in Whole-Mount Mouse Embryonic Organs. *Current Protocols in Cell Biology* **83**, (2019).

8. Saver MA, Wilkens JL, Syed NI. In Situ and In Vitro Identification and Characterization of Cardiac Ganglion Neurons in the Crab, *Carcinus maenas*. *Journal of Neurophysiology* **81**, 2964-2976 (1999).